Core-Shell Composite Nanoparticles: Synthesis, Characterization, and Applications

by

Sriya Sanyal

A Dissertation Presented in Partial Fulfillment
of the Requirements for the Degree
Doctor of Philosophy

Approved September 2012 by the
Graduate Supervisory Committee:

Lenore Dai, Chair
Hanqing Jiang
Mary Laura Lind
Patrick Phelan
Kaushal Rege

ARIZONA STATE UNIVERSITY

December 2012

ABSTRACT

Nanoparticles are ubiquitous in various fields due to their unique properties not seen in similar bulk materials. Among them, core-shell composite nanoparticles are an important class of materials which are attractive for their applications in catalysis, sensing, electromagnetic shielding, drug delivery, and environmental remediation. This dissertation focuses on the study of core-shell type of nanoparticles where a polymer serves as the core and inorganic nanoparticles are the shell. This is an interesting class of supramolecular building blocks and can "exhibit unusual, possibly unique, properties which cannot be obtained simply by co-mixing polymer and inorganic particles".

The one-step Pickering emulsion polymerization method was successfully developed and applied to synthesize polystyrene-silica core-shell composite particles. Possible mechanisms of the Pickering emulsion polymerization were also explored. The silica nanoparticles were thermodynamically favorable to self-assemble at liquid-liquid interfaces at the initial stage of polymerization and remained at the interface to finally form the shells of the composite particles.

More importantly, Pickering emulsion polymerization was employed to synthesize polystyrene/poly(N-isopropylacrylamide) (PNIPAAm)-silica core-shell nanoparticles with N-isopropylacrylamide incorporated into the core as a co-monomer. The composite nanoparticles were temperature sensitive and could be up-taken by human prostate cancer cells and demonstrated effectiveness in drug delivery and cancer therapy. Similarly, by incorporating poly-2-(N,N)-dimethylamino)ethyl methacrylate (PDMA) into the core, pH sensitive core-shell

composite nanoparticles were synthesized and applied as effective carriers to release a rheological modifier upon a pH change. Finally, the research focuses on facile approaches to engineer the transition of the temperature-sensitive particles and develop composite core-shell nanoparticles with a metallic shell.

ACKNOWLEDGMENTS

With my deepest regards I would like to express my thanks to everyone who has contributed and helped me during the time which I conducted my research and completed this doctoral dissertation. It would not have been possible to do so without the help and support of the kind people around me. First and foremost I offer my sincerest gratitude to my advisor, Professor Lenore L. Dai, who has supported me throughout my research whilst allowing me the room to work in my own way. This dissertation would not have been possible without her patient help, encouragement and support. Her guidance despite her many other academic and professional commitments, has been invaluable for which I am extremely grateful. Her wisdom, knowledge and commitment to the highest standards inspired and motivated me and I consider myself extremely fortunate to have her as my graduate advisor and mentor. I am also grateful to the members of my thesis committee, Professor Hanqing Jiang, Professor Mary L. Lind, Professor Patrick Phelan and Professor Kaushal Rege for their encouragement and for their insightful suggestions about my research.

I would like to acknowledge several collaborators and group members who contributed to a portion of the experimental work in this dissertation. Dr. Mingxiang Luo and Dr. Huan Ma initiated the project of synthesizing composite particles using Pickering emulsions. It has been a great pleasure working with Professor Kaushal Rege and Dr. Huang C. Huang for the experimental work involving the cancer cell research in the dissertation and Dr. Patrick Phelan and Mingmeng Zhang for the metal shell collaboration work. I also thank all past and

present group members of Professor Dai's research group for various supports, including their hard work on several experiments and collection of data. During my research, I had the privilege to access some instruments in Professor Jerry Lin's lab as well as have inspiring discussions with members of his group; especially Dr. Matthew B. Anderson and Teresa M. Rosa. I truly appreciate their generosity and kindness. Also, I am grateful for access to instruments to Dr. Paul Westerhoff, the Center for Solid State Sciences and the Biodesign Institute at the Arizona State University.

Most importantly I would like to extend my sincere gratitude toward my parents, who have always supported, encouraged and believed in me, in all my endeavors and my grandmother for her encouragement and profound love, faith and understanding.

TABLE OF CONTENTS

Page

CHAPTER Page

LIST OF FIGURES

Chapter 1

INTRODUCTION

Nanoparticles have generated great interest in chemistry, physics, biology, and engineering. This is due to the fact that nanoparticles have properties that are significantly different than those of bulk materials (Jain et al., 2006, Liu et al., 2001). The high surface-to-volume ratio of nanoparticles makes them a suitable carrier or delivery system for drugs, proteins or genes which can be either delivered locally or targeted specifically (Ding et al., 2006). The development of fabrication routes for inorganic polymer nanocomposites has considerable interest as, organic-inorganic hybrid morphologies can provide enhanced mechanical and physical properties for a breadth of application areas especially in biological and medical applications such as in artificial bones, dental fillings, and drug delivery (Sanchez et al., 2005). Among them, core-shell composite nanoparticles are a unique class of materials which are attractive for their potential applications as delivery vehicles (for drugs, dyes, cosmetics, ink etc.) (Caruso, 2000; Huang et al., 1999). Core-shell composite particles can be synthesized by methods of post-surface-reaction (Lynch, Nawaz, Bostrom, 2005; Ding et al., 2004) electrostatic deposition (Dokoutchaev et al., 1999), and layer-by-layer self-assembly (Caruso, 2001; Caruso, Susha, Giersig M, Möhwald H, 1999; Caruso, Susha A, Caruso, 2001). Here we employ the concept of Pickering emulsions to synthesize core-shell composite particles. Pickering emulsion polymerization is superior in several aspects: (1) no sophisticated instrumentation is needed; (2) a commercialized nanoparticle powder or solution can be used without further treatment; (3) the

synthesis can be completed in one-step; and (4) the produced particle dispersion is surfactant-free which makes it easier to purify and an excellent material for biological applications. Despite these advantages, efforts made to explore and utilize the Pickering approach have been scarce, although some related synthesis methods have been documented including miniemulsion polymerization (Bon, Colver, 2007; Cauvin, Colver, Bon, 2005), dispersion polymerization (Schmid et al., 2007; Yang et al., 2008), inverse suspension polymerization (Duan et al., 2009; Gao et al., 2009), and inverse emulsion polymerization (Voorn et al., 2006) stabilized by fine solid particles. It is worthwhile to note that the composite nanoparticle structure in this study is opposite to the often reported core-shell structure in which inorganic particles serve as the core and polymer serves as the shell (Caruso 2001; Bourgeat-Lami & Lang, 1998; Gu et al., 2004; Guo et al., 2008; Nagao et al., 2008; Tianbin & Yangchuan, 2006). Here the polymer serves as the core and the inorganic particles serve as the shell. Such materials provide a new class of supramolecular building blocks and can "exhibit unusual, possibly unique, properties which cannot be obtained simply by co-mixing polymer and inorganic particles." (Barthet et al., 1999)

In addition to nanoparticles, environmentally responsive materials have recently been subjects of great interest due to their versatile applications (Nayak & Leon, 2005). Such materials are sometimes termed ''smart'' since their properties allow them to react in a specific way to external stimuli. Hence, such ''smart'' materials can be made responsive to various parameters, such as temperature, (Pelton, 2000; Hoshino et al., 1987) pH, (Jones & Lyon, 2000;

Dupin et al., 2006) light, (Nayak & Lyon, 2004), ionic strength (McPhee et al., 2006), and magnetic fields (Zrinyi, 2000). Applications of these systems range from drug delivery (Das et al., 2006; Nayak et al., 2004; Soppinath et al., 2005), biosensing (Hu et al., 1998), chemical separation (Kawaguchi & Fujimoto, 1999), biomaterials (Sahiner et al., 2006; Bouillot & Vincent, 2000) to catalysis (Bergbreiter et al., 1998; Biffis et al., 2003; Lu et al., 2006; Lu & Mei 2006). Some of these systems are based on polymeric materials such as poly(N-isopropylacrylamide) (PNIPAAm) or related copolymers (Nayak & Leon, 2005; Pelton, 2000). "Smart" polymers typically respond by large changes triggered by small changes in environment. The "smart" polymers studied during the course of this dissertation usually undergo fast and reversible changes in the microstructure from a hydrophilic to a hydrophobic state that are in response to a stimulus in the environment. This phenomenon is reversible, the system returning to its initial state when the trigger is removed. The driving force behind these transitions varies, with common stimuli including neutralization of charged groups by either a pH shift or the addition of an oppositely charged polymer, changes in the efficiency of the hydrogen bonding with an increase in temperature or ionic strength, and collapse of hydrogels and interpenetrating polymer networks. Even the latest among these have been the electric, magnetic, light or radiation induced reversible phase transitions. Such a change in the property of "smart" polymers has shown various applications in biological systems as will be detailed later on in the dissertation. In this study, N-isopropylacrylamide (NIPAAm) is incorporated as a co-monomer in order to impart temperature sensitivity to the

core-shell nanoparticles. In aqueous media, PNIPAAm exhibits a lower critical solution temperature (LCST) at about 32°C, which is close to the physiological temperature (Heskins & Guillet, 1968; Schild, 1992; Wu & Wang, 1998; Hellweg et al., 2004; Cho et al., 1997; Jones & Lyon, 2003; Dingenouts et al., 2001). Below the LCST, the polymer chains are soluble in water due to the formation of hydrogen bonds between the water molecules and the amide side chains. When the temperature increases, the polymer undergoes a volume phase transition. Water is expelled from the interior, thus causing a drastic decrease in volume above the LCST of the polymer.

The main theme of this dissertation is to apply the concept of nanoparticle self-assembly in Pickering emulsions to synthesize organic-inorganic core-shell structured composite particles and understand the polymerization mechanisms. Furthermore, facile approaches have been developed to validate the environmental responsiveness of the core-shell composite particles and to engineer their physical properties. Several applications of these composite particles are explored, for example, the polystyrene/PNIPAAm-silica nanoparticles have demonstrated efficiency in targeted drug delivery and cancer therapy.

This dissertation is structured as follows. Chapter 2 offers the background of Pickering emulsions which are the basis of this dissertation. In Chapter 3, synthesis and characterization of core-shell composite particles via Pickering emulsion polymerizations and exploration of polymerization mechanisms are addressed. Chapter 4 focuses on the temperature responsiveness of the composite

nanoparticles and their application as a drug delivery vehicle. Chapter 5 summarizes how to tune the transition temperature of the thermally responsive nanoparticles using methods during synthesis as well as post synthesis. Whereas, Chapter 6 details the development of pH responsive composite nanoparticles and the effort of changing the shell material from silica to gold and the challenges resolved during this process. The dissertation concludes with a summary and suggestions for future work, presented in Chapter 7.

Chapter 2

BACKGROUND OF PICKERING EMULSIONS AND THEIR APPLICATIONS

2.1 Introduction

The concepts of self-assembly at liquid-liquid interfaces and consequently Pickering emulsions can be extended to design environmentally sensitive nanoparticles. The adsorption of solid particles onto the interface between two immiscible liquids is a spontaneous process towards a lower total free energy configuration. Small molecule surfactants near the liquid interfaces tend to have continuous adsorption and desorption behaviors (Binks, 2002), in sharp contrast with most solid particles which attach to liquid interfaces irreversibly. The particle desorption energy quantifies how strongly the particles can be held at the interface. This desorption energy equals the negative value of the particle adsorption energy and can be expressed by the equation for spherical particles (Binks, 2002; Binks & Horozov, 2006; Horozov, Binks, Aveyard, & Clint, 2006)

$$\Delta G_{de} = \pi \mathrm{a}^2 \gamma_{\mathrm{ow}} (1 \pm \cos\theta)^2 \qquad (2.1)$$

where a is the particle radius, γ_{ow} is the oil-water interfacial tension, θ is the three-phase contact angle measured through the water phase, and the sign inside the bracket is positive for desorption into or adsorption from oil and negative for desorption into or adsorption from water. The contact angle (θ) of colloidal particles determines the preferable position of particles at liquid interfaces (Binks,

2002). For a spherical colloidal particle with smooth surface at an oil-water interface, according to Young's equation,

$$\cos\theta = \frac{\gamma_{po} - \gamma_{pw}}{\gamma_{ow}} \qquad (2.2)$$

where γ is the interfacial tension of particle-oil (po), particle-water (pw), or oil-water (ow) interface (Binks & Horozov, 2006).

According to Equation 2.1, the desorption energy depends on the square of the particle radius, as plotted in Figure 2.1a taking θ = 90° and γ_{ow} = 50 mN/m (Binks, 2002). For particles with intermediate hydrophobicity (θ = 90°) in the size range from several nanometers to several microns, the desorption energy is significantly higher than the thermal energy of several kT, so that particles are attached at the interface irreversibly (Binks, 2002). For extremely small particles (radius ≤ 1 nm), the detachment energy becomes comparable to the thermal energy (kT) and the particles might detach from the interface. The wettability of the particles is another important parameter in Equation 2.1, which determines how strongly the particles can be held at the interface. The particle is most strongly held at the interface for θ = 90°, when particles are equally wetted by both oil and water ($\gamma_{po} = \gamma_{pw}$), and the strength falls rapidly on either side of 90° (Denkov, Ivanov, Kralchevsky, & Wasan, 1992). This is illustrated in Figure 2.1b, which shows the dependence of the energy required to remove a 10-nm spherical particle from the oil-water interface with an interfacial tension γ_{ow} = 36 mN/m on the contact angle (Binks & Lumsdon, 2000c).

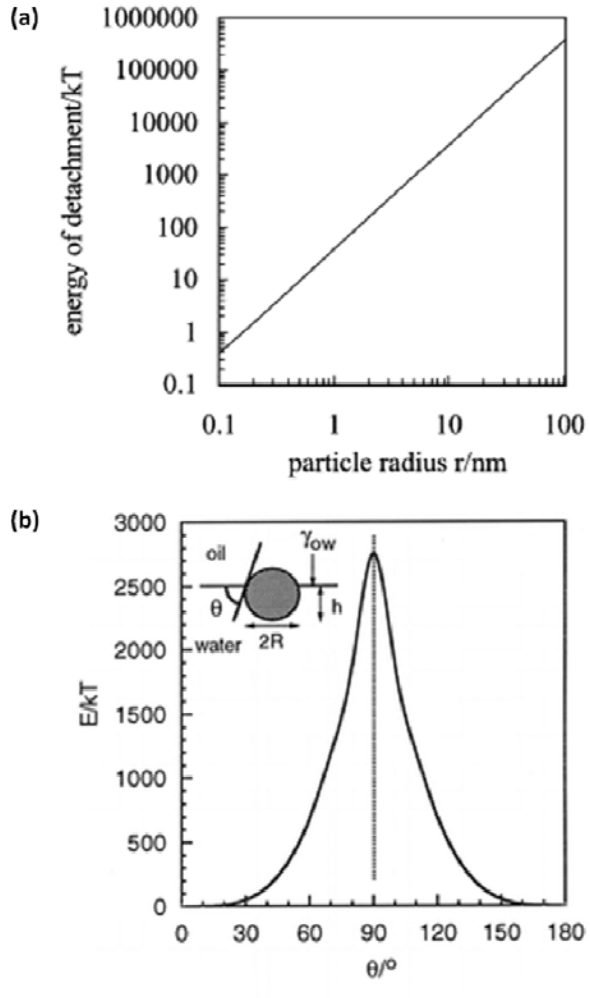

Figure 2.1

Variation of the energy (E) required to remove a spherical particle from a planar oil-water interface at 298 K with (a) the particle radius r and (b) the water contact angle θ. Adapted from (Binks, 2002) and (Binks & Lumsdon, 2000c) respectively.

Solid particles self-assembled at liquid interfaces could function as surfactants to stabilize an emulsion. An emulsion is commonly defined as a mixture of one liquid phase dispersed in another immiscible liquid. Typically, emulsions are stabilized by emulsifying agents, such as amphiphilic small

molecule surfactants or polymers. Solid particles were identified as another type of emulsifying agent since the pioneering studies by Ramsden in 1903 (Ramsden, 1903) and Pickering in 1907 (Pickering, 1907). Such emulsions stabilized by solid particles are often referred to as Pickering emulsions, solid-stabilized emulsions, or particle-laden emulsions. Interfacial energy calculations show that the surface roughness may influence particle adsorption at the interface. Quantitatively, the surface area of a rough particle can be defined as r times larger than that of a spherical particle having a smooth surface (Y. Nonomura, Komura, & Tsujii, 2005; Nonomura, Komura, & Tsujii, 2006). By plotting the normalized interfacial adsorption energy $\Delta G_{ad}/\pi a^2 \gamma_{AB}$ versus normalized immersion depth z/a for particles with various roughness at γ_{AP}/γ_{AB} =0.4 and γ_{BP}/γ_{AB} =0.5 (Figure 2.2), the immersion depth at minimum interfacial energy for particle adsorption is determined to be $z_{\min} = (1 - r\cos\theta)a$. So, the surface roughness makes hydrophilic (or hydrophobic) particles appear even more hydrophilic (or hydrophobic) and consequently the range of particle wettability suitable for interfacial adsorption becomes narrower (Nonomura et al., 2005; Nonomura et al., 2006).

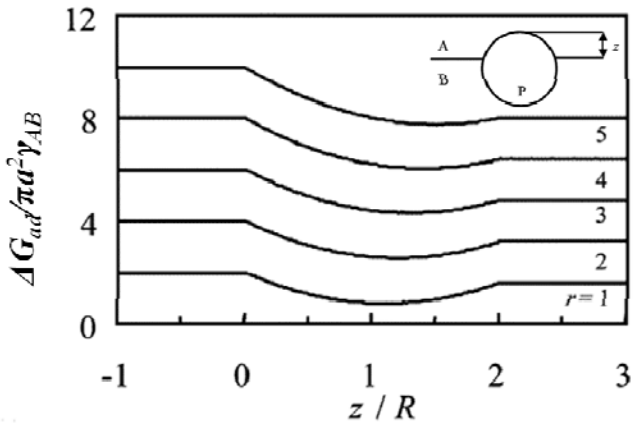

Figure 2.2

The plot of the normalized interfacial adsorption energy versus normalized immersion depth for particles with various roughnesses. The inset scheme illustrates a particle (P) adsorbing at the Liquid A-Liquid B interface at an immersion depth z. Adapted from (Nonomura et al., 2005).

For non-spherical particles, the preferred particle orientation at the interface may be predictable based on interfacial free energy evaluations, as the orientation leading to a maximum interfacial energy reduction is preferred (Boker, He, Emrick, & Russell, 2007). The order of stability for prolate, spherical, and oblate nanoparticles equally wetted by the two immiscible phases at various orientations with respect to the liquid interface is shown in Figure 2.3 (Bresme & Oettel, 2007; Bresme & Faraudo, 2007; Faraudo & Bresme, 2003; Faraudo & Bresme, 2004). For example, the parallel orientation is preferred to the perpendicular orientation for tri-n-octylphosphine oxide (TOPO) covered CdSe nanorods (~8 nm in diameter, 39-40 nm in length) adsorbed at toluene-water interfaces, since the interfacial energy is lowered ~40 times more when the

nanorods are oriented parallel to the interface (He et al., 2007). Similar to elongated nanoparticles, micron-sized ellipsoids also prefer to stay at liquid interfaces in the orientation parallel to the liquid interface (Loudet, Alsayed, Zhang, & Yodh, 2005; Loudet, Yodh, & Pouligny, 2006; Madivala, Fransaer, & Vermant, 2009). The ellipsoid microparticle is equilibrated at a position with less volume in the water phase at the water-decane interface than at the water-air interface (Madivala et al., 2009).

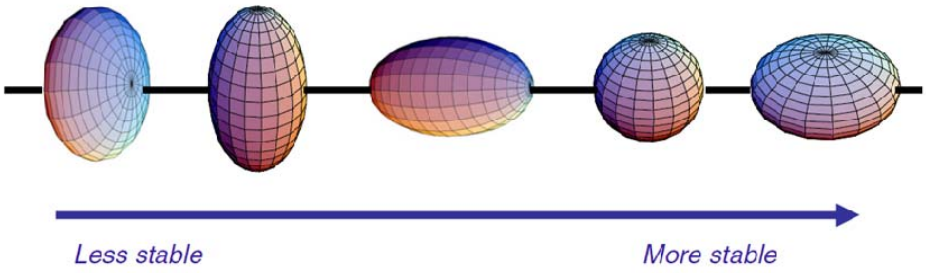

Figure 2.3

Relative stability of non-spherical nanoparticles at fluid interfaces depending on the particle shape and orientation. Adapted from (Bresme & Oettel, 2007).

Most previous studies focus on the emulsifier function of colloidal particles to stabilize a Pickering emulsion (Akartuna et al., 2008; Chen, Colver, & Bon, 2007; Madivala, Vandebril et al., 2009; Melle, Lask, & Fuller, 2005; Stancik, Kouhkan, & Fuller, 2004; Tsuji & Kawaguchi, 2008). In comparison, the self-assembled particle structures and the underlying particle interactions at liquid-liquid interfaces are much less understood, despite the importance in various applications. Pickering emulsions are known for their high stability which is a direct consequence of the large adsorption energy of colloidal particles at an

oil/water interface. This provides a large energy barrier against the particle desorption that usually accompanies droplet coalescence. For microparticles in a small amount of water with continuously reduced thickness due to evaporation, Pieranski (Pieranski, 1980) observed that the particles adsorb onto the air-water interface from the bulk only when the thickness of water phase decreases "very rapidly". When depositing particles at planar liquid interfaces, an alcohol is usually used to aid particle adsorption onto the liquid interfaces, which would create strong convective fluxes and turbulence near the interface (Horozov et al., 2006). In many Pickering emulsions, not all the particles adsorb onto the droplet interfaces and free particles dispersed in the liquid phase are usually observed (Tarimala & Dai, 2004). Particle wettability studies show that this energy is proportional to the square of the particle radius and is of the order of 10^7 kT for micrometer scale particles and interfacial tensions as shown in equation 2.3 (Pieranski, 1980).

$$E = \frac{-\pi \mathrm{R}^2}{\gamma_{\mathrm{ow}}} \left(\gamma_{\mathrm{ow}} - \gamma_{\mathrm{pw}} + \gamma_{\mathrm{po}}\right)^2 \qquad (2.3)$$

This equation assumes the particles are spherical and the contact angle obeys the Young's equation. The adsorption energy for bare particles is a function of the interfacial tensions between oil and water and the particle with both phases (γ_{ow}, γ_{po}, γ_{pw}). This means that larger particles are more strongly attached to the interface than nanoparticles and micrometer scale particles typically act as more efficient emulsifiers than nanoparticles. For droplet coalescence to take place, particles must desorb from the interface due to the decrease in the overall surface area. However, the high adsorption energy of Pickering emulsifiers prevents

particles from desorbing and effectively stabilizes droplets from coalescing together. Typically Pickering emulsions follow the empirical Bancroft rule where, the phase that initially contains the dispersed particles becomes the continuous phase in the emulsion. There may be exceptions to this rule, usually the preferred emulsion type is normally determined by particle wettability. For a contact angle measured through water (<90°), the particle mostly stays in the aqueous phase and an oil-in-water (o/w) emulsion forms. For a more hydrophobic particle, the contact angle being (>90°) a water-in-oil emulsion (w/o) forms. The "preferred" emulsion type is defined as the type of emulsion (o/w or w/o) that forms at a 1:1 oil:water ratio, however some emulsion systems have the potential to catastrophically phase invert by increasing the content of the discontinuous phase. Previous studies by Binks and Lumsdon found that hydrophilic and hydrophobic silica stabilized oil-in-water (o/w) and water-in-oil (w/o) emulsions, respectively and each dispersed 70 volume% of the discontinuous phase in the emulsion. When the discontinuous phase was increased above this volume fraction, the emulsions catastrophically phase inverted (o/w becoming w/o, or vice versa), representing an "anti-Bancroft" emulsion. Charges on the particle result in complex particle-particle interactions that affect adsorption behavior at the droplet interface. Weak particle attractions could cause an enrichment of particles on the droplet interface, enhancing emulsion stability. However, too large of an attraction would result in particle clusters that may destabilize the droplets. Particles also exhibit long range repulsive forces due to the dipole moment they adopt upon adsorption to the oil/water interface. These particle interactions are

expected to influence the packing of particles at the interface and particle adsorption energy, and thus the interfacial response to bending and dilatational forces. Pre-flocculated particles before emulsification can enhance emulsion stability, however this behavior is system dependent. Dense particle clusters can form a protective network around droplets preventing droplet coalescence.

The structure of self-assembled microparticles at the emulsion droplet interface is rich, depending on the particle concentration and chemistry (A rough schematic is shown in Figure 2.4a). Dai and coworkers (Dai et al., 2008; Tarimala & Dai, 2004; Tarimala et al., 2006) reported the rich morphology of polystyrene microparticles when they self-assemble onto poly(dimethylsiloxane) (PDMS, 5 cSt)-in-water emulsion interfaces, as shown in Figure 2.4. For single-species sulfate-treated polystyrene (S-PS) particles of 1.1 μm (bulk concentration of 0.3%), the particles self-assemble at the emulsion interface, but do not fully cover it, although there is excess number of particles in the water phase (Figure 2.4b). The partial coverage does not seem to be dynamically affected by time since there is no noticeable change in the interfacial particle concentration during a three-day sample aging. At the oil–water interface, the particles form small patches with local hexagonal order; these domains are separated by other particle-free domains. The type of aggregation is likely to be the diffusion limited cluster aggregation (DLCA) (Tarimala & Dai, 2004).

Dai and coworkers also reported the self-assembly of particles with different size and hydrophobicity on the same emulsion droplet interface (Tarimala & Dai, 2004). Figure 2.4c shows a mixture of the S-PS particles with

diameters of 1.1 and 4.0 μm that are simultaneously assembled at the Pickering emulsion droplet interface. Similar observations have been made on systems involving mixtures of 0.2 and 1.1 μm S-PS particles, although the images are not shown. Figure 2.4d shows the sequential scanning result of a three-dimensional fluorescent image of a PDMS (5 cSt)-in-water Pickering emulsion droplet containing S-PS (sulfate-treated polystyrene, relatively hydrophobic, in green, excited by the argon laser) and C-PS (carboxylate-treated polystyrene, relatively hydrophilic, in red, excited by the He–Ne laser) particles of 1.1 μm, which is the result of assembly from equal bulk concentration of 0.15% by particles. It is hypothesized that the particles form a semi-double-layer configuration at the oil-water interface, in that the distance from the particle center positions to the liquid interface does not equal for different types of particles. To maintain the three phase contact angle determined by particle surface and liquid phase properties, hydrophilic C-PS particles may prefer the position with more particle volume in the aqueous phase, while hydrophobic S-PS particles may be positioned towards the oil phase.

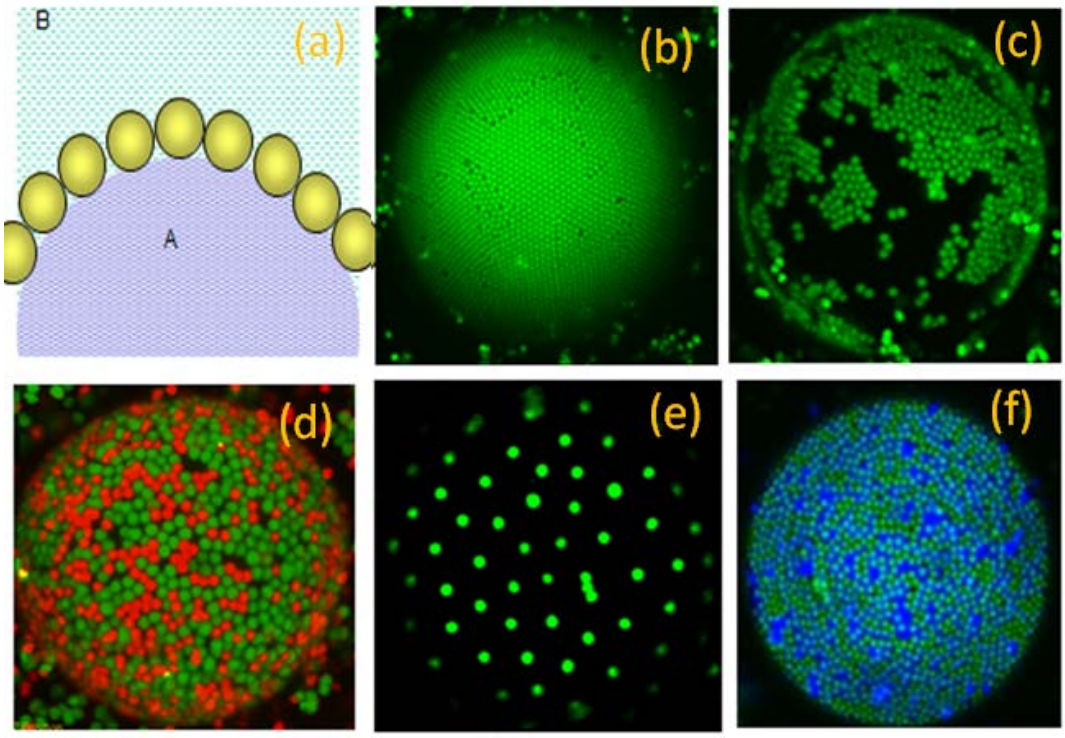

Figure 2.4

Confocal laser scanning microscope images showing the rich morphology of microparticles at PDMS-in-water Pickering emulsion interfaces. The solid particles are S-PS except in (d) which is a mixture of S-PS (in green) and C-PS particles (in red). Adapted from (Dai et al., 2008); (a) is a schematic representation of the other figures.

Pickering emulsions are often encountered in various industrial processes, consumer products, and research and development (R&D) challenges. For example, in the chemical flooding processes in tertiary (enhanced) oil recovery, solid particles in the oil well, such as clays, scales and corrosion products, can self-assemble at the oil–water interfaces (Kokal, 2005). Emulsification is

necessary and beneficial in the extraction process, and demulsification to separate the water and surface active molecules or solids from the oil is required after the extraction (Sullivan & Kilpatrick, 2002; Yan & Masliyah, 1995a; Yan & Masliyah, 1995b; Yan & Masliyah, 1996; Yan, Kurbis, & Masliyah, 1997; Yan, Gray, & Masliyah, 2001). In the cosmetics industry, emulsions stabilized by metal oxide particles, such as titanium oxides, are potential attractive alternatives to replace conventional surfactants, leading to new skincare and sunscreen formulations (Stiller et al., 2004). In many daily food emulsions, the emulsion stabilization is provided by solid particles (Dickinson, 2010; McClements, 2004; Rousseau, 2000), such as egg yolk particles in mayonnaise (Kim et al., 2009; Kiosseoglou, 2003; Santipanichwong & Suphantharika, 2009) and fat crystals in margarine (Garti, Binyamin, & Aserin, 1998). Recently, using Pickering emulsion droplets as delivery vehicles for controlled release of therapeutic substances in pharmaceutical formulations has received increasing attention (Frelichowska et al., 2009; Frelichowska, Bolzinger, Pelletier, Valour, & Chevalier, 2009; Simovic & Prestidge, 2007). For instance, Frelichowska and coworkers demonstrated the topical delivery of lipophilic drugs using oil-in-water (o/w) Pickering emulsion droplets (Frelichowska, Bolzinger, Pelletier et al., 2009) and hydrophilic drugs using water-in-oil (w/o) Pickering emulsion droplets (Frelichowska et al., 2009).

Solid-stabilized emulsions, also have the ability to provide a simple and convenient experimental template to meet various requirements, such as changing property of solid particles, oil phase viscosity and interfacial curvature. The confocal laser scanning microscope (CLSM) is a useful and convenient tool to

investigate the dynamics of particles at emulsions interfaces. Pickering emulsions have been employed as an experimental template and confocal laser scanning microscopy as a tool to study the dynamics of solid particles at liquid-liquid interfaces by Dai and coworkers. More specifically, the diffusion behavior of colloidal particles at oil-water interfaces were studied using Pickering emulsions as templates. The solid particles are sulfate modified polystyrene microparticles with diameters of 1.1 μm and the oil phase as polydimethylsiloxane oil (PDMS) or octamethyltrisiloxane with different viscosities (Wu and Dai, 2006).

The two most interesting characteristics for Pickering emulsions are the excellent long-term stability and the unique structure. First, emulsion stability is particularly enhanced by the particle-laden interfaces compared to using surfactant molecules as the stabilizer. The densely-packed particles at the interface could serve as a mechanical barrier to droplet coalescence (Ashby & Binks, 2000), and Ostwald ripening can be slowed down or arrested because of the high desorption energy of the particles and capillary effects (Ashby & Binks, 2000; Tcholakova, Denkov, & Lips, 2008).

The unique structure of Pickering emulsions open a new avenue to engineer advanced materials, such as core-shell structured composite particles (Fortuna et al., 2009; Li et al., 2008), colloidosomes (Cayre et al., 2004), and microcapsules (Bon & Chen, 2007). For example, Weitz and coworkers (Dinsmore et al., 2002; Hsu et al., 2005) prepared hollow particles with permeable shells based on the self-assembly of colloidal particles at emulsion droplet interfaces, as shown in Figure 2.5. The shell is a monolayer of colloidal particles

with tunable properties, such as the permeability, elastic moduli, and breaking forces. The hollow particles have potential applications in encapsulation and controlled release of active ingredients such as drugs, vitamins, and fragrances. Wu and coworkers (Wu et al., 2009) synthesized magnetic hollow particles with a permeable shell of silica and Fe_3O_4 particles with the potential application as a magnetic adsorbent for wastewater treatments. The synthesis is via interfacial sol-gel reactions of silica at Fe_3O_4 particle-laden interfaces in Pickering emulsions. Pickering emulsions also offer a new approach to synthesize core-shell structured composite particles as detailed in Chapter 3.

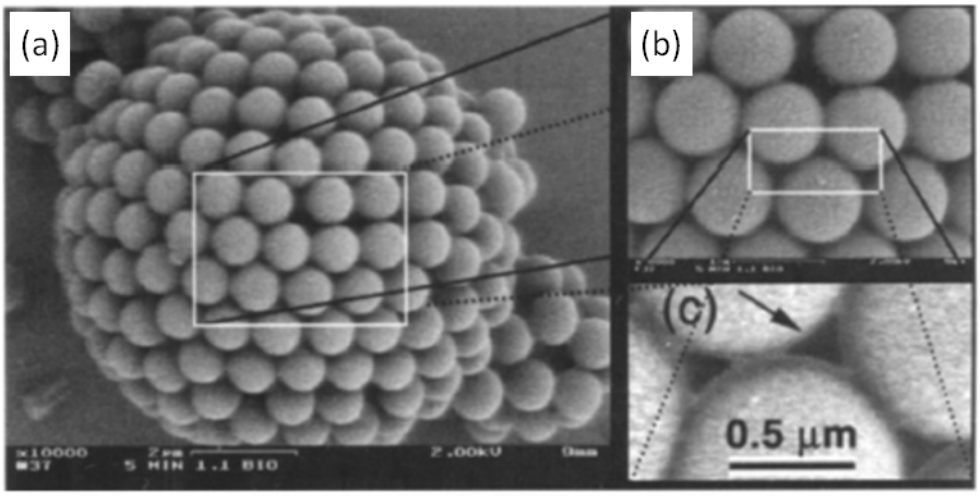

Figure 2.5

(a) Scanning electron microscope image of a dried, 10-µm-diameter colloidosome composed of 0.9-µm-diameter polystyrene spheres. (b and c) Close-ups of (a) and (b), respectively. The arrow points to one of the 0.15-µm holes that define the permeability. Adapted from (Dinsmore et al., 2002).

Another recent and exciting development in the field of Pickering emulsions has been the study of particle self-assembly in ionic liquid-water emulsions (Ma & Dai, 2010). Ionic liquids are a unique collection of liquid materials composed solely of ions. Under ambient conditions, room temperature ionic liquids (RTILs) stay as liquids, whereas conventional salts are in the crystalline state. This is because, in RTILs, the Coulombic attractions of ion pairs are damped due to the large ion size and the lattice-packing is frustrated due to the sterical mismatch of irregular shaped ions (Hayes, Warr, & Atkin, 2010). Ionic liquids may be either composed of an organic cation and an inorganic anion or completely inorganic (Ohno, 2005). The organic cations can be either aprotic or protic (Angell, Byrne, & Belieres, 2007; Freemantle, 2010; Ohno, 2005). The protic cations are formed by the transfer of a proton from a Brønsted acid to a Brønsted base, which lead to the assembly of H-bonded networks mimicking water (Fumino, Wulf, & Ludwig, 2009; Greaves, Weerawardena, Fong, Krodkiewska, & Drummond, 2006; Greaves & Drummond, 2008b; Hayes et al., 2010; Ohno, 2005). Ionic liquids, especially RTILs, have many unique properties, such as the negligible volatility, non-flammability, high thermal and chemical stability, high ionic conductivity, and large electrochemical window (Zhang, Sun, He, Lu, & Zhang, 2006). In addition, the chemical and physical properties of ionic liquids can be custom tailored via the choice of cations and anions. They have been given attractive nicknames such as “green solvents” and “designer solvents” (Freemantle, 2010), ionic liquids have broad applications. For example, ionic liquids have been used as solvents in polymerizations (Kubisa, 2009; Lu, Yan, &

Texter, 2009), inorganic syntheses (Alammar & Mudring, 2009; Khare et al., 2010), enzymatic reactions (Yang & Pan, 2005), and extractions (Chapeaux et al., 2008; Huddleston, Willauer, Swatloski, Visser, & Rogers, 1998; Poole & Poole, 2010; Visser et al., 2001). They have also been employed as advanced materials including ionic lubricants (Bermudez, Jimenez, Sanes, & Carrion, 2009; Zhou, Liang, & Liu, 2009) and ionic gels (Lu et al., 2009; Torimoto, Tsuda, Okazaki, & Kuwabata, 2010; Ueki & Watanabe, 2008).

Ionic liquids can be selected or designed to be immiscible and form liquid interfaces with an organic solvent or water (Freemantle, 2010). Common ionic liquids which have been used in biphasic liquid systems include aprotic imidazolium-based ionic liquids with hexafluorophosphate ($[PF_6]$), tetrafluoroborate ($[BF_4]$), bis(trifluoromethylsulfonyl)imide ($[NTf_2]$), and chloride anions, as well as protic ionic liquid ethylammonium nitrate (EAN) (Binks, Dyab, & Fletcher, 2003; Greaves & Drummond, 2008a; Qiu & Texter, 2008). The miscibility with water or organic solvents is primarily determined by the anions, although the cations may also affect the hydrophobicity and hydrogen bonding ability (Huddleston et al., 1998; Welton, 1999). For example, 1-butyl-3-methylimidazolium tetrafluoroborate ($[BMIM][BF_4]$) and 1-ethyl-3-methylimidazolium chloride ([EMIM]Cl) are miscible with water and immiscible with the oils hexadecane, toluene, and Miglyol 810N (a medium chain length triglyceride with 8-10 carbons in each chain supplied by S. Black, UK) (Binks et al., 2003); $[BMIM][NTf_2]$ and $[EMIM][NTf_2]$ are immiscible with both water and the above three oils (Binks et al., 2003); and 1-butyl-3-methylimidazolium

hexafluorophosphate ([BMIM][PF_6]) is immiscible with water (Wong, Chen, Chang, & Chou, 2002).

In recent years, ionic liquid based microemulsions have received significant attention (Greaves & Drummond, 2008a; Qiu & Texter, 2008). Such microemulsions contain two liquid phases, at least one of which is ionic liquids, and are stabilized by small molecule surfactants. Nonionic surfactants Triton X-100 (TX-100) (Behera, Malek, & Pandey, 2009; Cheng et al., 2007; Gao et al., 2004; Gao, Zhang et al., 2006; Gao et al., 2005; Gao et al., 2007), Tween 20 (Gao et al., 2006), and Tween 80 (Zheng & Eli, 2009) have been demonstrated to effectively stabilize microemulsions of ionic liquids, such as [BMIM][PF_6] and [BMIM][BF_4], and water or other organic solvents (Greaves & Drummond, 2008a). In comparison to the microemulsions, which are often considered thermodynamically stable, very few studies on thermodynamically unstable but kinetically stable ionic liquid based emulsions have been reported, especially for those stabilized by solid particles. In the pioneering work by Binks and coworkers (Binks et al., 2003; Binks, Dyab, & Fletcher, 2007), a series of stable ionic liquid emulsions stabilized solely by fumed silica nanoparticles were successfully prepared and the emulsion stability and phase inversions were investigated (Binks et al., 2003; Binks, Dyab, & Fletcher, 2007). However, it is still unclear what the particle self-assembled structure at ionic liquid-water interfaces are and how the particles partition in the dispersed and continuous phases. These two questions are important in various fundamental researches and applications, such as in the active debate on the complicated interactions between interfacial particles

(McGorty et al., 2010; Oettel & Dietrich, 2008) and in the synthesis of novel materials using Pickering emulsion droplets as templates (Bon & Chen, 2007; Cayre et al., 2004; Fortuna et al., 2009; Li et al., 2008).

Comparisons are drawn between ionic liquid-in-water Pickering emulsions and oil-in-water Pickering emulsions containing the same particles. First, aggregates of fully covered droplets were frequently observed in ionic liquid-in-water emulsions containing S-PS/A-PS binary particles, whereas in PDMS oil-in-water emulsions containing the same particles, there were hardly any fully covered Pickering emulsion droplets. The absence of fully covered emulsion droplets were also noticed in other PDMS-water emulsion systems including S-PS, C-PS, and AS-PS particles, as reported in previous publications (Dai et al., 2008; Tarimala & Dai, 2004; Tarimala et al., 2006). The contrast seems to suggest that the S-PS/A-PS particles have a stronger affinity to the ionic liquid-water interfaces than the PDMS-water interfaces, although free particles not attached to interfaces are still present. The distinction between the ionic nature of the ionic liquid and the molecular nature of PDMS should be at least one of the important factors, if not the primary factor, in determining the affinity of particles to liquid interfaces.

Second, particles form aggregates instead of colloidal lattices at ionic liquid-water droplet interfaces despite the surface packing densities being high (Figure 2.6) or low (Figure 2.7). Long-range ordered non-close packed colloidal lattices observed in oil-in-water Pickering emulsions, due to the enhanced electrostatic repulsion through the oil phase (Aveyard, Clint, Nees, & Paunov,

2000; Aveyard et al., 2002; Leunissen, Zwanikken et al., 2007), were not observed at ionic liquid-water emulsion interfaces. Obviously, the enhanced electrostatic interactions through the oil phase due to the residual charge at particle-oil interface are no longer valid for particles at ionic liquid-water interfaces. The ionic strength of [BMIM][PF_6] is calculated to be 4.86 M. When the PDMS is substituted by [BMIM][PF_6], the electrostatic repulsion through the ionic liquid phase between charged colloidal particles is screened beyond the Debye length, which is normally in the range of several nanometers (Min et al., 2009), and thus eliminates long-range lattice structure formation at the [BMIM][PF_6]-water interfaces. This is consistent with the melting of the colloidal lattice with large lattice spacing at oil-water interfaces with increasing electrolyte concentration in the oil phase reported previously (Leunissen, Zwanikken et al., 2007), which also supports the importance and necessity of Coulomb repulsion through the oil phase in the lattice structure formation. The formation of particle aggregates at partially covered droplets might be driven by attractive interparticle forces although the origin of the attraction is still debatable. An early study on particle monolayers at air-water interfaces attributes the driving force for particle aggregation to the van der Waals force (Robinson & Earnshaw, 1992).

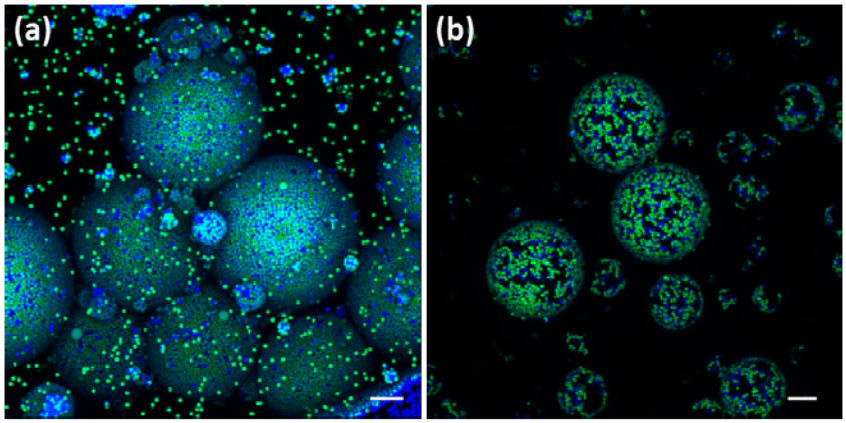

Figure 2.6

Confocal microscope images (overlays of depth-series images) of [BMIM][PF_6]-in-water emulsion droplets with 0.004 g (a) S-PS/A-PS and (b) S-PS/AS-PS binary particles. The scale bars represent 10 µm.

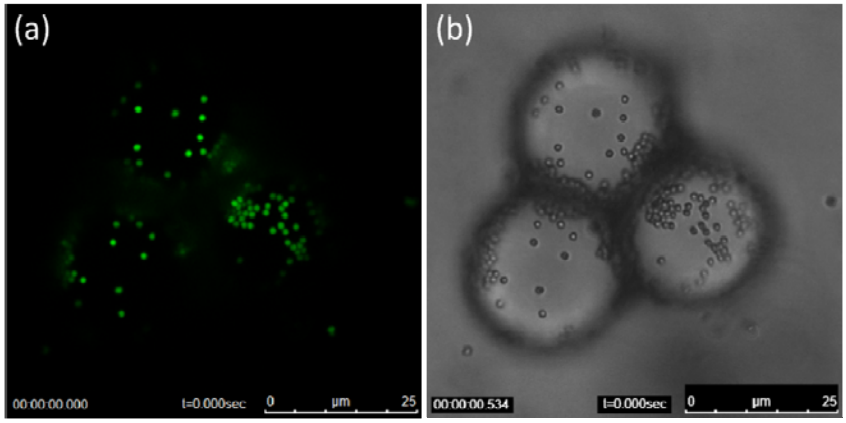

Figure 2.7

A representative confocal microscope image (a) and the corresponding transmitted light image (b) of a [BMIM][PF_6] droplet in water with a low coverage of A-PS particles.

2.2 Important Factors in Pickering Emulsion Formation and Stability

A brief introduction about the relevant factors involved in forming and stabilizing a Pickering emulsion is presented, keeping in mind these challenges were studied before embarking on the synthesis route.

2.2.1 Particle Type

Pickering emulsions may be stabilized by solid particles of various chemical compositions. The most commonly studied particle stabilizers include silica particles, clay minerals, and polystyrene latex particles. Silica particles with various degrees of silanization, including amorphous fumed silica powders and silica colloidal particle dispersions, have been used to investigate various aspects of oil-water emulsification such as phase inversion (Binks & Lumsdon, 2000a; Binks & Rodrigues, 2003), oil phase polarity (Binks & Lumsdon, 2000b; Binks & Clint, 2002), aqueous phase composition (Binks & Lumsdon, 2000b), and temperature-dependent stability (Binks & Whitby, 2003). The clay particles form "card-house structures" due to their plate shape and unique distribution of surface charging sites, which add complexities to the stability and phase transition properties of Pickering emulsions (Ashby & Binks, 2000; Li et al., 2009; Nonomura & Kobayashi, 2009). Polystyrene latex particles can be surface modified by various functional groups, such as sulfate (Binks & Lumsdon, 2001; Golemanov, Tcholakova, Kralchevsky, Ananthapadmanabhan & Lips, 2006; Tarimala & Dai, 2004), aldehyde-sulfate (Binks & Lumsdon, 2001), or carboxylate groups (Tarimala & Dai, 2004), to tune the surface wettability. Using polystyrene particles with different surface functional groups labeled with

different fluorescent dyes, Dai and coworkers studied the simultaneous self-assembly of particles with different wettability to emulsion droplet interfaces, investigated the dynamics of particles, and developed microrheology at liquid-liquid interfaces (Dai et al., 2008; Tarimala & Dai, 2004; Tarimala et al., 2006; Wu, Song & Dai, 2009; Wu & Dai, 2006; Wu & Dai, 2007).

2.2.2 Particle Concentration

Increasing particle concentration has been shown to enhance the stability of a Pickering emulsion by reducing the droplet size or increasing the continuous phase viscosity (Binks & Whitby, 2004; Yang et al., 2006; Yang, Niu, Lan & Sun, 2007). The inverse of droplet size increases linearly with the particle mass, as reported by Gautier and coworkers, for 145 nm silica particle-hexadecane-water systems (Gautier et al., 2007), which is roughly consistent with Binks and Whitby's study on 25 nm silica particle-poly(dimethylsiloxane)-water systems at low particle concentrations (Binks & Whitby, 2004). At higher silica particle concentrations, the droplet size remains constant and the continuous phase viscosity increases with particle concentration, which enhances the emulsion stability (Binks & Whitby, 2004). Significant continuous phase viscosity increase, up to gelation, has been reported and attributed to the formation of three-dimensional particle networks in the particle-concentrated continuous phase (Abend, Bonnke, Gutschner & Lagaly, 1998; Binks & Lumsdon, 2000a; Neuhausler, Abend, Jacobsen & Lagaly, 1999; Yang et al., 2006; Yang et al., 2007). Although the high continuous phase viscosity is beneficial to the emulsion stability, it may cause problems in the production and applications of the

emulsion, and thus a proper particle concentration needs to be selected with caution.

Increasing particle concentration may also induce phase inversions in some special cases. One example is the phase inversion from o/w to w/o with increasing particle concentration in silicone oil-water emulsions stabilized by silica particles with intermediate wettability initially dispersed in the oil phase (Binks, Philip & Rodrigues, 2005). This might be explained by a wettability change at increasing particle concentration in the oil phase. Since the particles form aggregates in the oil phase, the increase in particle concentration promoted more hydrogen bond formation between silanol groups at particle surfaces, which leads to the decrease of effective surface silanol group content and the corresponding increase of hydrophobicity (Binks et al., 2005).

Although the effect of particle concentration to the emulsion stability and phase transition has been studied, the determination of a proper particle concentration to stabilize an emulsion remains a challenge. Theoretically, the amount of particles needed to stabilize an emulsion can be easily calculated if the total volume of the dispersed phase and the droplet diameter are known, assuming the droplets are fully covered and all the particles are attached at the interface. However, the real problems are much more complicated, since the above assumptions are not always true. First, emulsion droplets can be stabilized by either fully covered or partially covered particle layer at the interface. Binks and Whitby (Binks & Whitby, 2004) proposed that droplet stability requires a close-packed layer of particles, supported by scanning electron microscope images

showing continuous, densely packed layers of silica particles at the poly(dimethylsiloxane)-water interface.

The emulsion stability is likely explained by the static steric hindrance mechanism. However, Vignati and coworkers (Vignati, Piazza & Lockhart, 2003) discovered that emulsions can be stabilized with only approximately 5% particle coverage at the interface. A closer observation on the self-assembled particle structure at the contact region of two droplets reveals a monolayer structure, which suggests a single layer of particles is bridging two droplet interfaces to prevent film drainage. Second, free particles dispersed in the continuous phase are frequently observed in Pickering emulsions (Tarimala & Dai, 2004). The degree of interfacial particle attachment, defined by the weight percentage of interfacial particles in all the particles, is related to the particle wettability (Horozov & Binks, 2006), which is difficult to accurately determine especially for colloidal particles. The partial droplet coverage and the fractional interfacial adsorption should be taken into account when estimating the proper particle concentration in a Pickering emulsion system.

2.2.3 Particle Wettability

The intrinsic particle wettability is largely determined by the surface functional groups. In most cases, hydrophilic particles tend to stabilize o/w type Pickering emulsions and hydrophobic particles tend to stabilize w/o type Pickering emulsions (Midmore, 1998; Tambe & Sharma, 1994), as the positions of particles at the interface being more protruded into the water or oil phase. For example, in silicone oil-water systems, the emulsion type is w/o when stabilized

by highly hydrophobic silica particles, but o/w when stabilized by less hydrophobic silica particles (Binks et al., 2005). However, the opposite scenario is observed in triglyceride oil-water systems (Binks & Rodrigues, 2003). When a mixture of hydrophobic and hydrophilic particles is used as the stabilizer, transitional phase inversion in either direction is demonstrated by changing the ratio of hydrophobic and hydrophilic particles (Binks & Lumsdon, 2000d). The transitional phase inversion is induced by changing the effective wettability of particle stabilizers, analogous to changing the system hydrophile-lipophile balance (HLB) in conventional emulsions while keeping the volume ratio of the two liquid phases constant (Binks & Lumsdon, 2000d). This is consistent with Dai and coworkers' microscopic observation that both hydrophobic particles and hydrophilic particles can simultaneously self-assemble onto the same droplet interface (Tarimala & Dai, 2004).

The effective particle wettability can be influenced by the initial location of the particle due to contact angle hysteresis. In emulsions stabilized by silica particles with intermediate wettability, catastrophic inversion induced by increasing the fraction of the dispersed phase is dependent on the phase in which the particles are initially dispersed (Binks & Lumsdon, 2000b; Binks & Rodrigues, 2003). During the transition from w/o to o/w or w/o/w with increasing water phase fraction, the water phase fraction at inversion was found to be below 0.5 for particles starting in water and above 0.5 for particles starting in oil. At water phase fraction of 0.5, particles with intermediate hydrophobicity prefer to stabilize emulsions with the continuous phase being the phase in which the

particles were initially dispersed, possibly due to the contact angle hysteresis (Binks & Lumsdon, 2000b; Binks & Rodrigues, 2003). For particles entering the interface from the oil phase, an advancing water contact angle is preferred, while for particles entering from the water phase, a receding water contact angle is preferred. The advancing contact angle is normally greater than the receding contact angle, which renders the particles to be more hydrophobic and prefer w/o emulsions when starting from the oil phase (Binks & Rodrigues, 2003). The effective particle wettability may also be tuned by the surrounding liquid phases, such as the adsorption of surfactants or polar species onto the particle surface or the effect of aqueous phase pH on the surface group dissociation. These factors will be discussed in the following sections.

2.2.4 Presence of Surfactants

The stability of Pickering emulsions may be influenced by the addition of surfactants. Through systematic investigations using hydrophilic silica particles with nonionic surfactants (Binks, Desforges & Duff, 2007), negatively charged silica particles with cationic surfactants (Binks, Rodrigues & Frith, 2007), and positively charged silica particles with anionic surfactants (Binks & Rodrigues, 2007), Binks and coworkers identified the competition of surfactant adsorption on the particle surface or the liquid-liquid interface and found that the particle flocculation caused by surfactant adsorption at silica colloidal particle surfaces enhances emulsion stability. Different from Binks' approach of mixing the surfactant with particles before emulsification, Whitby and coworkers (Whitby,

Fornasiero & Ralston, 2009) diluted the prepared particle-stabilized emulsion in a surfactant and salt solution.

At surfactant concentrations below the critical micelle concentration, adsorption of surfactants onto the fumed partially hydrophobised silica is not significant and the emulsion stability is not affected by the presence of surfactants. Above the critical micelle concentration, the surfactant destabilizes the emulsion by causing rapid creaming and flocculation of drops. The presence of surfactants may also affect the phase inversion behavior of emulsions. Binks and Rodrigues (Binks & Rodrigues, 2009) reported the double inversion of silica particle stabilized emulsions induced by double-chain cationic surfactants. The first inversion is due to the adsorption of double-chain cationic surfactants on particle surface in a monolayer which increases hydrophobicity and reduces the negative surface charge.

Further adsorption of the surfactants on particle surfaces makes the particles more hydrophilic and positively charged by forming a surfactant bilayer. The combined effect of surfactant adsorption on both particle surfaces and droplet interfaces triggers the second inversion. On the contrary, Nonomura and Kobayashi (Nonomura & Kobayashi, 2009) reported the hindering effect of an oil soluble silicone surfactant (polyoxyethylene-methylpolysiloxane copolymer, KF-6015) to the phase inversion of water/silicone oil emulsion stabilized by plate-shaped clay particles from w/o state to o/w state with the increase of water phase fraction. In the presence of surfactants, the affinity of the particles to the oil phase is tuned too high for phase inversion.

2.2.5 Liquid Phase Polarity

The polarities of the two immiscible phases are important in determining the preferred position of particles at the interface and the emulsion type. For emulsions composed of water and oils of various polarities, the particle contact angle measured from the aqueous phase increases as the liquid-liquid interfacial tension decreases (Binks & Lumsdon, 2000b; Binks & Clint, 2002). At polar oil (ester and alcohols)-water interfaces, particles of intermediate wettability appear relatively hydrophobic and prefer to stabilize w/o emulsions. In comparison, at non-polar oil (alkanes)-water interfaces, particles of intermediate wettability appear relatively hydrophilic and prefer to stabilize o/w emulsions (Binks & Lumsdon, 2000b).

As illustrated in Figure 2.8, the volume fraction of water at emulsion phase inversion (ϕ_w) depends on the work of adhesion of the two liquid phases ($W_a = \gamma_{po} + \gamma_{pw} - \gamma_{ow}$), which increases as the polarity of the oil increases. The oil phase of the emulsions shown in Figure 2.8 (with W_a values in the brackets, in the unit of mJ/m^2) are eugenol (99.3), undecan-1-ol (90.9), cineole (83.2), methyl myristate (76.2), isopropyl myristate (71.1), toluene (65.0), 50 cSt poly(dimethylsiloxane) (54.9), 0.65 cSt poly(dimethylsiloxane) (49.2), cyclohexane (45.1), dodecane (44.4), heptanes (41.0), and perfluoroheptane (28.0). Except for the perfluoroheptane system (W_a = 28.0 mJ/m^2), the phase inversion occurs at higher volume fraction of water with increasing W_a (or oil polarity), until above W_a = 72 mJ/m^2, when the oil has very high polarity, emulsion remains w/o at all ϕ_w. Furthermore, the addition of polar oils to the non-

polar oil phase of a silica particle stabilized emulsion, up to a critical polar/non-polar oil ratio, makes the hydrophilic silica particles appear more hydrophobic and improves the emulsion stability through adsorption of the polar species on silica surfaces via hydrogen bonding (Binks & Whitby, 2005).

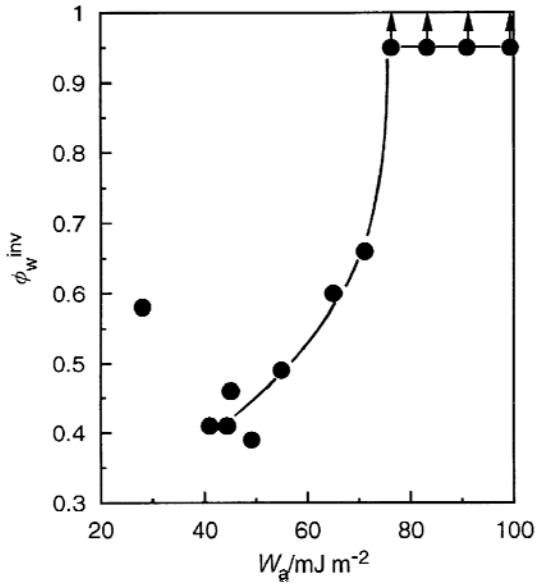

Figure 2.8

Volume fraction of water at inversion of emulsions vs. work of adhesion between oil and water for oil-water emulsion systems stabilized by partially hydrophobic SLM 081 silica particles. Arrows indicate that emulsions remain w/o up to at least $\phi_w = 0.95$. Adapted from (Binks & Lumsdon, 2000b).

2.2.6 Aqueous Phase pH

The aqueous phase pH tunes the particle wettability and surface charge which influences the emulsion stability. For emulsions stabilized by silica or clay particles, with the increase of aqueous phase pH, emulsions initially being w/o experience a transitional phase inversion to o/w emulsions (Binks & Lumsdon, 2000b) and emulsions originally being o/w are destabilized (Yan & Masliyah,

1996; Yan et al., 1997; Yan & Masliyah, 1996). A possible explanation is that, in the high pH environment, uncharged silanol groups at particle surface dissociate to negatively charged SiO^- groups and thus make the particles more hydrophilic (Binks & Lumsdon, 2000b). In the case of transitional phase inversion, adjusting aqueous phase pH provides an alternative way to change the system hydrophile-lipophile balance (HLB) other than adding surfactants (Binks & Lumsdon, 2000b). In the case of destabilization, important applications can be found in oil recovery aiming to demulsify the crude oil in water emulsions after extraction and obtain a higher percentage of recovery (Yan et al., 1997). It is worthwhile to note that, for acidic pH, although the particles have less negative surface charges, silica particles have been shown not to coagulate, even at a NaCl concentration of 5 M below pH of 5, which excludes the contribution of coagulation to the higher emulsion stability (Binks & Lumsdon, 1999; Simovic & Prestidge, 2003). This non-DLVO colloid stability behavior is attributed to particle hydration; the coagulation is prevented by a water layer formed at the particle surface through forming hydrogen bonding with silanol groups (Allen & Matijevi, 1969; Abend et al., 1998; Allen & Matijevi, 1970; Simovic & Prestidge, 2003). Different from silica or clay particles, plate-like layered double hydroxides (LDHs) particles are positively charged and the surface charge density decrease with increasing pH (Yang et al., 2007). Losing part of the surface charge, LDHs particles have a stronger tendency to aggregate and adsorb at liquid interfaces to stabilize the emulsion, except that, at very high pH (pH = 12.47), particles aggregate into large flocculates and become sediments instead of adsorbing at the oil-water interface.

For emulsions stabilized by LDHs particles, the stability of o/w emulsions to coalescence and creaming improves with increasing pH up to pH = 11.98 (Yang et al., 2007).

2.2.7 Ionic Strength

The main effect of electrolytes in the aqueous phase is to screen the particle charge, which would lead to particle coagulation. Weak flocculation facilitates particle adsorption at liquid interfaces and improves emulsion stability, but demulsification might occur when the flocculation extent is too high (Aveyard et al., 2003). This is illustrated by Binks and coworkers in a fumed silica stabilized emulsion with salt $LaCl_3$ (Binks & Lumsdon, 1999), as shown in Figure 3.2. At low pH, emulsions are unstable as the particles are stabilized from coagulation. At high pH, with increasing salt concentration, the emulsion becomes more stable as particles start to coagulate, but demulsifies due to extensive coagulation at even higher salt concentration. Furthermore, Yang and coworkers reported the effect of NaCl salt in promoting particle adsorption at interfaces in a liquid paraffin-in-water emulsion stabilized by plate-like layered double hydroxides (LDHs) particles (Yang et al., 2006). The enhanced particle adsorption is supported by the experimental observation that, in the particle concentration range of 2 to 4 wt% in water, the aqueous phase separated from the emulsion phase changes from aqueous dispersion of particles to clear aqueous phase as the salt concentration is increased to 0.1 M.

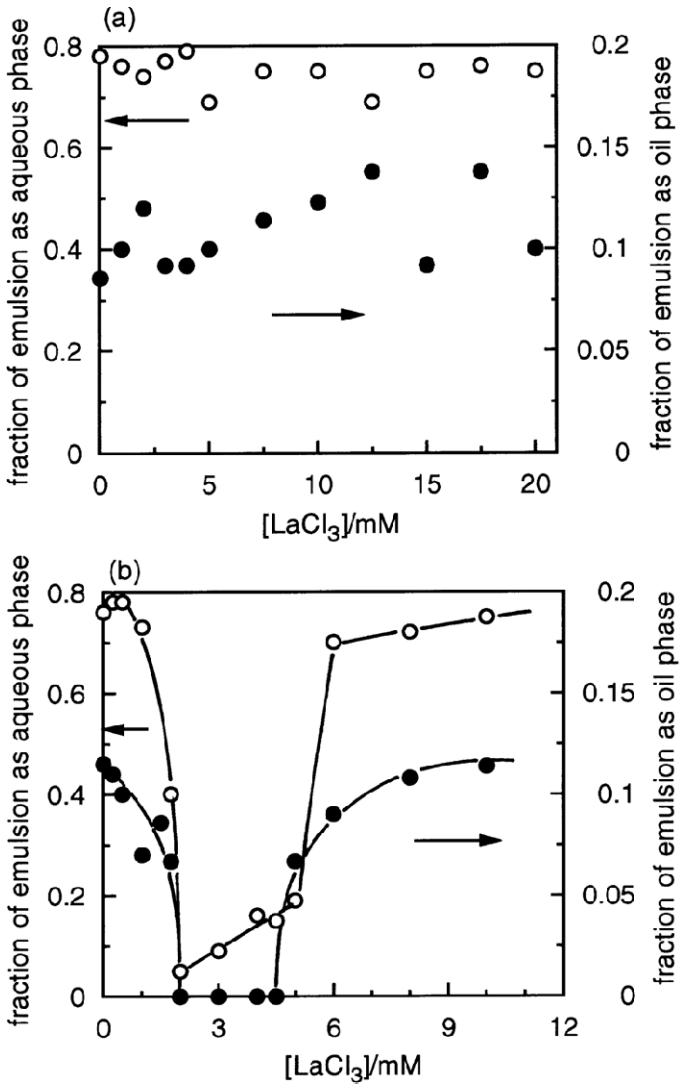

Figure 2.9

Stability to creaming (open points, left hand ordinate) and coalescence (filled points, right hand ordinate) after 30 min of 20 vol% toluene-in-water emulsions stabilised by 0.5 wt.% Aerosil 200 as a function of $LaCl_3$ concentration. (a) pH 2, (b) pH 10. Adapted from (B. P. Binks & Lumsdon, 1999).

2.2.8 Liquid Phase Viscosity

Liquid phase viscosities may affect emulsion formation during the process of particle attaching to the interface. Fournier and workers (Fournier, Fradette & Tanguy, 2009) studied the effect of dispersed phase viscosity on Pickering emulsions using a series of silicone oils of varying viscosities dispersed in distilled water stabilized by fine iron powders. Experimental results show that the emulsified oil volume fraction decreases with the increasing of oil phase viscosity, which might be explained by the increased resistance to particle penetration across the interface during the particle attachment at the interface. The resistance increases with the oil viscosity and becomes a barrier at an o/w viscosity limiting ratio of ~1250-1400, above which emulsions could not be generated with the specific oil-water mixing ratio and procedure in their experiments. This limit is proposed to be "governed by equilibrium between the anchoring time needed for the particle to attach itself at the interface and the shear forces in the fluid that can remove the particle from the interface." (Fournier et al., 2009) However, higher continuous phase viscosity improves the emulsion stability, as discussed earlier, when excess particles increase the continuous phase viscosity at increasing particle concentration.

2.2.9 Particle Shape and Surface Roughness

Although spherical particles with relatively smooth surface have been employed in most of the studies for simplicity, non-spherical particles and rough particles are present in many industrial processes. The emulsifying power of non-spherical particles has been shown to be stronger than spherical particles.

Madivala and coworkers (Madivala, Vandebril, Fransaer & Vermant, 2009) reported that non-spherical particles with an aspect ratio (AR) above the critical value 4.4 for 1 wt% hematite particles in decane-water systems can function as emulsifiers (Figure 2.10d-f), while spherical or lower aspect ratio particles with the same surface wettability fail to stabilize an emulsion (Figure 3.3a-c). Moreover, the amount of emulsified phase increases with the particle aspect ratio, similar to the effect of increasing the concentration of particles at the same aspect ratio. Particles with rough surfaces have been shown to provide less emulsion stability than smooth particles, probably because the surface roughness modifies the surface wettability and reduces the fraction of particle adsorption at the interface (Vignati et al., 2003).

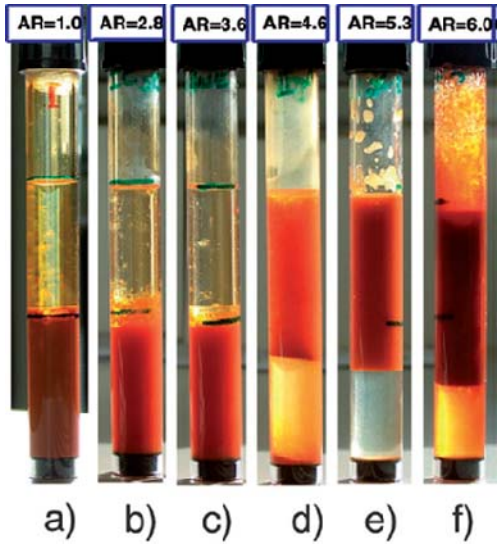

Figure 2.10

Effect of particle aspect ratio (AR) on the emulsifying behavior of decane-water system (1:1) with 1 wt% hematite particles in the aqueous phase. Adapted from (Madivala, Vandebril et al., 2009).

Chapter 3

CORE-SHELL COMPOSITE NANOPARTICLES VIA PICKERING EMULSION POLYMERIZATION

3.1 Emulsion Polymerization

As discussed previously, solid particles can self-assemble at liquid interfaces and function as emulsifiers in Pickering emulsions. In this chapter, particles are used as the stabilizers in emulsion polymerizations to synthesize organic-inorganic core-shell composite particles. To understand Pickering emulsion polymerization we must first be familiar with the process of emulsion polymerization. Traditionally, emulsion polymerization has been used to generate micro and nanoparticles. As we shall proceed with this discussion, we shall find that emulsion polymerization has many advantages (van Herk, 2005). Emulsion polymerization is a type of radical polymerization that usually starts with an emulsion incorporating water, monomer, and surfactant. The most common type of emulsion polymerization is an oil-in-water emulsion, in which droplets of monomer (the oil) are emulsified (with surfactants) in a continuous phase of water. Water-soluble polymers, such as certain polyvinyl alcohols or hydroxyethyl celluloses, can also be used to act as emulsifiers/stabilizers.

The name "emulsion polymerization" is a misnomer that arises from a historical misconception. Rather than occurring in emulsion droplets, polymerization takes place in the latex particles that form spontaneously in the first few minutes of the process. These latex particles are typically 100 nm in size, and are made of many individual polymer chains. The particles are stopped from

coagulating with each other because each particle is usually surrounded by the surfactant ('soap'); for example in ionic surfactants, the charge on the surfactant repels other particles electrostatically. When non-ionic water-soluble polymers are used as stabilizers instead of soap, the repulsion between particles arises because these water-soluble polymers form a 'hairy layer' around a particle that repels other particles, because pushing particles together would involve compressing these chains.

Emulsion polymerization is used to manufacture several commercially important polymers. Many of these polymers are used as solid materials and must be isolated from the aqueous dispersion after polymerization. In other cases the dispersion itself is the end product. A dispersion resulting from emulsion polymerization is often called a latex (especially if derived from a synthetic rubber). They are finding increasing acceptance and are preferred over solvent-based products in these applications as a result of their eco-friendly characteristics due to the absence of VOCs (Volatile Organic Compounds) in them (Odian, 2004). Additionally, emulsion polymerization is used in the production of a wide range of specialty polymers including adhesives, paints, and binders for nonwoven fabrics, additives for paper, textiles and construction materials, impact modifiers for plastic matrices, diagnostic tests, and drug-delivery systems. The development of this industry has been due to both the possibility of producing polymers with unique properties. The term emulsion polymerization encompasses several related processes: (1) conventional emulsion polymerization, (2) inverse emulsion polymerization, (3) miniemulsion polymerization, (4) dispersion

polymerization, and microemulsion polymerization. Conventional emulsion polymerization accounts for the majority of the world's production (~20 X 10^6 tons/year). All these techniques, which are leading to various kinds of polymer dispersions, are characterized by their heterogeneous nature. Polymer dispersions are defined as colloidal systems where the polymer is finely distributed in a liquid-dispersion medium in the form of stable individual particles. It might be useful to define emulsion polymerization in a general way as polymerization or copolymerization in aqueous systems of any combinations of monomers, which lead to water-insoluble polymers or copolymers in the form of individual polymer particles with a size distribution of diameters in a range typically lower than 1 μm. The polymer or copolymer particles swell after nucleation with the monomers. These swollen particles represent the nucleus where most of the monomer is polymerized. In many cases (especially in industrial systems), emulsifiers are present during the polymerization to stabilize the large interfacial area.

The mechanism of emulsion polymerization has been reviewed several times during the last decade (van Herk, 2005; Tauer et al., 2008). In general, particle nucleation is assumed to take place either via micellar or homogeneous nucleation in dependence on the hydrophilicity of the monomer and the surfactant concentration. The micellar mechanism considers a smooth transition from a monomer swollen micelle to a polymer particle after entry of a free radical and is applied for hydrophobic monomers such as styrene. For more hydrophilic monomers such as methyl methacrylate, the homogeneous nucleation mechanism assumes that a single growing water-born oligomer radical precipitates when it

becomes insoluble in the aqueous phase. The amount of growth of the particles is mainly determined by both the monomer and the initiator concentration per particle. The analysis of particle nucleation, and eventually, formation requires slowing down the reaction rate and a combination of various methods. The studies that have been done, on this mechanism in literature, obtained so far do not specify the location nucleus or locus of particle formation. It has been observed that particle nucleation can take place outside the micelles and subsequent particle growth can thus occur.

Next we shall take a look of the various established advantages as well as disadvantages of the emulsion polymerization method:

Advantages of emulsion polymerization include (Odian, 2004):

- High molecular weight polymers can be made at fast polymerization rates. By contrast, in bulk and solution free radical polymerization, there is a tradeoff between molecular weight and polymerization rate.
- The continuous water phase is an excellent conductor of heat and allows the heat to be removed from the system, allowing many reaction methods to increase their rate.
- Since polymer molecules are contained within the particles, viscosity remains close to that of water and is not dependent on molecular weight.
- The final product can be used as is and does not generally need to be altered or processed.

Disadvantages of emulsion polymerization include (Odian, 2004):

- Surfactants remain in the polymer or are difficult to remove, especially if the remnants of the stabilizer are adsorbed on the particle surface.
- For dry (isolated) polymers, water removal is an energy-intensive process.
- The inability to run the process continuously, unless several batch reactors are alternated, then the process may be continuous from that point on.
- Emulsion polymerizations are usually designed to operate at high conversion of monomer to polymer. This can result in significant chain transfer to polymer. Chain transfer reactions reduce the average molecular weight of the final polymer leading to anomalies or defects in the final polymer product.

3.2 Pickering Emulsion Polymerization

Employing solid particles, instead of surfactants, as the sole stabilizer into emulsion polymerization (Pickering emulsion polymerization) offers a novel one-step method to synthesize organic-inorganic core-shell structured composite particles. In the past decade, several different methods have been developed to synthesize core-shell composite particles. These methods can be sorted in two categories. One is the deposition of inorganic nanoparticles on preformed organic particle surfaces via electrostatic attraction or chemical bondings formed in situ (Caruso, 2001; Caruso, Susha, Giersig, & Möhwald, 1999; Caruso, Susha, &

Caruso, 2001; Dokoutchaev et al., 1999). These methods usually require multiple steps and are tedious to implement. The other category is the heterophase polymerizations in the presence of nanoparticles, including emulsion polymerization (Chen, Zhou, You, & Wu, 2005; Cheng, Chen, Zhou, & Wu, 2006), dispersion polymerization (Hong, Han, Hong, & Shim, 2008; Percy et al., 2003; Schmid, Fujii, & Armes, 2005; Schmid, Fujii, & Armes, 2006; Schmid et al., 2007; Yang et al., 2008), miniemulsion polymerization (Bon & Colver, 2007; Cauvin et al., 2005; Luo, Dai, & Chiu, 2008; Qiao, Chen, Zhou, & Wu, 2007; Tiarks, Landfester, & Antonietti, 2001), inverse emulsion polymerization (Voorn, Ming, & van Herk, 2006), and suspension polymerization based on inverse Pickering emulsions (Gao et al., 2009). In these heterophase polymerizations, pretreatment of nanoparticles are sometimes required and the stabilizing effect is usually provided by surfactants, co-monomers, initiators, solely or cooperatively with nanoparticles, and the inorganic nanoparticles are incorporated via electrostatic interactions or acid-base interactions.

In comparison, to conventional emulsion polymerization, Pickering emulsion polymerization uses nanoparticles as the sole stabilizing agent and nanoparticles are incorporated due to their self-assembly at monomer-aqueous phase interface and continuous attachment until the end of the polymerization. This novel technique has several advantages: (1) no sophisticated instrumentation is needed; (2) a commercialized nanoparticle powder or solution can be used without further treatment; (3) the synthesis can be completed in one-step; and (4) the produced particle dispersion is water-based and surfactant-free. Despite the

above advantages, the effort to explore and utilize Pickering emulsion polymerizations is very limited, and the polymerization mechanism and the nanoparticle incorporation mechanism remain unclear.

An interesting approach is to use a soft interface, i.e. liquid-liquid or liquid-gas, as a tool to capture particles and guide their assembly, whereby the interface acts as a template. In our group we look at this interface-driven assembly process of colloidal particles and combine this with polymer chemistry to create a variety of complex supracolloidal structures. It has been found that Pickering Emulsion polymerization offers a facile approach to get the same result from emulsion polymerization excluding most of the disadvantages (Ma et al. 2010). A simple schematic of this is represented in Figure 3.1. Employing solid particles, instead of surfactants, as the sole stabilizer into emulsion polymerization (Pickering emulsion polymerization) offers a novel one-step method to synthesize organic-inorganic core-shell structured composite particles. This is in contrast to emulsion polymerization where surfactants are required as stabilizers.

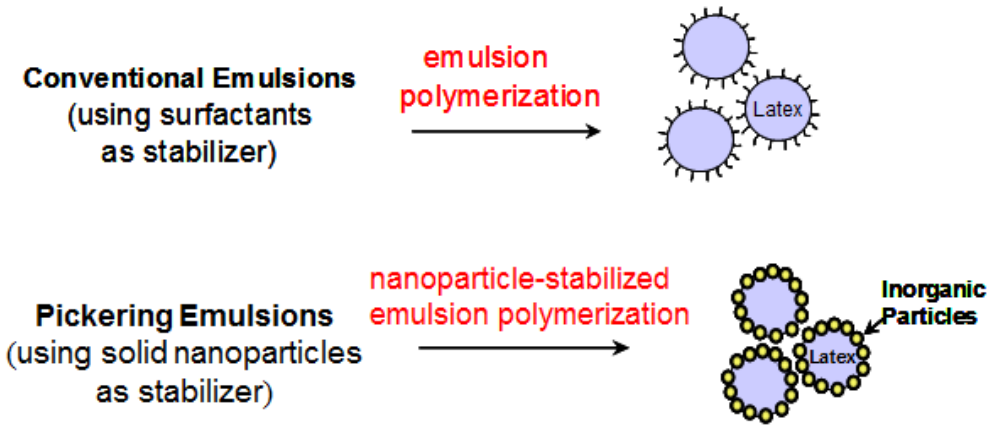

Figure 3.1

Schematic representation for Pickering emulsion polymerization process compared to conventional emulsion polymerization process.

The advantages of this novel technique have been listed in the introduction to this dissertation. Despite having its advantages, efforts to explore and utilize Pickering emulsion polymerizations have been limited, and the polymerization mechanism and the nanoparticle incorporation mechanism remain unclear. Lee and coworkers (Lee, Hong, Choe, & Shim, 2007) successfully synthesized polystyrene-silica composite particles using positively charged silica nanoparticles and anionic initiator KPS via soap-free emulsion polymerization; however, the silica nanoparticles needed to be added 30 minutes after the initiation which complicated the process. When silica nanoparticles were present at the initial stage of polymerization, the charge neutralization leads to irreversible particle agglomerations. The composite particle structure in this study is opposite to the often reported core-shell structure in which inorganic particles serve as the core and polymer serves as the shell (Bourgeat-Lami & Lang, 1998; F. Caruso,

2001; Gu, Kondo, & Konno, 2004; Guo et al., 2008; Nagao, Yokoyama, Saeki, Kobayashi, & Konno, 2008; Tianbin & Yangchuan, 2006); here the polymer serves as the core and the inorganic particles serve as the shell. Such materials provide a new class of supramolecular building blocks and can "exhibit unusual, possibly unique, properties which cannot be obtained simply by co-mixing polymer and inorganic particles." (Barthet, Hickey, Cairns, & Armes, 1999) For example, recent work (Schmid, Tonnar, & Armes, 2008) demonstrated that thin films made of polystyrene-silica core-shell composite particles remain transparent, even at silica loading as high as 39%. The transparency is due to the well-dispersibility of silica in the polymer matrix, which cannot be achieved simply by co-mixing the polystyrene and silica particles.

3.3 Synthesis Methodology

Materials

IPA-ST (Nissan Chemicals) is a dispersion of 10–15 nm silica nanoparticles in 2-isopropanol at a concentration of 30–31 wt %. Nonionic azo initiator VA-086 (98%, 2,2-azobis(2-methyl-N-(2-hydroxyethyl)propionamide), Wako Chemicals), anionic initiator potassium persulfate (KPS, 99%, Acros Organics), styrene monomer (99.9%, Fisher), N-isopropylacrylamide monomer (NIPAAm, 97%, Aldrich), 2-(N,N-Dimethylamino)ethyl methacrylate, (99%, Polysciences Inc.), L-α-Phosphatidylcholine, (Sigma Aldrich) and water (HPLC grade, Acro Organics) were used in the polymerization without further purification. The nonpolar dye BODIPY (493/503) (4,4-difluoro-1,3,5,7,8-

pentamethyl-4-bora-3a,4a-diaza-s-indacene) was obtained from Invitrogen, Molecular Probes.

Composite Particle Synthesis

The composite particles were prepared using the following procedure. First, water, IPA-ST and styrene were agitated mechanically with an IKA Ultra Turrax T25 homogenizer at 10,800 rpm for 2 minutes in an ice bath. Second, the emulsion was degassed with nitrogen and kept in nitrogen atmosphere under magnetic stirring. When the temperature was raised to 70 °C, the initiator aqueous solution was added to start the polymerization. In the synthesis using VA-086 as the initiator, a typical formulation includes 8 mL styrene, 52.5 mL water, 20 g IPA-ST silica nanoparticle dispersion, and 0.06 g initiator VA-086. In the synthesis of thermal sensitive composite nanoparticles, usually 0.66 g NIPAAm, 3.76 g styrene, 32 mL water, 4.1 g IPA-ST silica nanoparticle dispersion, 0.037 g initiator VA-086, and 1 μg BODIPY 493/503 were used. A typical formulation of the pH responsive nanoparticle type A includes 2.21 g DMA, 2.21 g styrene, 32 mL water, 4.1 g IPA-ST silica nanoparticle dispersion, 0.037 g initiator VA-086. The composite particles were sampled at different time intervals ranging from 3 h to 24 h for further characterizations. For experimental purposes the typical formulations varied for different setups and will be specified for the exceptions made.

3.4 Characterization of Composite Particles

Polystyrene-silica nanocomposite particles were successfully prepared by formulating 8 mL styrene, 52.5 mL water, 20 g IPA-ST silica nanoparticle dispersion, and 0.06 g initiator VA-086. The particle size, characterized by dynamic light scattering (DLS), is 203.9±51.6 nm in diameter with mono-distribution (the standard deviation here represents the half width of the particle size distribution). Figure 3.2a is a representative SEM image of the composite particles sampled at 5 hour reaction time. The roughness of the composite particle surfaces suggests that the composite particles are covered by silica nanoparticles. The core-shell structure can be clearly observed in the TEM image presented in Figure 3.2b. In many regions, the thickness of the shell is close to the size of one silica nanoparticle (10–15 nm), which may suggest a monolayer coverage.

The silica shell can be removed by excess amount of hydrofluoric acid (HF) solution. As shown in Figure 3.2c, after the HF etching treatment, the particle surfaces become smooth and reveal the polystyrene core. Energy dispersive x-ray (EDX) spectrum confirms that a substantial amount of Si and O exist, as shown in Figure 3.5d. Note that the relative intensity of the peak does not necessarily correspond to the true atom ratio in the sample, since the penetration depth of the electron beam is unknown. The penetration depth depends on various factors, such as the electron beam voltage, the nature of the sample, and the Au/Pd coating thickness. The EDX result only provides qualitative information regarding the existence of silica, which is composed of Si and O, in the composite particles.

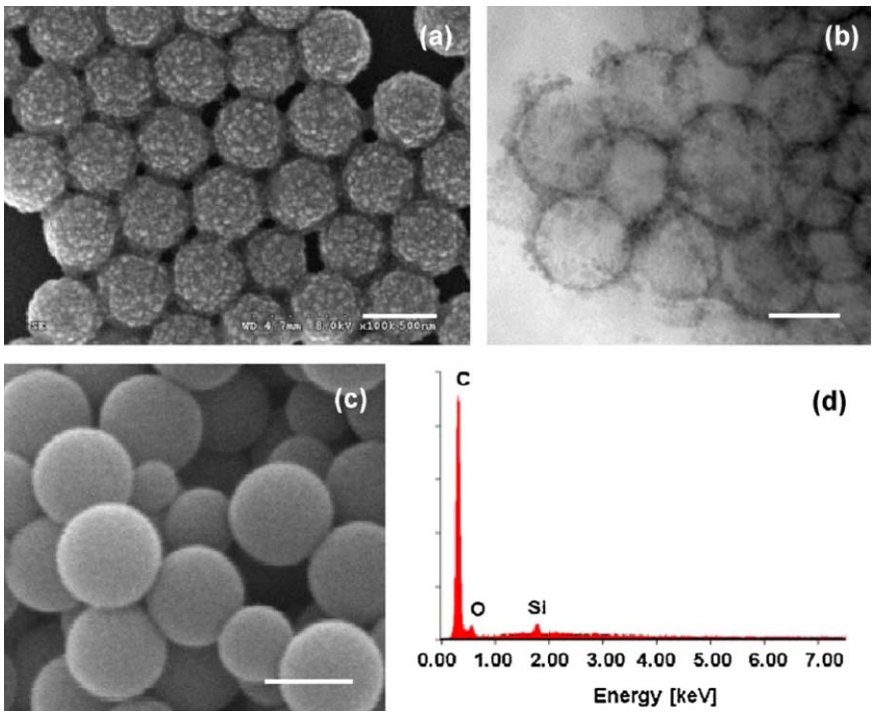

Figure 3.2

(a) An SEM image of composite particles, (b) a TEM image of cross-sectioned composite particles, (c) an SEM image of composite particles after HF etching, and (d) the EDX spectrum of composite particles. The scale bars represent 200 nm.

The silica content was quantitatively determined by TGA, as shown in Figure 3.3 (solid line). Two samples were measured: the composite particles (solid line) and the composite particles after removal of the silica component by hydrofluoric acid etching, which is essentially polystyrene cores (dashed line). The polystyrene cores have a residual weight of approximately zero at 800 °C. Thus it is reasonable to assume that the major weight loss during heating is associated with the thermo-oxidative degradation of polystyrene and the residue

close to 800 °C is solely silica. The silica content of the composite particles is approximately 20 wt %. Although some silica nanoparticles remain in the continuous phase and are washed off by centrifuging-redispersing cycles, the silica content of particles prepared *via* Pickering emulsion polymerization using nonionic initiator VA-086 is significantly higher than that of particles (1.1 wt %) prepared *via* dispersion polymerization using nonionic initiator AIBN (Schmid et al., 2007). The improvement is likely due to the distinct polymerization mechanisms. In contrast to the dispersion polymerization in which the polystyrene monomers are dissolved in alcohols, the emulsion polymerization here contains distinguished liquid-liquid interfaces due to the immiscibility between the monomers and the aqueous continuous phase.

Therefore the nanoparticles, even in the absence of electrostatic interactions, are thermodynamically favorable to self-assemble and remain at the liquid-liquid interfaces, following the same argument in Pickering emulsions (Binks & Horozov, 2006). At the initial stage of polymerization, the nanoparticles provide stability to the monomer droplets. During the nucleation stage, silica nanoparticles are at the interfaces between the monomer phase and continuous phase. It is worthwhile to note that the role of silica nanoparticles described here is not the same as that in the polymerization involving oppositely charged initiator and nanoparticles (Schmid et al., 2007). In the alcoholic dispersion polymerization presented by Schmid and coworkers, densely covered polystyrene-silica core-shell composite particles were successfully prepared by using cationic initiator AIBA (2,2'-azobis(isobutyramidine) dihydrochloride)

instead of the nonionic initiator AIBN (Schmid et al., 2007). The silica incorporation is likely promoted by the electrostatic attraction between the cationic initiator and the anionic nanoparticles. The initiator molecules or residues adsorb onto the silica nanoparticle surfaces after initiation (Schmid et al., 2007), and thus the silica nanoparticles function as the surface-active initiator residue. The mechanism of the core-shell structure formation in Pickering emulsion polymerization will be detailed later on.

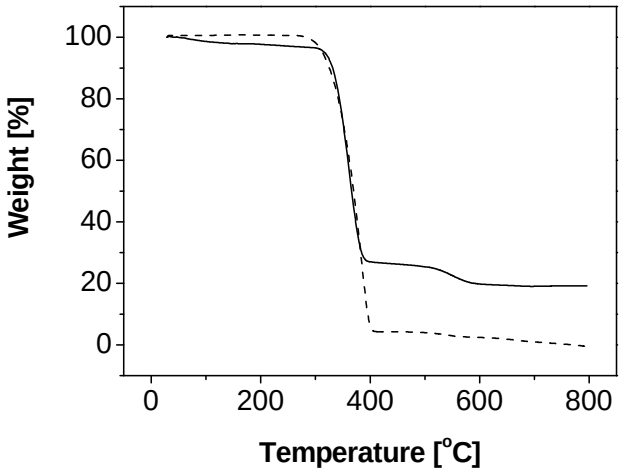

Figure 3.3

Thermogravimetric analysis of the nanocomposite particles prepared using VA-086 as the initiator before (solid line) and after (dashed line) HF etching treatment.

The glass transition temperatures (T_g) of the composite particles and HF treated particles, determined by DSC, are 103.8±0.2 °C and 100.7±0.1 °C respectively. The HF treated particles are assumed to be pure polystyrene and the T_g value is close to the reference value of 100 °C (Brandrup & Immergut, 1989).

The presence of the silica elevated T_g by approximately 3 °C, possibly due to the immobility of polymer chain at silica surface. It may also be worthwhile to note that, depending on the silica nanoparticle source, Percy and coworkers (Percy et al., 2004) observed either a slightly elevated T_g or a depressed T_g in polystyrene-silica composite particles prepared by emulsion polymerization using an anionic initiator APS (ammonium persulfate) and a catalyst TEMED (N,N,N',N'-tetramethylethylenediamine) at 25 °C.

In the above experiments, VA-086 was used as the initiator. VA-086 is a water-soluble nonionic initiator and no success has been reported in surfactant-free emulsion polymerization of styrene (Torii, Fujimoto, & Kawaguchi, 1996). In order to verify the sole stabilizing effect of silica nanoparticles, emulsifier-free emulsion polymerization using VA-086 as the initiator in the absence of nanoparticles was performed. No polystyrene particle formation was observed in the product, evidenced by SEM experiments. These experiments show that the initiator VA-086 has little effect on stabilizing the system in emulsion polymerization and therefore silica nanoparticles here are the only source of stabilizer. In addition, VA-086 is neutral in charge and thus is expected to minimize any electrostatic interactions with the negatively-charged silica nanoparticle surfaces.

3.5 Probable Mechanisms

The mechanism of conventional emulsion polymerization stabilized by surfactants has been under active discussion for over half a century and some consensus has been reached. Harkins proposed three loci of particle nucleation in

1947 (Harkins, 1947), which are later developed into at least three different nucleation mechanisms (Chern, 2006; Lovell & El-Aasser, 1997): the micellar nucleation, the homogeneous coagulative nucleation, and the droplet nucleation. Upon initiator addition and decomposition, free radicals form in the aqueous phase. The micellar nucleation (Chern, 2006; Tauer et al., 2008) begins with the capture of free radicals by micelles, proceeds with the continuous swelling and polymerization of monomers in the monomer-swollen particles, and finally terminates with the exhaustion of monomers. While some researchers believe that the micellar nucleation mechanism dominates at a surfactant concentration above the critical micelle concentration, doubts have also been raised on the insufficient experimental evidence (Tauer et al., 2008). In the absence of micelles, the homogeneous coagulative nucleation mechanism is likely dominant. In homogeneous coagulative nucleation (Chern, 2006; Feeney, Napper, & Gilbert, 1984; Feeney, Napper, & Gilbert, 1987; Yamamoto, Kanda, & Higashitani, 2004; Yamamoto, Kanda, & Higashitani, 2006), monomers dissolve in water and undergo radical polymerization to form oligomers. The oligomers coagulate to form embryos, nuclei, and primary particles sequentially. These primary particles, stabilized by the adsorption of surfactant molecules, could grow either *via* swelling of particles by monomers or deposition of oligomers onto their surfaces (Yamamoto, Nakayama et al., 2006). Finally, droplet nucleation is another possible mechanism in conventional emulsion polymerization. Here the monomer droplets may be subjected to the oligomeric radical entry and solidify into particles, following the droplet nucleation mechanism. Droplet nucleation is

usually minor in emulsion polymerization, except in miniemulsion polymerization when hydrophobic initiators are used.

Based on the fundamental understandings in conventional emulsion polymerization, possible Pickering emulsion polymerization mechanisms are proposed, taking into account the differences between fine solid particles and surfactant molecules. Since the nanoparticles do not form micelles like surfactant molecules, micellar nucleation is excluded. Thus there are two possible nucleation mechanisms involved in the initial stage of Pickering emulsion polymerization. Homogeneous coagulative nucleation is likely to be the dominating mechanism here, which yields the sub-micron-sized particles. The droplet nucleation might also occur, which yield micron-sized particles. The two mechanisms are illustrated in Figure 3.4. Upon initiator addition, monomers dissolved in the aqueous phase, react with decomposed initiators and form oligomers with radicals. In homogeneous coagulative nucleation, the oligomers coagulate into nuclei, which subsequently become monomer swollen particles. Nanoparticles self-assemble at the interfaces between monomer and the continuous phase to provide stability. With the continuous supply of monomer molecules from the monomer droplets through diffusion, the particle size growth is mainly achieved by monomer swelling into the core and polymerizing within the core. In contrast, in droplet nucleation, initiated oligomers with radicals enter monomer droplets, which subsequently polymerize into solid cores without significant size growth.

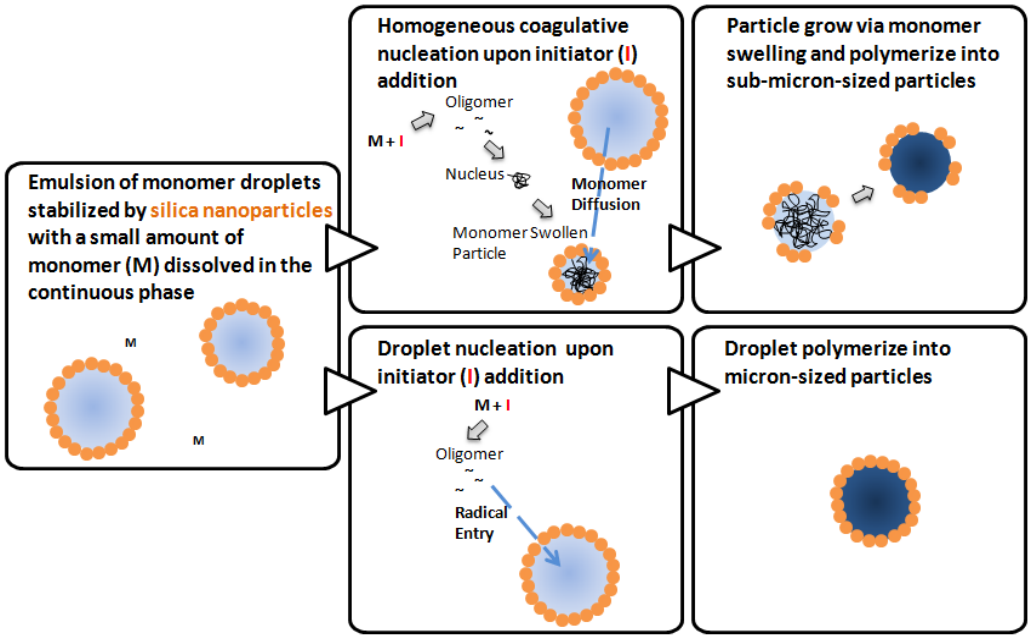

Figure 3.4

Schematic illustration for possible mechanisms of Pickering emulsion polymerization.

Figure 3.5 shows the dependence of particle size and surface coverage on reaction time and initiator concentration. The composite particles were sampled from 3 h to 24 h reaction time and the initiator concentration relative to the monomer amount was selected to be 0.83, 2.5, and 4.2 wt % respectively. At 3 h reaction time, well after the nucleation stage, nanocomposite particles with dense silica coverage were obtained. Since VA-086 initiator residues cannot provide sufficient stabilization to the monomer-swollen particles, silica nanoparticles would self-assemble at interfaces to provide stabilization and thus lead to high silica coverage.

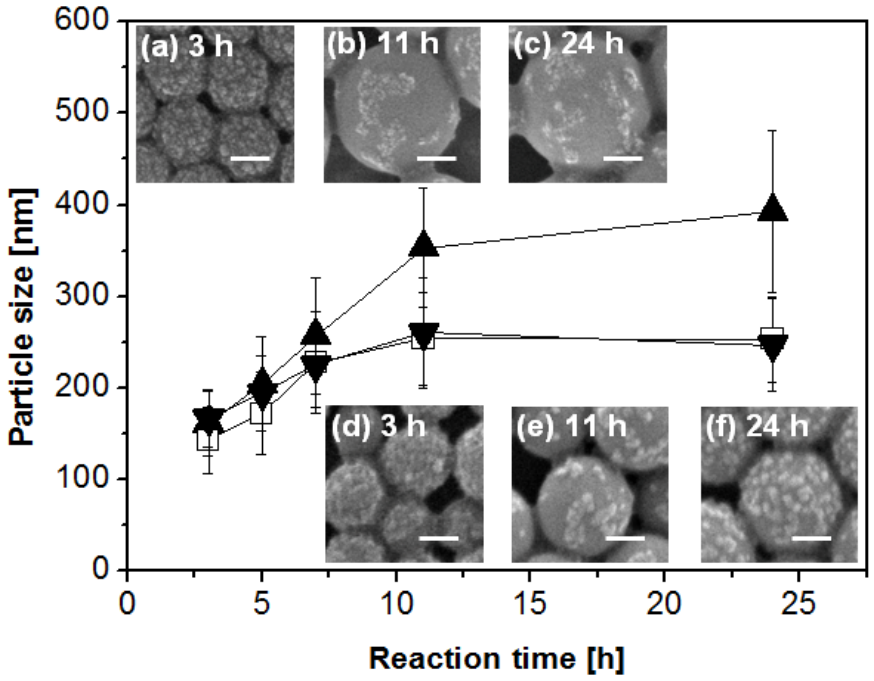

Figure 3.5

The Plot of particle size versus reaction time and SEM images in polymerizations using: 0.83 wt % (▲, a-c), 2.5 wt % (□) and 4.2 wt % (▼, d-f) VA-086. The error bars indicate the width of the particle size distribution and the scale bars represent 100 nm.

During the first 3 to 7 hours of reaction, the particles in all three systems experienced comparable particle size growth. The two systems with higher initiator concentrations ceased to grow soon after 7 hours of reaction time, whereas the system with the lowest initiator amount continued to grow significantly and produced the largest size of composite particles at 24 hour reaction time. The trend was confirmed by SEM experiments (images not shown). At initiator concentration 0.83 wt %, the silica coverage decreased with the particle size growth and the silica nanoparticles formed patches on the composite

particle surface with a low coverage. This might be an indication that the surface area of the polystyrene core increases with the particle growth without a significant increase of silica continuously attaching onto the polystyrene core. The particle growth mechanism is likely due to the swelling of particles by monomers in the continuous phase. The same mechanism explains the surface coverage decrease in the system containing 2.5 wt % of initiator (images not shown) and from 3 h to 11 h in the system containing 4.2 wt % of initiator. Comparing the particle sizes at 24 hour reaction time, a decrease in particle size occurred when the initiator amount was increased from 0.06 g to 0.18 g. The dependence of particle size on initiator concentration herein is in reverse trend with that in solid-stabilized alcoholic dispersion polymerization (Schmid et al., 2007). The difference probably originates from the distinct particle growth mechanisms (Yamamoto, Nakayama et al., 2006). In this emulsion polymerization, a larger number of nuclei likely formed at the initial stage of polymerization, so the particle size decreased with increasing initiator concentration, given a fixed amount of monomer and assuming the same monomer conversion. Further increasing the initiator amount from 0.18 g to 0.30 g did not have significant influence on particle size.

One possible explanation would be that the available amount of silica nanoparticles did not provide sufficient stability to an even larger number of nuclei, and thus oligomers, embryos, and nuclei coagulate until the remaining smaller number of nuclei could be sufficiently stabilized. These observations suggest that the Pickering emulsion polymerization using VA-086 as the initiator

mainly follows the homogeneous coagulative nucleation mechanism. One remaining mystery is the unexpected silica coverage from 11 h to 24 h in the system with 4.2 wt % initiator. Although the origin is unclear, it is tentatively attributed to the unusual silica coverage increase to the deposition of oligomers on the polystyrene core, which adsorbed onto silica nanoparticles in the continuous phase (Yamamoto, Nakayama et al., 2006). Excess initiator molecules might generate a large number of oligomers in the continuous phase, which could possibly adsorb onto silica nanoparticles. Thus when the oligomers on silica nanoparticles attach to preformed polystyrene surfaces, the silica nanoparticles are anchored there. It is also possible that the surface coverage increase might be due to the adsorption of depleted or close to depleted monomer droplets with a size below that of particles. It is also worthwhile to note that the continuous phase contains approximately 21% isopropanol. The existence of isopropanol might increase the solubility of the monomer and the degree of polymerization required for an oligomer to be insoluble in the continuous phase, however, the solubility of monomer in the continuous phase is still low enough to enable emulsification and subsequent emulsion polymerization.

Influence of particle size on the core-shell composite particles

As discussed before in the last chapter, the size and shape of the stabilizing nanoparticle in the Pickering emulsion can influence the final composite particle yielded. Previous composite nanoparticles discussed in this section were synthesized using IPA-ST which is a spherical silica nanoparticle dispersion of the size order 10-15 nm. Further studies were done using IPA-ST-L

which is a spherical silica dispersion of the size order of 40-50 nm. In general the concentration of the nanoparticle dispersion used to stabilize the emulsion was also varied as a parameter. However, as pointed out earlier in this dissertation, higher concentration than the weight percentage used for synthesis led to gelation. Lower concentrations, did not form an emulsion and synthesis could not be carried out. In the case of the larger size of silica particles, micron as well as sub-micron size of particles were observed (Figure 3.6a, b). This implies that of the mechanism types discussed previously in this chapter, both types of mechanisms are applicable in the formation of these composite particles. As discussed in the previous section, based on the fundamental understandings in conventional emulsion polymerization, possible Pickering emulsion polymerization mechanisms have been proposed, taking into account the differences between fine solid particles and surfactant molecules. Thus there are two possible nucleation mechanisms involved in the initial stage of Pickering emulsion polymerization. Homogeneous coagulative nucleation, which yields the sub-micron-sized particles as well as, droplet nucleation, which yield micron-sized particles seem to occur. The two mechanisms have been illustrated in Figure 3.4.

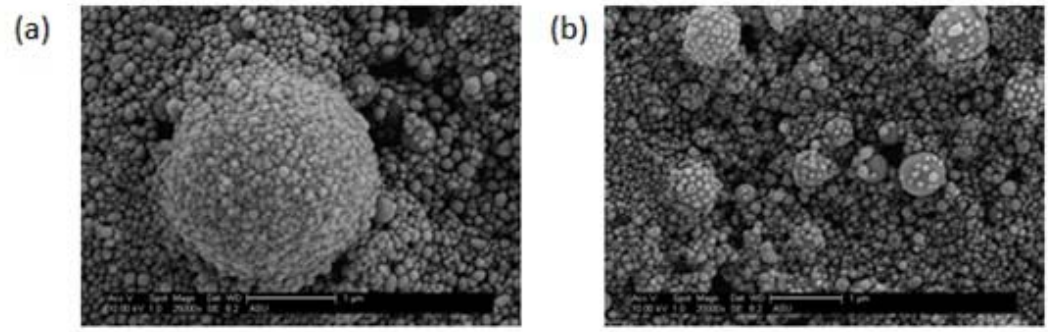

Figure 3.6

SEM images of composite particles synthesized with varied types of silica nanoparticles. Scale bars of each sub figures are as follows: (a) 1µm (b) 1µm.

Chapter 4

TEMPERATURE RESPONSIVE COMPOSITE NANOPARTICLES WITH SILICA AS SHELL MATERIAL

4.1 Introduction

"Smart" materials that respond to environmental changes, such as temperature or pH, are attractive means for designing "intelligent" drug carrier systems. In this study, N-isopropylacrylamide (NIPAAm) is incorporated as a co-monomer in order to impart temperature sensitivity to the core-shell nanoparticles. Poly (N-isopropylacrylamide) (PNIPAAm) is a well-understood temperature sensitive gel, which undergoes volume shrinkage at a transition temperature of approximately 32°C in pure water (Lee et al., 2007). Below this temperature which is referred to as the lower critical solution temperature (LCST), the polymer chain is hydrophilic because the hydrogen bonding between the hydrophilic groups and water molecules dominates; above the LCST, the polymer chain becomes hydrophobic due to the weakened hydrogen bonding at elevated temperatures and the interactions among hydrophobic groups (Schild, 1992). To synthesize PNIPAAm chains in solutions, techniques such as free radical initiation in organic solutions, redox initiation in aqueous medium, ionic initiators, and radiation of aqueous medium are used (Teo et al., 2010). One advantage of using PNIPAAm is that it can be engineered to possess transition temperatures slightly above physiological temperatures (e.g., at 38-39 °C) (Qiu & Park, 2001), that can be exploited for selective and controlled delivery at the tumor site using external stimuli (e.g. laser irradiation) which is suitable for

triggered *in vivo* drug delivery. Recently a "nanopump" system was reported using a block copolymer poly(L-lactide-star block-N-isopropylacrylamide) (PLLA-sb-PNIPAAm) for controlled drug release (Wang et al., 2008). The PNIPAAm block leads to the shrinkage of the complex micelles and pumps the drug out when the temperature is above the LCST. However, the nanoparticles constructed out of the block polymer have a tendency to aggregate together if the temperature is above the LCST (Wei et al., 2007). This was likely due to the loss of amphiphilic property of the block copolymer above the LCST as PNIPAAm blocks transformed into their hydrophobic character. In this work, we report a different synthetic pathway and use Pickering emulsion polymerization which provides adequate stability as evidenced by zeta potential measurements. Cancer drug candidate 17-(Allylamino)-17-demethoxygeldanamycin (17-AAG), an ansamycin antibiotic which binds and inhibits Hsp90 (Heat Shock Protein 90), is incorporated into the core during synthesis and used as a hydrophobic drug in the release experiments. Figure 4.1 illustrates a hypothesized core-shell "smart" nanoparticle and its release of drugs upon temperature change.

A major problem associated with the controlled release of drugs is the sensitivity of the dosage from properties to the variations of pH and transit in the human gastrointestinal (GI) tract (Moe¨s, 1989). Consequently in some cases, the drug targeting to some specific areas of the GI tract, like the colon is difficult. Several innovative approaches have been considered to overcome those difficulties and among these, the use of stimuli-sensitive materials is promising. Different kinds of stimuli such as temperature (Cammas et al., 1992; Yoshida et

al., 1992; Serres et al., 1996; Ichikawa and Fukumori, 1997; Kono et al., 1999; Ichikawa and Fukumori, 2000; Peppas et al., 2000), pH (Okatata et al., 1982; Dong et al., 1992; Kim et al., 1994; Brazel & Peppas, 1996; Serres et al., 1996), pressure (Tanaka et al., 1998) or electric fields (Eisenberg & Grodzinsky, 1984) can be used in order to provoke the drug release. Thermosensitive polymers such as Poly-N-isopropylacrylamide (PNIPAAm) and its copolymers have recently been proposed for the delivery and selective release of drugs (Okano et al., 1990; Yoshida et al., 1992; Kiolchob et al., 1998; Kono et al., 1999). PNIPAAm is a water soluble polymer that precipitates out of water when the solution is heated above its cloud point of about 32 °C (Heskins & Guillet, 1968; Kubota et al., 1990; Wu & Zhou, 1995). It therefore exhibits an inverse solubility curve with a lower critical solution temperature (LCST), contrary to most polymers, which exhibits an upper critical solution temperature (UCST) in organic solvents. This inverse behavior is neither novel nor unique to PNIPAAm since most non-ionic water-soluble polymers that owe their solubility to hydrogen bonding (with water) also exhibit similar behavior. However, unlike poly(acrylamide) or poly(ethylene oxide) (Ataman & Boucher, 1982; Ataman, 1987; Plate et al., 1999), which have LCST values near or above the boiling point of water, the PNIPAAm LCST is close to the physiological temperature which makes it a very attractive candidate in the field of controlled-drug delivery. Moreover, the transition is found to be reversible and rather abrupt (Wu & Zhou, 1997). Finally, the LCST of PNIPAAm that is about 32 °C in water can be easily modified by co-polymerization (Ringsdorf et al., 1992; Feil et al., 1993) with hydrophilic (increase) or

hydrophobic (decrease) monomers, or by addition of salts (Schild & Tirrell, 1990) or surfactants (Schild & Tirrell, 1991) to the aqueous polymer solutions. The practical applications of PNIPAAm and its copolymers can be found in comprehensive review papers published by Schild (Schild, 1992) and Ichikawa (Ichikawa & Fukumori, 1997). It is the relatively recent recognition of the transition of PNIPAAm as a potential thermosensitive shrinking device that prompted a surge of interest in the polymer. However, the need of a certain environmental temperature change to obtain significant variations of the polymer properties is an important limiting factor for the potential in vivo applications of thermosensitive polymers like PNIPAAm.

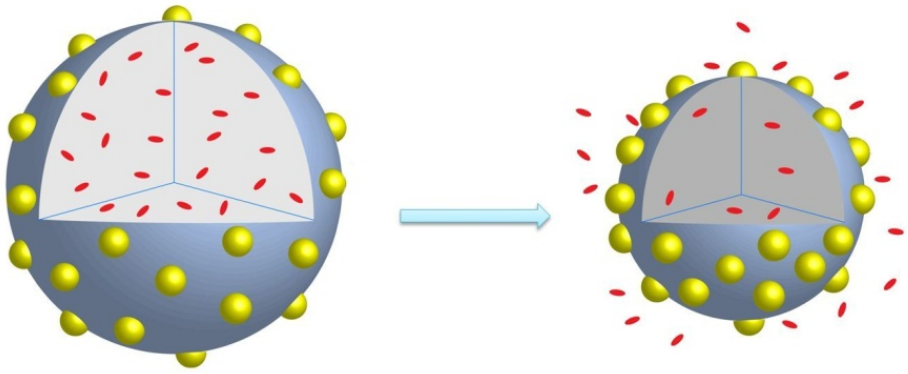

Figure.4.1

Schematic illustration of the polystyrene/PNIPAAm composite nanoparticles responding to temperature change and releasing encapsulated drugs.

Controlled release systems deliver a drug at a predetermined rate for a definite time period. In general, release rates are determined by the design of the system and may be dependent of environmental conditions, such as temperature or pH. These systems can also deliver drugs for long time periods (days to years). Although vesicles or drug macromolecule conjugates may prolong release, optimal control is obtained if the drug is placed in a polymeric material or pump. Controlled release systems differ from older "sustained release" or "slow release" preparations that include complexes (to salts or ion- exchange resins), suspensions, emulsions, slowly dissolving coatings that do not dissolve in the stomach yet do dissolve in the intestine (enteric coatings), and compressed tablets. Cellular uptake and cytotoxicity were studied in prostate cancer cells incubated at 37°C, with composite nanoparticles encapsulating 17-AAG and their controls.

The synthesis and characterization methods used for these experiments are typically the same as outlined in section 3.2, however to evaluate the effectiveness of the temperature sensitive composite nanoparticles as controlled release systems cellular uptake, cytotoxicity and drug release experiments were done.

4.2 Thermoresponsiveness of the Composite Particles

Different ratios of styrene/NIPAAm were used in the formulation of the polystyrene/PNIPAAm-silica core-shell nanoparticles. The work reported here contain 0%, 5%, 10%, 15%, 25%, 50%, and 75% of NIPAAm by weight during the synthesis; the percentage of 15% NIPAAm is used for all studies unless noted. Pickering emulsion polymerization was performed using VA-086 as the initiator. In order to verify the sole stabilizing effect of silica nanoparticles, emulsifier-free

emulsion polymerization using VA-086 as the initiator in the absence of silica nanoparticles was also conducted. No particle formation was observed in the product, as evidenced by SEM images. These experiments suggest that the initiator VA-086 has little effect on stabilizing in emulsion polymerization and therefore silica nanoparticles are the only source of stabilizer when present (Ma & Dai, 2009; Ma et al., 2010). Figure 4.2a is a representative SEM image of the composite particles sampled at 5-hour reaction time which shows that the particles tend to be spherical. The roughness of the composite particle surfaces suggests that the composite particles are covered by silica nanoparticles; this is contrasted by the smooth surface of the hydrofluoric acid (HF)-treated particles in Figure 4.2b. HF dissolves the silica layer and leaves behind the smooth polymer surface. It is also evidenced by the blue line in the FTIR spectrum in Figure 4.2c which shows that the composite particles have a characteristic strong peak at 1104 cm^{-1}, corresponding to the asymmetrical vibration of the Si-O-Si bond. Such a peak is absent in the red line in Figure 4.2c which represents the HF-treated composite particles. FTIR is a strong analytical tool which gives information about specific chemical bonds simply by interpreting the infrared absorption spectrum; here it is used to identify the presence of silica. The measurement of zeta potential allows predictions about the storage stability of a colloidal dispersion. Particle aggregation is less likely to occur for charged particles (high zeta potential) due to electric repulsion. The mean zeta potential for the drug loaded polystyrene/PNIPAAm-silica nanoparticles was -48.1 mV. Therefore, this system has a relative good stability and dispersion quality.

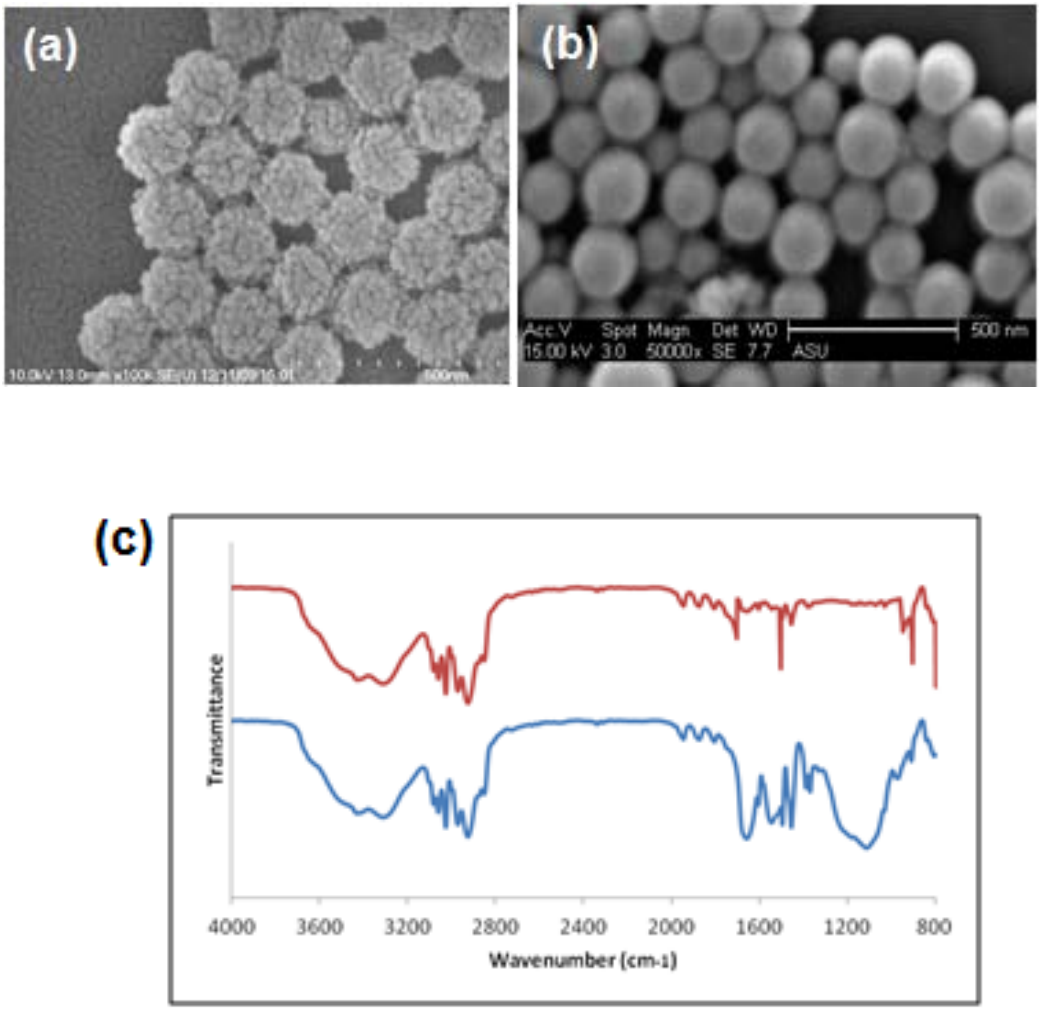

Figure 4.2

(a) An SEM image of the composite particles (b) SEM image taken after HF etching process (the scale bar represents 500 nm). (c) An FTIR spectrum of the composite nanoparticles where the blue line represents the composite particles and the red line is a sample of composite particles treated with HF. The box highlights the difference between the two spectra near 1104 cm^{-1} which corresponding to the asymmetrical vibration of the Si-O-Si bond.

To supplement the results summarized in Figure 4.2, the surface morphology of these composite nanoparticles were also studied using atomic force microscopy (AFM). AFM or scanning force microscopy (SFM) is a very high-resolution type of scanning probe microscopy, with demonstrated resolution on the order of fractions of a nanometer, more than 1000 times better than the optical diffraction limit. The AFM is one of the foremost tools for imaging, measuring, and manipulating matter at the nanoscale. The information is gathered by "tapping" the surface with a mechanical probe. Piezoelectric elements that facilitate tiny but accurate and precise movements on (electronic) command enable the very precise scanning. In some instruments, electric potentials can also be scanned using conducting cantilevers. In newer more advanced versions, currents can even be passed through the tip to probe the electrical conductivity or transport of the underlying surface.

The aim of this study was to compare the surface morphology of the composite nanoparticles with or without silica. Four types of nanoparticles were synthesized: 1. Polystyrene nanoparticles without silica, stabilized by the surfactant SDS (Figure 4.3a). 2. Polystyrene nanoparticles with silica (Figure 4.3b). 3. Polystyrene/PNIPAAm nanoparticles without silica, stabilized by SDS (Figure 4.3c). 4. Polystyrene/PNIPAAm-silica nanoparticles with silica (Figure 4.3d). Tapping mode images were taken using a Agilent Technologies 5500 system AFM.

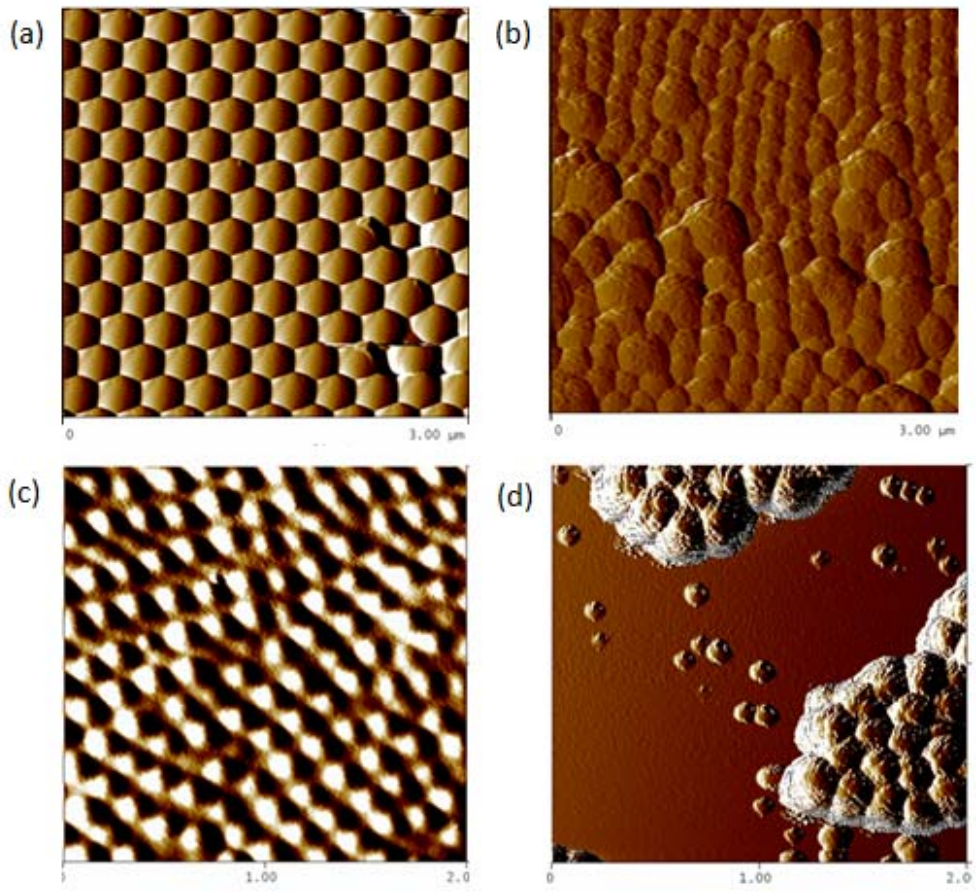

Figure 4.3

AFM images depicting the surface roughness of the various types of nanoparticles studied: (a) Polystyrene nanoparticles without silica, stabilized by the surfactant SDS (b) Polystyrene nanoparticles with silica (c) Polystyrene/PNIPAAm nanoparticles without silica, stabilized by SDS (d) Polystyrene/PNIPAAm-silica nanoparticles.

The images gathered from this AFM study reiterate that the surface roughness is a direct consequence of the silica shell of these composite nanoparticles. For Figure 4.3 (a) and (c) the surface of the spheres are smooth as there is no silica present, which is a contrast to Figure 3.6 (b) and (d) where the surface of the spheres are rough due to the presence of silica on their surface.

The synthesized polystyrene/PNIPAAm-silica core-shell nanoparticles are responsive to thermal stimuli. Figure 4.4 shows the dependence of average diameter of the composite particles on temperature. The average particle size at 25°C is approximately 92 nm. The size decreases sharply as the temperature reaches 32°C, around the LCST for homopolymer PNIPAAm and size change is nearly reversible upon cooling. Control experiments of polystyrene-silica nanoparticles did not show a size transition over a temperature range of 25-45°C (data not shown). The transition temperature is not shifted by the silica nanoparticle encapsulation. This is consistent with the recently reported composite microspheres with a PNIPAAm core and a silica shell which also show a volume transition starting at 32°C (Duan et al., 2009). It is likely due to the fact that silica particles are physically adsorbed on the surfaces of PNIPAAm microspheres thus no chemical bond formation with silica occurs which might change the transition temperature. Moreover, the copolymerization with styrene has no significant effect on the transition temperature. One hypothesis is the relative phase separation of PNIPAAm and polystyrene within the core. Duracher et al. studied PNIPAAm-polystyrene particles and suggest a PNIPAAm-rich shell and a polystyrene-rich core structure (Duracher et al., 1998). Such phase

separation may also occur in the core of the composite particles here although detailed morphology is unknown. The hydrodynamic sizes of polystyrene/PNIPAAm-silica of various compositions of core-shell nanoparticles were measured by DLS at different temperatures. It was found that when the concentration of PNIPAAm is high, the volume change is more significant with temperature change.

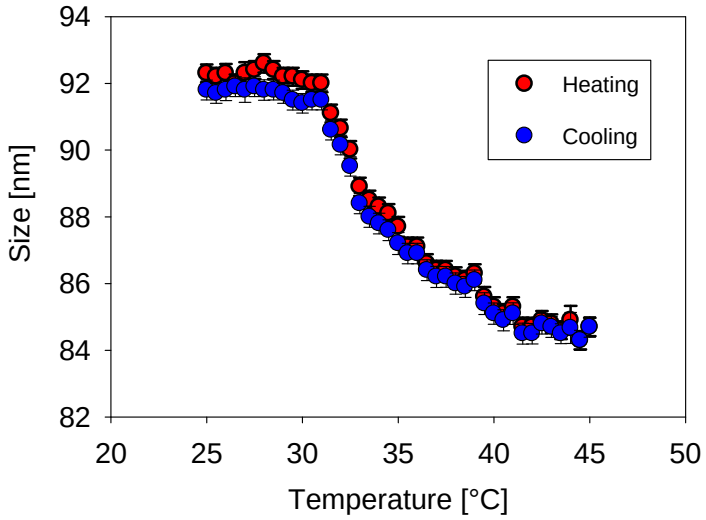

Figure 4.4

(a) The dependence of average diameter of composite nanoparticles (15% NIPAAm) on temperature. The error bars show standard deviations of particles made in three different batches. The transition temperature is around 32°C. Their size transition is nearly reversible.

Effect of Styrene/NIPAAm Ratio

The hydrodynamic sizes of polystyrene/PNIPAAm-silica of various compositions of core-shell nanoparticles were measured by DLS at different temperatures, and the results are shown in Figure 4.5. The hydrodynamic sizes of

the nanoparticles decreased as the temperature increased from 25°C to 40°C, and the transition temperature for the various compositions of nanoparticles was observed to be 32°C. From Figure 4.5 we infer that when the concentration of PNIPAAm is high, the volume change is more significant upon temperature change.

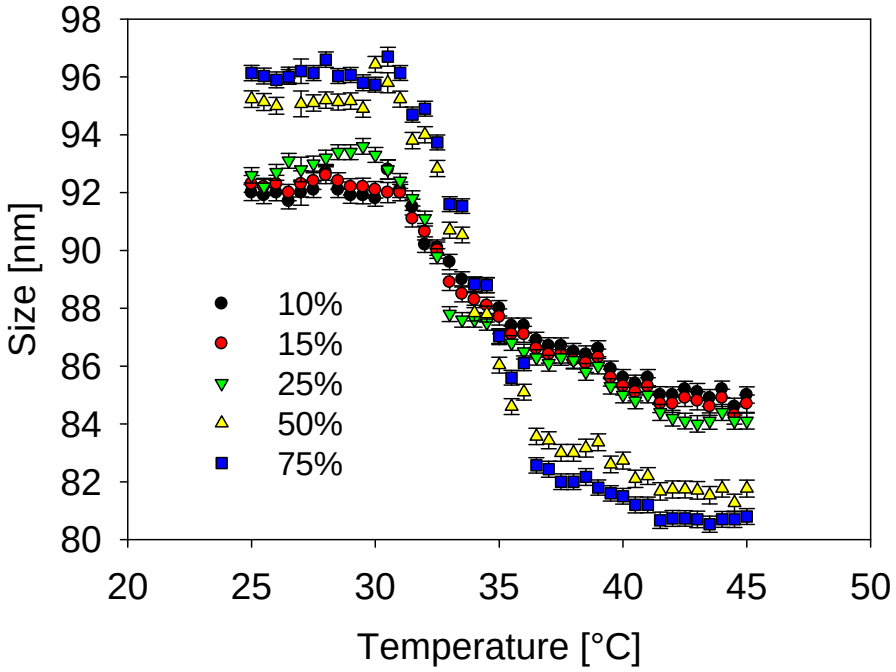

Figure 4.5

The dependence of average diameter of composite nanoparticles with different amounts of NIPAAm on temperature. The error bars show standard deviations of particles made in three different batches.

4.3 Temperature Responsive Composite Nanoparticles and their Potential Applications in drug delivery

Effect of Temperature and NIPAAm Concentration on Drug Release

The drug candidate used in the release experiment is 17-AAG, an ansamycin antibiotic which binds to Hsp90 (Heat Shock Protein 90). Hsp90 plays a key role in regulating the physiology of cells exposed to environmental stress and in maintaining the malignant phenotype of tumor cells. Hsp90 client proteins are important in the regulation of the cell cycle, cell growth, cell survival, apoptosis, and oncogenesis. 17-AAG binds with a high affinity into the domain of adenosine triphosphate (ATP) binding pocket in Hsp90 and induces the degradation of proteins that require it for conformational maturation. Heat Shock Protein 90 (Hsp90) is of significant interest in cancer therapy because it helps in cell survival and tumor cell proliferation.

The main obstacle to the delivery of 17-AAG is its poor water solubility and it requires complicated formulations with Cremophor EL (CrEL), DMSO, or EtOH before parenteral administration (Shin et al., 2009). This is undesirable as CrEL is known to induce hypersensitivity reactions and anaphylaxis, and requires patient pretreatment with antihistamines and steroids before administration (Xiong et al., 2009). A safer administration of 17 AAG can be made by a surfactant free delivery system rather than using harmful surfactants to solubilize the drug. . Therefore, it requires a viable drug carrier for its time-controlled release. Composite core-shell nanoparticles loaded with 17AAG were used for the drug release experiments. The amount of drug released was determined by UV

analysis. Absorbance (at a wavelength of 332 nm) of a number of standard solutions of the reference substance at concentrations encompassing the sample concentrations was measured using a Biotek Microplate Reader and the calibration graph was constructed.

The release study of 17-AAG from the nanoparticles was first performed in deionized water. The composite nanoparticles encapsulated with 17-AAG to be tested were divided into two parts. The first portion was kept at room temperature and the second was in a temperature-controlled water bath at 40°C during the duration of the experiment. At regular time intervals, the samples were taken out and then centrifuged at 10,000 rpm for 3 min in a Beckman Coulter tabletop centrifuge and 100 μL of the supernatant was drawn out from release system for analysis. We have also performed DLS experiments on the supernatant to verify the absence of nanoparticles. Cumulative drug release measurements were performed. Figure 4.6 depicts the cumulative fractional drug release-time plot of 17-AAG from drug loaded nanoparticles at various time intervals at room temperature and 40°C. At room temperature there was no significant release of the drug. However, at a higher temperature of 40°C, the drug release from the nanoparticles reached a maximum after 7 h.

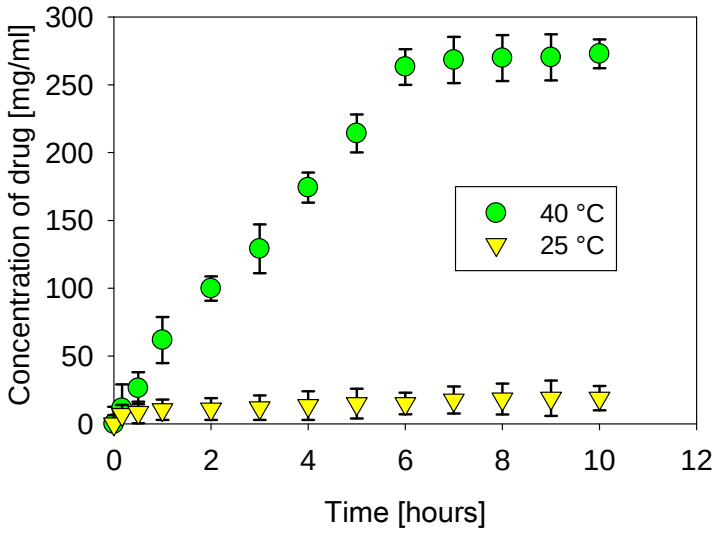

Figure 4.6

Drug release versus time curve indicating release at room temperature (yellow triangles) and at 40°C (green circles). There is no release at 25°C which is below the transition temperature of the composite particle. The cumulative fractional release is shown as an inset where the maximum amount of drug release value is taken at 40°C for 10 hours; diffusion model parameters have been calculated from these data.

Drug release was triggered upon heating at 40°C. As seen previously drug release is suppressed below the LCST at 25°C and there is no release from polystyrene-silica nanoparticles which served as the control. Figure 4.7 shows maximum release occurs from 15% of NIPAAm formulation. The release is quantified using concentration, which is obtained from the plate reader. 17-AAG release from the nanoparticles is summarized in Figure 4.7. This representation clearly shows the difference in amounts of release for different samples which would not have been possible if the cumulative fractional release representation

was used. Figure 4.8 suggests that the most efficient drug releasing concentration of NIPAAm is 15% and the least efficient is 75%. Obviously, this observation is inconsistent with the size change measured in Figure 4.5. To further understand how the maximum release of drug from 15% NIPAAm sample takes place, we performed a drug encapsulation efficiency experiment. In order to calculate the encapsulation efficiency, the amounts of drug present in the nanoparticles before and after the polymerization reaction were determined using the plate reader. The supernatant was measured for absorbance in each case and the background readings were taken into consideration after performing the same experiment using polystyrene/PNIPAAm-silica core-shell nanoparticles without drug loaded. Although an increase in the PNIPAAm concentration results in greater size reduction, it is observed that 17-AAG encapsulates less at high PNIPAAm concentrations, as shown in Figure 4.8. This is likely due to the fact that 17-AAG is a hydrophobic drug and is encapsulated less when there is a low percentage of polystyrene in the nanoparticle.

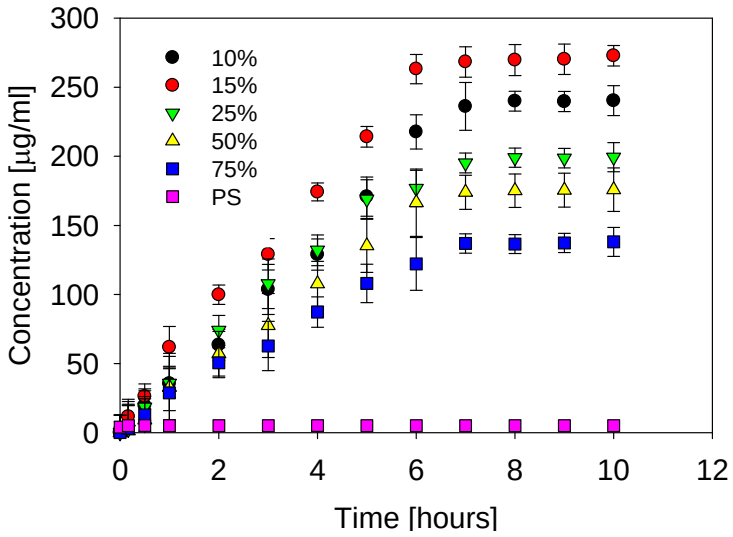

Figure 4.7

Drug release versus time curve for nanoparticles with different amounts of NIPAAm. For Polystyrene(0% NIPAAm) nanoparticles there is hardly any release observed.

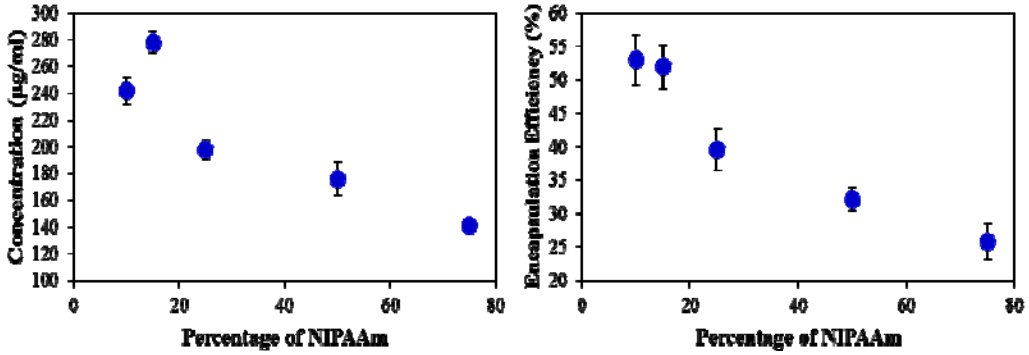

Figure 4.8

Summary of the cumulative drug release and encapsulation efficiencies for the different types of nanoparticles.

For further uptake, cytotoxic and analysis studies, (unless mentioned) the 15% NIPAAm containing nanoparticles was chosen and used as these are the most efficient i.e. release the maximum amount of drug compared to the other formulations of nanoparticles.

For decades, polymeric systems have been used for pharmaceutical applications, especially to provide controlled release of drugs. Drug–polymer systems may also be useful in protecting the drug from biological degradation prior to its release. The development of these devices started with the use of non-biodegradable polymers, which rely on the diffusion process, and subsequently progressed to the use of biodegradable polymers, in which swelling and erosion take place. Based on the physical or chemical characteristics of polymer, drug release mechanism from a polymer matrix can be categorized in accordance to three main processes (systems) (Leong & Langer, 1987), which are:

1. Drug diffusion from the non-degraded polymer (diffusion-controlled system).
2. Enhanced drug diffusion due to polymer swelling (swelling-controlled system).
3. Drug release due to polymer degradation and erosion (erosion-controlled system).

In all three systems, diffusion is always involved. For a non-biodegradable polymer matrix, drug release is due to the concentration gradient by either diffusion or matrix swelling (enhanced diffusion). For biodegradable polymer matrix, release is normally controlled by the hydrolytic cleavage of polymer chains that lead to matrix erosion, even though diffusion may be still dominant when the erosion is slow. This categorization allows mathematical models to be

developed in different ways for each type of system. Mathematical modeling of drug release provides insights concerning mass transport and chemical processes involved in drug delivery system as well as the effect of design parameters, such as the device geometry and drug loading, on drug release mechanism. Thus, the optimized device design for a required drug release profile can be predicted using a systematic approach with a minimum number of experimental studies.

The "anomalous" transport of drug release is often identified in swelling controlled systems since both diffusion and dissolution occur altogether and they are quite indistinguishable. Here, the drug transport is commonly modeled as diffusion in which the diffusion coefficient depends strongly on polymer concentration since polymer swelling and relaxation enhance the drug mobility, whereas the polymer dissolution is modeled to follow first-order kinetics at the interface with surrounding medium. In the simplest manner, researchers (Korsmeyer et al. and Yasuda et al.) developed a semi-empirical equation based on a power-law expression to describe the drug release from swelling-controlled systems as follows:

$$\frac{M(t)}{M(\infty)} = kt^n$$

Where, k is a constant and n is the diffusional exponent. The power-law equation can be observed as the superposition of two processes of Fickian diffusion and "Case-II transport". It has a feature to identify the relative importance between Fickian diffusion (n=0.5) and "Case-II transport" (n=1). The "anomalous transport" takes place where phenomena of both processes are coupled. For spheres, the n values are in the range of 0.43 and 0.85 for diffusion and "Case-II

transport" drug release, respectively. Besides the dependence on the geometry, the value of n may also be influenced by particle size distribution as observed by Ritger et al. (2003). For a hypothetical mixture of 20% 20-μm, 60% 100-μm, and 20% 500-μm spheres, the n values for Fickian diffusion and the "Case-II transport" become 0.30 and 0.45, respectively. In comparison to the release profile from monodispersed particles, this mixture shows an acceleration of drug transport at early times due to the portion of particles smaller than the mean size and retardation at longer times due to the portion of particles larger than the mean size.

A major challenge in drug delivery for anticancer agents is the poor aqueous solubility of many anticancer drugs. Due to the low aqueous solubility of the drug and low diffusivity within the polymer matrix, the release profile is generally very slow. An example is in the delivery of a promising anticancer agent paclitaxel which is found to be useful against a wide spectrum of carcinomas, especially in breast and ovarian cancer. Its low aqueous solubility and high crystallinity make it difficult to be encapsulated in biodegradable microparticles at reasonably high drug loading (>30%) and the drug release by diffusion is generally very low. The use of nanoparticles provides a solution to the slow release profile by providing a much larger surface area, but compromised with the slower diffusivity in the polymer matrix due to the more compact structures resulted from the fabrication techniques. For a monolithic system with uniform drug distribution with the polymeric matrix, release is generally governed by diffusion or erosion mechanisms. Drug release from common polymeric

nanoparticles, such as PLA and PLGA, is mainly due to diffusion, drug dissolution and subsequently surface erosion or bulk degradation. The effective diffusion coefficient of drug follows the combined effects of diffusion through particle pores and diffusion through an intact polymer matrix and is a function of the tortuosity and porosity of the polymer (Arifin et al., 2006). The release profile of highly hydrophobic drug from polymeric systems is mainly influenced by drug diffusion mechanism as detailed in the following paragraphs.

The cumulative fractional drug release is calculated as M_t/M_∞, where t is the release time, M_t is the amount of drug released at a time t and M_∞ is the amount of drug released at time infinity. Infinity is taken to be when the maximum amount of drug gets released and there is no subsequent release after infinity. The concentration of the drug in the sample solution was read from the calibration curve as the concentration corresponding to the absorbance of the solution. To determine the release mechanisms of the composite nanoparticle system an equation proposed by Yasuda et al. (Yasuda et al., 1968) was used, which analyses the release behavior of a solute from a polymer matrix, $\frac{M(t)}{M(\infty)} = kt^n$ where M(t) is the amount of drug released at time t, $M(\infty)$ is the total amount of drug released at a time ∞ which is taken to be the saturation time when no further amount of drug is released, k is a constant related to the physical properties of the system, and the index, n, is the diffusional component that depends on the release mechanism.

When n=0.5, the solute is released by Fickian diffusion; when 0.5<n<1.0, the solute is released by non-Fickian diffusion and when n=1, there is zero order

release (Yasuda et al., 1968). For example for 15% of NIPAAm as monomer amount, the calculated *n* value is 0.73 which indicates the non-Fickian diffusion. The mathematical model indicates that the drug diffusion behavior is non-Fickian and the rate of drug release is due to the combined effect of drug diffusion and polymer response due to increase in temperature. Several non-degradable drug-releasing systems have been found to have this kind of non-Fickian release behavior as reviewed by Fu (Fu & Kao, 2010). Especially in the comprehensive study by Grassi and colleagues (Grassi & Grassi, 2005) studying theophylline release from different kinds of HPMC tablets (hydroxyl propyl methylcellulose), propose a semi-empirical model based on the fact that release kinetics is in their case primarily determined by drug diffusion through the gel layer surrounding the dry tablet core. Also this builds on the physical frame of the model suggested by Higuchi (Higuchi, 1963) because in addition to drug diffusion, Grassi et al., thought that relaxation of the gel layer of the tablets they studied, contributed to the non-Fickian type of diffusion they observed.

The "n" value along with their standard deviation corresponding to each formulation of the different type of composite nanoparticles used in this study has been summarized in table 4.1. In general, drug diffusion, polymeric matrix swelling, and material degradation are suggested to be the main driving forces for solute transport from drug containing polymeric materials (Arifin et al., 2006). Specifically, Fick's law of diffusion provides the fundamental understanding for the description of solute transport from polymeric materials. Fickian diffusion refers to the solute transport process in which the polymer relaxation time (t_r) is

much greater than the characteristic solute diffusion time (t_d). This t_d can be defined as the ratio of the release liquid diffusion coefficient at equilibrium and the square of a characteristic length (radius in case of spherical matrices) (Coviello et al., 2005) and experimentally may be determined by knowing the above physical properties of the system.

NIPAAm %	**"n" value**	**S.D.**
10	0.69	0.0021
15	0.73	0.0081
25	0.66	0.0055
50	0.63	0.0032
75	0.60	0.0074

Table 4.1

"n" values of each type of nanoparticle used in the study.

The solute diffusion coefficient can be characterized in terms of the diffusion coefficient of the solute in the pure solvent (D_{iw}) as well as the network porosity (ε) and tortuosity (τ). Additionally, the manner in which the solute partitions itself within the pore structure of the network will affect the diffusion of the drug. This phenomenon is described in terms of the partition coefficient, K_p. These parameters can be incorporated to describe the transport of the drug in the membranes in terms of an effective diffusion coefficient (D_{eff}):

$$D_{eff} = D_{iw} \frac{K_p \varepsilon}{\tau}$$

When $t_r \approx t_d$, the macroscopic drug release becomes anomalous or non-Fickian (Grassi & Grassi, 2005). The purpose of mathematical modeling is to simplify the complex release process and to gain insight into the release mechanisms of a specific material system. In literature, well-established models have been developed to describe drug release based on the mechanisms related to Fickian and non-Fickian diffusion. However, it is also acknowledged that the disparities that exist between theories and experimental data are present since there are multiple driving forces involved in a single type of release process. In particular, non-degradable polymers have been widely applied in the fabrication of drug delivery vehicles (Pillai & Panchangula, 2001). These polymers include polyurethanes, silicone rubber, polyethylene vinyl acetate, just to name a few. Solute transport from non-degradable polymeric systems is mainly considered as diffusion driven (Katz et al., 2004). Non-degradable polymers can be classified into "reservoir-" and "matrix-" type vehicles (Fung & Saltzman, 1997). By definition, reservoir-type devices refer to those having an inert coating material, which functions as a rate-controlling membrane. The release rate remains relatively constant and is not affected by concentration gradient, but most likely is related to the thickness and permeability of polymeric membrane. In contrast, for matrix-type devices, drug release is more likely to be Fickian diffusion driven, which is associated with concentration gradient, diffusion distance, and the degree of swelling (Siepmann & Siepmann, 2008; Lin et al., 1985). As discussed, diffusion, erosion, and degradation are the most important mechanisms for solute transport from polymeric matrices (Arifin et al., 2006). In the thermoresponsive

system we are studying, we can discard erosion and degradation as possible mechanisms as the composite nanoparticles consist of neither erodible nor degradable polymers. The release in our system is due to a combination of drug diffusion and the thermal response of PNIPAAm which constitutes a non-Fickian release. Several studies on PNIPAAm release similary indicate a non-Fickian type of release (Akdemir & Apohan, 2007; Jones et al., 2008; Molina et al., 2011). Several commonly used power law equations for modeling release kinetics are summarized (Table 4.2). These models are easy to use and the established empirical rules may help explain transport mechanism(s). For instance, Ritger-Peppas equation has been applied to describe the release of sodium salicylate from HPMC tablets, indicating a non-Fickian drug release mechanism. The study also revealed that polymer swelling was involved in the release process and the authors suggested that the conclusion of a non-Fickian drug release mechanism, can be simply based on the diffusional exponent, n, of the Peppas models (Ferrero et al., 2009). Comparing the models in Table 4.2 and the diffusional exponents we have derived from experimental results in Table 4.1, we find that the more general Ritger-Peppas model still conforms with our system. This is because all “n” values lie between 0.5 and 1 which has the physical interpretation of following non-Fickian diffusion.

Model	**Expression**	**Application**	**Reference**
Higuchi	$\frac{M(t)}{M(\infty)} = kt^{1/2}$	Fickian diffusion	(Higuchi, 1963)
Ritger-Peppas	$\frac{M(t)}{M(\infty)} = kt^{n}$	n=1, 0 order diffusion n=0.5, Fickian diffusion 0.5<n<1, non-Fickian diffusion	(Ritger & Peppas, 1987)
Zero-order	$\frac{M(t)}{M(\infty)} = kt$	0 order diffusion	(Serra et al., 2006)

Table 4.2

Review of mathematical models for drug release kinetics.

Cellular Uptake and Cytotoxicity Studies

Composite core-shell nanoparticles, loaded with BODIPY 493/503 dye in the core for imaging and as a model drug, were used in cellular uptake experiments. Prostate cancer cells (PC3 and PC3-PSMA) were seeded in a 24-well plate at a density of 50,000 per well and incubated overnight at 37°C and 5% CO_2. Dye-containing nanoparticles were added to cancer cells in the absence of serum for 0.5, 1.0, 1.5, and 5 h (Figure 4.9) following which, nanoparticles and serum-free medium were removed and cells were washed five times using 1X phosphate buffered saline (PBS). Cells were stained with the nuclear stain Hoechst 33258 (MP Biomedicals) and then mounted for analysis using a laser

scanning Nikon C2 confocal microscope (Nikon Instruments Inc., Melville, NY). Images were acquired and stacked using NIS-Elements Microscope Imaging Software (Nikon Corporation) at 60× water objective with a z-step of 0.4 μm slice and with PMT scanners at 1024 × 1024 pixels. The cytotoxicity of nanoparticles (NPs) was determined using 3-(4, 5- dimethylthiazol-2-yl)-2, 5-diphenyl tetrazolium bromide (MTT) assay. Prostate cancer cells were cultured in medium (RPMI 1640 plus 10 % fetal bovine serum and 1% penicillin/streptomycin) under 5% CO_2 at 37^{o}C. Cells were seeded in a 96-well plate at a cell density of 5,000 cells per well and allowed to attach overnight prior to NP treatment (0.01-1 μg/ml). At 72 h after treatment with different doses of NPs, 10 μl of MTT reagent was added to each well and incubated under 5% CO_2 at 37°C for 4 h, followed by addition of detergent. Absorbance at 570 nm was determined with microplate reader (Biotek Synergy 2). Studies were performed with at least 4 individual samples and repeated 3 times. Any interference from NPs alone (i.e. without cells) was normalized for all samples. Two-tailed Student's t-test was employed for statistical analysis.

It was hypothesized that polystyrene/PNIPAAm-silica core-shell nanoparticles are sufficiently small to be taken up by cancer cells. Cell uptake experiments were performed using human prostate cancer cells (50,000/well in 24 well plates). The uptake of the composite nanoparticles by PC3 and PC3-PSMA cells following incubation for 0.5, 1, 1.5 and 5 h (Figure 4.9 & 4.10) was visualized using confocal microscopy. In Figure 4.9, at a nanoparticle dosage of 0 (control), 0.025 and 0.05 μg/ml, the human prostate cancer cells take up dye-

loaded composite nanoparticles and traffic them throughout the cytoplasm while remaining viable after incubation for 5 h. Visible green fluorescence in Figure 4.9 suggests that composite nanoparticles are internalized in both the PC3 and PC3-PSMA cells. Initial internalization of nanoparticles in both PC3 and PC3-PSMA cells was observed after 1 h of incubation (Figure 4.10). A control was kept under observation at the different times with no nanoparticles. Uptake was observed at lower concentration of 0.025 μg/ml and at a higher concentration of 0.05 μg/ml. The higher concentration case shows presence of some debris which may be due to some cell death as indicated by cytotoxicity experiments. Nanoparticles could be transported into the cell by either specific (receptor-targeted) or nonspecific cellular uptake mechanisms depending on the surface properties. Since the nanoparticles are not conjugated with any antibody, the uptake behavior here is nonspecific. Nonspecific uptake of nanoparticles has recently attracted much attention in the development of new strategies for designing efficient nano-carriers, though specific uptake is a more developed strategy as more control is possible and effects on cell functions are easier to predict. Our findings suggest that the thermally sensitive composite nanoparticles can be taken up by prostate cancer cells, which opens new opportunities in controlled drug delivery. Further research in our laboratory will involve conjugation of targeting biomolecules on the surface of these nanoparticles in order to facilitate selective delivery to prostate cancer cells.

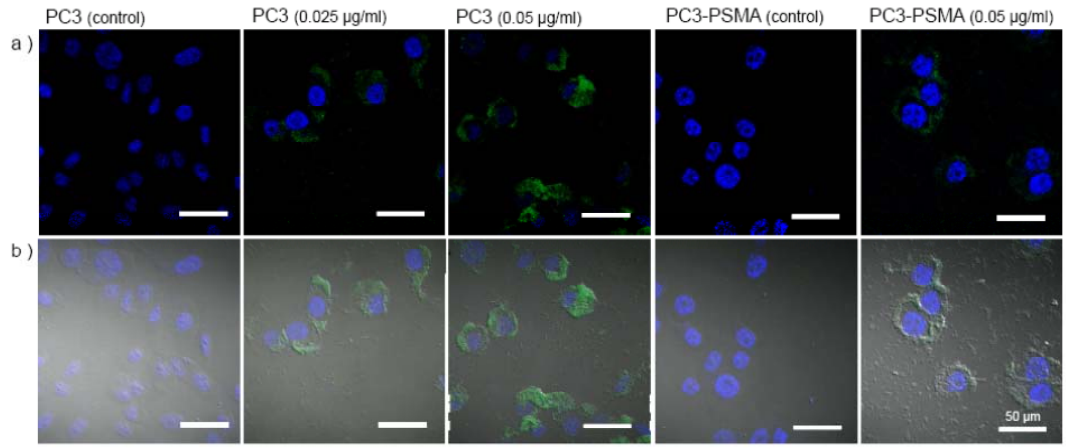

Figure 4.9

Cellular uptake of BODIPY 493/503 dye -loaded core-shell nanoparticles by PC3 and PC3-PSMA human prostate cancer cell lines following 5 h treatment. Untreated PC3 and PC3-PSMA cells were used as controls. In all cases, cellular nuclei were stained using Hoechst 33258. The top row shows overlays of green (BODIPY) and blue (Hoechst) fluorescence images. The bottom row shows overlays of fluorescence images and their corresponding differential interference contrast (DIC) images.

Additionally, from figure 4.10 we can infer that the fluorescent dyes were present in the cytoplasm and at the same focal plane of the cancer cell nuclei, which is a consequence of nanoparticle internalization inside the cells. We saw the presence of the particles in the nuclear plane in approximately 60-90 min after incubation. Some BODIPY fluorescence in the cytoplasm could be due to the presence of dye that diffuses from the nanoparticles. However, the presence of punctate structures in the nuclear plane is a likely indication that the nanoparticles are present in cytoplasmic vesicles. Freely diffusing dye would likely show a

uniform spread throughout the cytoplasm, which is not the case. This demonstrated the capability of delivering molecules into cancer cells using the temperature sensitive composite nanoparticles. Eventually, this strategy can result in lower toxicities towards non-malignant cells and other organs in vivo. We next compared the ability of 17-AAG-containing polystyrene/PNIPAAm-silica core-shell nanoparticles (17-AAG-PS/PNIPAAm) to induce death in prostate cancer cells, and compared it with cell death induced by polystyrene-silica nanoparticles (PS), 17-AAG-loaded polystyrene-silica nanoparticles (17-AAG-PS) and polystyrene/PNIPAAm-silica nanoparticles (PS/PNIPAAm). Two-tailed student's t-test was employed to compare the two groups, 17-AAG- PS/PNIPAAm and PS/PNIPAAm.

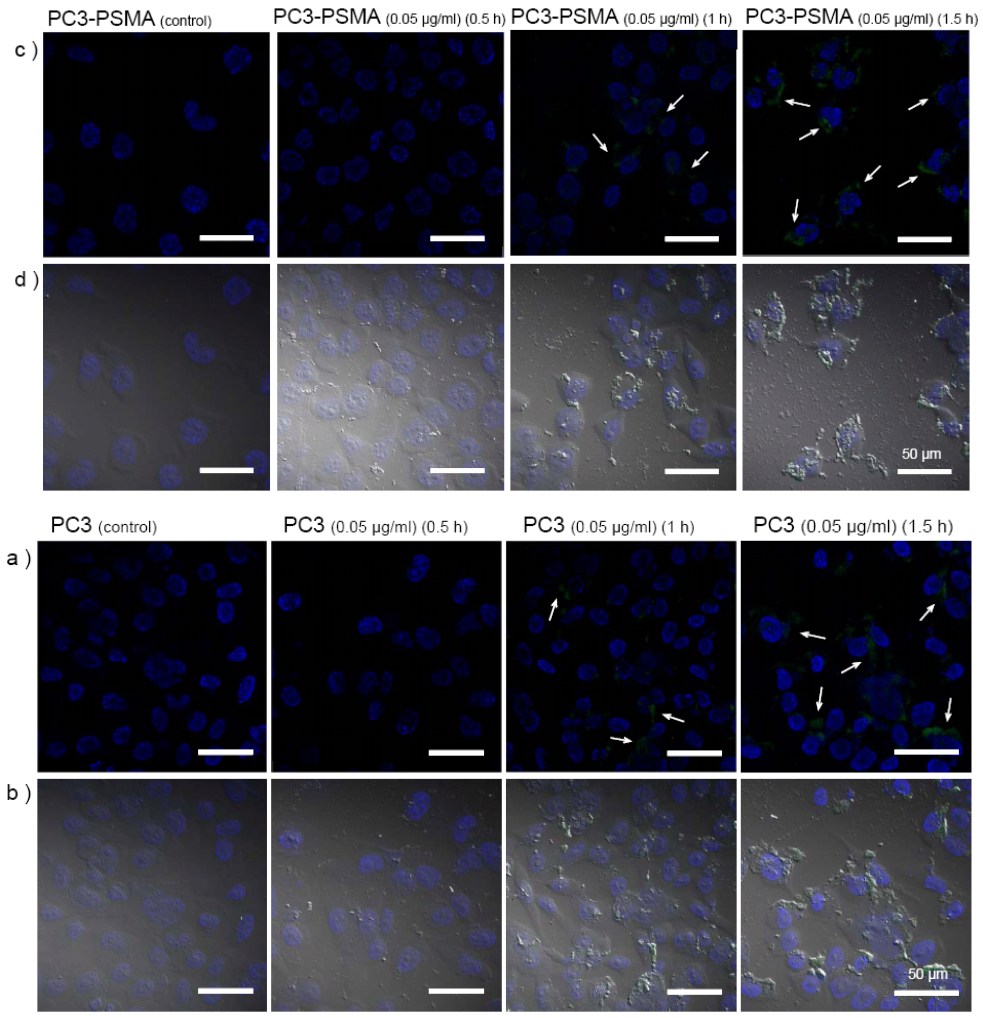

Figure 4.10.

Cellular uptake of BODIPY 493/503 dye -loaded core-shell nanoparticles by PC3 and PC3-PSMA human prostate cancer cell lines following 0.5, 1 and 1.5 h treatment. Untreated PC3 and PC3-PSMA cells were used as controls. In all cases, cellular nuclei were stained using Hoechst 33258. The top row (a and c) shows overlays of green (BODIPY) and blue (Hoechst) fluorescence images. The bottom row (b and d) shows overlays of fluorescence images and their corresponding differential interference contrast (DIC) images.

As seen in Figure 4.11a, thermoresponsive nanoparticles loaded with 17-AAG (17-AAG-PS/PNIPAAm) induced the greatest dose-dependent death in PC3 cells at nanoparticle dosages from 0.01 to 1 μg/ml compared to other nanoparticle formulations. Drug-loaded nanoparticles are minimally toxic at lower doses (0.01 μg/ml), but induce death in 35 – 90% of the PC3 population at doses from 0.03-0.3 μg/ml. This is statistically significant from other nanoparticle formulations tested under similar conditions (Figure 4.11a), indicating that uptake and drug release of the 17-AAG containing nanoparticles resulted in death of PC3 cells. The nanoparticles were not as efficacious in inducing death in PC3-PSMA cells compared to PC3 cells (Figure 4.11b). While 17-AAG containing nanoparticles demonstrated higher average losses in cell viability in PC3-PSMA cells compared to other nanoparticle formulations, these differences were not statistically significant except at the highest concentration (0.3 μg/ml). This can be explained in part by the susceptibility of this cell line to nanoparticles without the drug; while 'bare' nanoparticles do not result in loss of viability of PC3 cells, they induce death in a large population of PC3-PSMA cells in a dose-dependent fashion. In addition, previous results in our laboratory have demonstrated differential therapeutic efficacy in these cell lines due to differential intracellular trafficking and localization of nanoparticles (Barua & Rege, 2009; Barua & Rege, 2010). These differences in closely related cell lines underscore the role of the cancer cell phenotype in determining efficacy of delivered nanoparticle therapeutics and are currently under investigation in our laboratories. In addition, it is hypothesized that conjugation of prostate cancer cell specific biomolecules

(e.g. antibodies to the Prostate-Specific Membrane Antigen (Rege et al., 2007)) will help receptor-mediated uptake of these nanoparticles leading to increased efficacies.

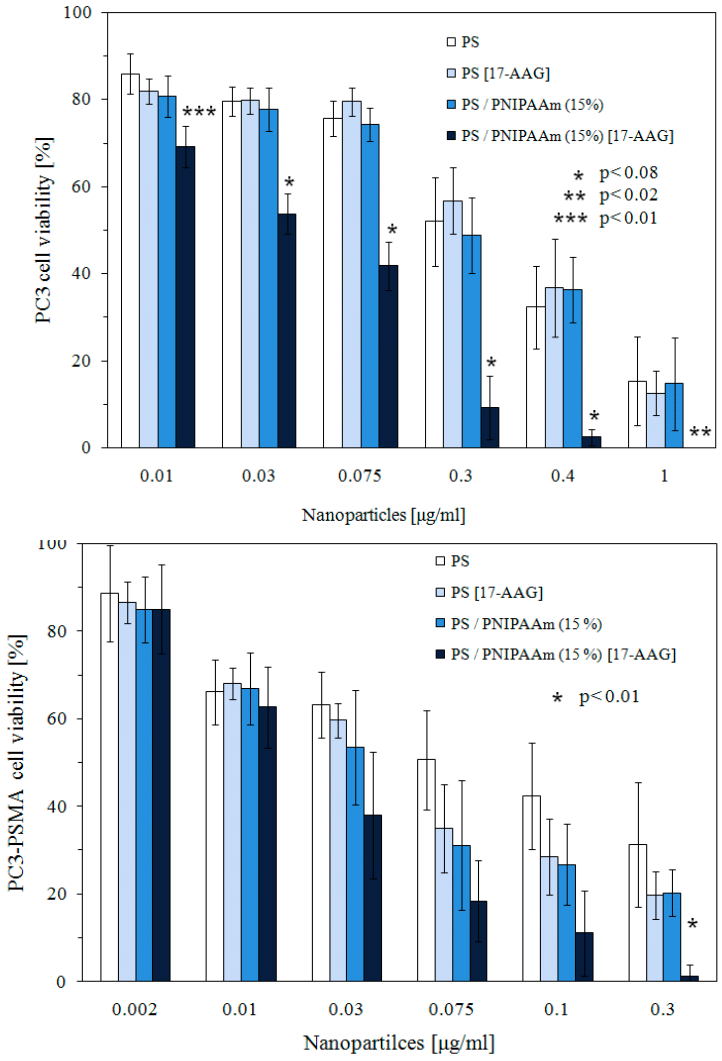

Figure 4.11

Cytotoxicity of 17-AAG loaded particles against prostate cancer cell lines (a) PC3 (b) PC3-PSMA Two-tailed student's t-test was employed to compare between 17-AAG-PS/PNIPAAm and PS/PNIPAAm treatment.

Additionally, above a concentration of 0.3 µg/ml of nanoparticle dosage considerable aggregation was observed as confirmed by DLS studies summarized in Figure 4.12. Over successively higher periods of time, the size of the composite nanoparticles increases drastically indicating aggregation. The zeta potential data were measured at pH 7. In water, there is no aggregation observed in various concentrations. However aggregation is observed in serum free media (SFM) at and above 0.3 µg/ml, possibly due to the high concentration of salt in the solution of SFM which may be classified as salt induced aggregation.

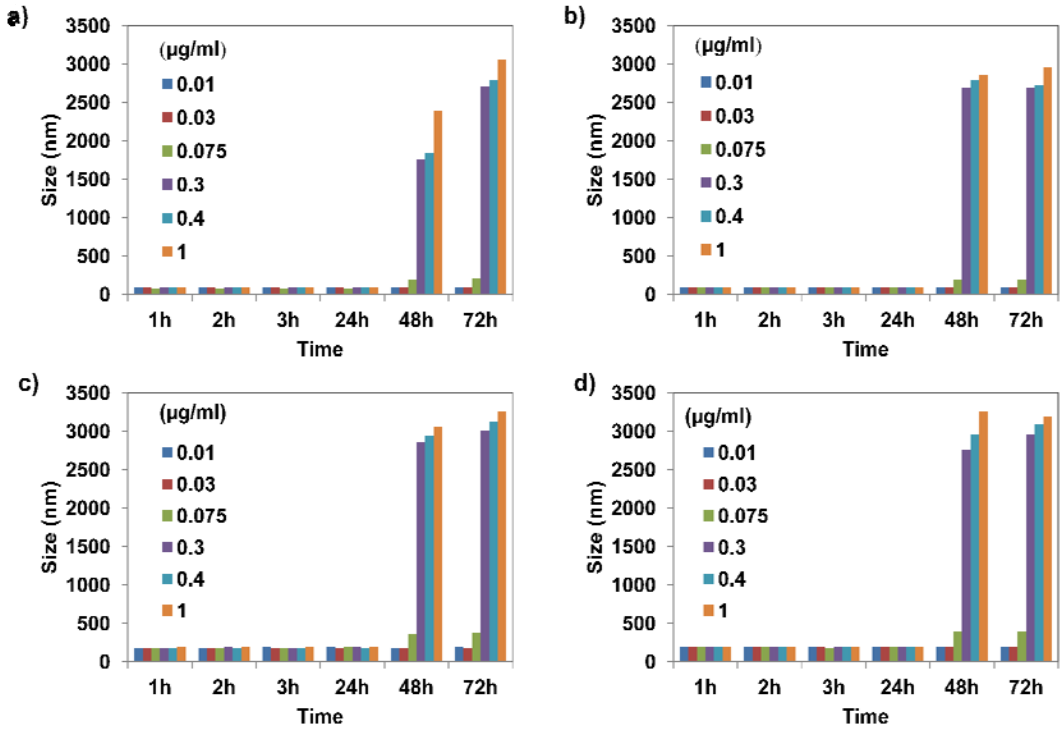

Figure 4.12

Stability of the composite nanoparticles in serum free media summarized by DLS studies each sub figure represents a particular type of composite nanoparticle:- (a) PS-PNIPAAm (b) PS-PNIPAAm (17-AAG) (c) PS (d) PS (17-AAG)

The focus of this section was to employ a unique drug delivery vehicle which can be taken up by cancer cells and can release the loaded drug. Polystyrene/PNIPAAm-silica core-shell nanoparticles were successfully synthesized with N-isopropylacrylamide incorporated into the core of the nanocomposite as a co-monomer. The work has demonstrated the temperature sensitivity, controlled drug release properties of the synthesized core-shell nanoparticles, and their effectiveness for inducing death of human prostate cancer cells. The collapse of the PNIPAAm resulted in the shrinkage of composite particles at temperatures above the LCST which makes them promising as a unique drug delivery vehicle. The next chapter will focus on further understanding of modification of the transition temperature of the composite particles to just above physiological temperature (i.e. 37 °C) for *in vivo* drug delivery for destruction of the human prostate cancer tumors.

Chapter 5

TUNING THE TRANSITION TEMPERATURE OF POLY(N-ISOPROPYLACRYLAMIDE) BASED CORE-SHELL COMPOSITE NANOPARTICLES

5.1 Introduction

The focus of this chapter is to tune the transition temperature of the thermo-responsive composite core-shell nanoparticles synthesized using Pickering emulsion polymerization. As discussed in the previous chapter, the synthesized PS/PNIPAAm-silica core-shell nanoparticles are temperature sensitive with a transition near 32°C in pure water; an increase of the N-isopropylacrylamide monomer enhances the degree of transition. PNIPAAm is a well-understood temperature sensitive gel, which undergoes volume shrinkage at a transition temperature (lower critical solution temperature (LCST)) of approximately 32°C in pure water (Lee et al., 2007). This temperature effect is due to the disruption of hydrogen bonds with water and the increasingly hydrophobic interactions among isopropyl groups (Qiu & Park, 2001). One specific goal of the work is to investigate how to manipulate the transition temperatures of the polystyrene/PNIPAAm-silica composite nanoparticles, and what the effects of crosslinker, co-monomer, surfactant, and co-solvent are on their transition temperature and dimension change. The ease of changing the transition temperature and thus the stimulus response of these composite nanoparticles can consequently make them suitable for temperature responsive applications. By making these composite nanoparticles tunable to a particular temperature range

would significantly expand their applications as sensing probes, functional materials, and drug delivery vehicles. In addition, such tunability has been less explored at the nanoscale, especially in a complicated structural hierarchy. For example research has been done on bulk PNIPAAm, to change the transition temperature for various applications: Kanazawa et al. (1997) recognized the possibility of changing the LCST parameter through the addition of different chemical groups. Kanazawa's group investigated the reversible changes of PNIPAAm once modifying it with a carboxyl end. They attached the carboxyl-terminated PNIPAAm chains to (aminopropyl)silica and used it as packing material for HPLC analysis of steroids. Similarly, Okano's group (1996) expanded on their success by using different modifiers to enhance hydrophobicity of bulk PNIPAAm through the attachment of butyl methacrylate (BMA), a hydrophobic comonomer. In this work, we comprehensively attempt to change the transition temperature of the composite nanoparticles using facile methods during as well as post synthesis.

5.2 Experimental

Materials

The following materials are used for the core-shell composite nanoparticle synthesis: IPA-ST (Nissan Chemicals), which is a dispersion of 10-15 nm silica nanoparticles in 2-isopropanol at a concentration of 30-31 wt %. Nonionic azo initiator VA-086 (98%, 2,2-azobis(2-methyl-*N*-(2-hydroxyethyl)propionamide), Wako Chemicals), styrene monomer (99.9%, Fisher), N-isopropylacrylamide monomer (NIPAAm, 97%, Aldrich), N,N,-dimethylaminoethylmethacrylate

(DMA, Polysciences, Inc.) water (HPLC grade, Acros Organics), and N-N'-methylenebisacrylamide (MBA, 99.5%, Fluka) were used in the polymerization without further purification.

After the synthesis, sodium dodecyl sulfate (SDS, 99.7% Fisher Scientific), Cetyl tetra ammonium bromide (CTAB, 99.8% Sigma Aldrich), Triton X-100 (laboratory grade, Sigma Aldrich), methanol (99.5%, Acros Organics), and tetrahydrofuran (THF, 99.9%, Acros Organics), were used, respectively, without further purification.

Materials Synthesis

Water, IPA-ST, NIPAAm and styrene were agitated mechanically with an IKA Ultra Turrax T25 homogenizer at 10,800 rpm for 2 min in an ice bath to emulsify. The emulsion was then degassed with nitrogen and kept in a nitrogen atmosphere under magnetic stirring. When the temperature was raised to 70 °C, the initiator aqueous solution was added to start the polymerization, which lasted for 5 hours. A typical formulation of the thermo-responsive nanoparticle includes 0.66 g NIPAAm, 3.76 g styrene, 32 mL water, 4.1 g IPA-ST silica nanoparticle dispersion, and 0.037 g initiator VA-086. Before characterization, the synthesized nanoparticles were washed twice by centrifuging-redispersing cycles using an Eppendorf 5810R centrifuge.

Characterization Techniques

Particle size distributions of the composite nanoparticles were measured using a Brookhaven 90Plus Particle Size Analyzer with the dynamic light scattering (DLS) technique. The washed composite nanoparticles were further

dispersed in water to appropriate concentrations before measurements. The specimens for scanning electron microscope (SEM) were then sputter coated with gold and viewed by SEM-XL30 (FEI). Specimens for SEM experiments were prepared by placing a droplet of the nanoparticle samples onto mica substrates and dried in air. Fourier transform infrared spectra (FTIR) were scanned over the range of 400-4000 cm^{-1} with potassium bromide pellets on a Bruker IFS 66V/S FTIR spectrometer. Surface tension measurements were conducted using an Attension 701 tensiometer using the Du Nuoy ring method.

5.3 Results and Discussion

5.3.1 Polystyrene/PNIPAAm-silica core-shell nanoparticles

The hydrodynamic sizes of polystyrene/PNIPAAm-silica of core-shell nanoparticles were measured by DLS at different temperatures, and the results are shown in Figure 5.1. The hydrodynamic sizes of the nanoparticles decreases as the temperature increased from 25°C to 40°C, and the transition temperature for the various compositions of nanoparticles is observed to be 32°C. This is consistent with the recently reported composite microspheres with a PNIPAAm core and a silica shell made by inverse suspension polymerization, which also show a volume transition starting at 32°C (Duan et al., 2009). They reported that the phenomenon was most likely due to the fact that silica particles are physically adsorbed on the surfaces of PNIPAAm microspheres. Thus, there is no chemical bond formation with silica which might change the transition temperature. Interestingly, the co-polymerization with styrene here has no significant effect on the transition temperature as well. One hypothesis is the relative phase separation

of PNIPAAm and polystyrene within the core. Duracher et al. studied PNIPAAm-polystyrene microparticles and suggested a PNIPAAm-rich shell and a polystyrene-rich core structure by analyzing SEM images taken during the reaction (Duracher et al., 1998). Such phase separation may also occur in the core of the composite nanoparticles here, although detailed morphology is difficult to reveal.

Figure 5.1 also suggests that when the concentration of the PNIPAAm is high, the maximum diameter change is more significant. Control experiments of polystyrene-silica nanoparticles did not show a size transition over a temperature range of 25-45°C (data not shown). The percentage dimension change of the nanoparticles vs. the amount of NIPAAm monomer in the synthesis is shown in the inset of Figure 5.1. Over the experimental range, there seems to exist a linear relationship, which reveals a simple way to tune the degree of the transition.

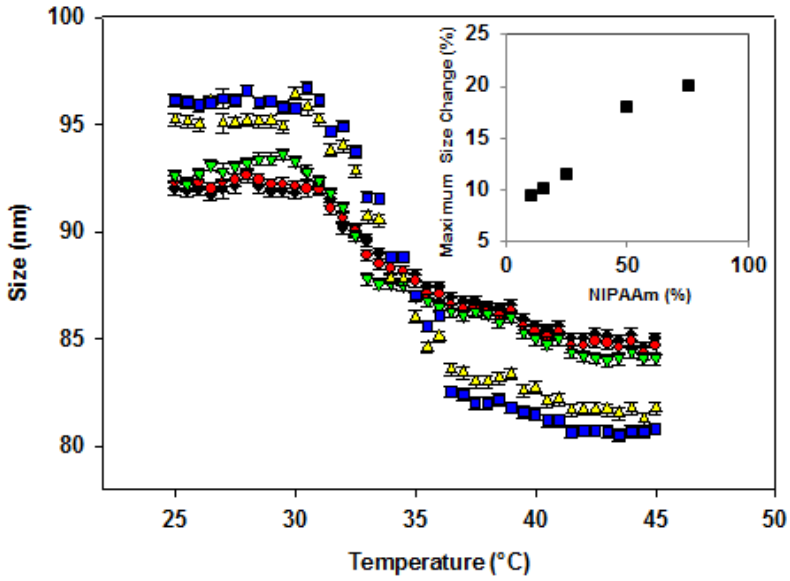

Figure 5.1

Dependence of average diameter of the composite nanoparticles on temperature. Each colored symbol signifies a different amount of NIPAAm percentage used during synthesis: blue squares for 75%, yellow triangles for 50%, green inverted triangles for 25%, red circles for 15% and black diamonds for 10%of NIPAAm. The error bars show standard deviations of particles made in three different batches. The inset shows the maximum size change of the composite nanoparticles as a function of the amount of NIPAAm content in the synthesis.

5.3.2 Effect of a crosslinker or an additional co-monomer

We next evaluate the effect of a crosslinker or an additional co-monomer on the thermal transition of the composite nanoparticles. A crosslinker, N-N'-Methylenebisacrylamide (MBA), was incorporated into the synthesis. Figure 5.2 shows that with successively higher crosslinker content, the transition temperatures and the degree of size transition change in different directions. The

temperature dependent hydrodynamic radius shows a continuous decrease when approaching the transition temperature. The results indicate that there is only a slight increase in the transition temperature with increasing crosslinker amount; this implies that the transition temperature is only slightly influenced by the network crosslink density. As anticipated, the composite nanoparticles with a lower crosslinker content are more "flexible" in nature having a greater size transition. As the figure reveals, the composite nanoparticles with the highest crosslinking amount undergo the most ''flat" transition, the more crosslinker present, the more the "rigidity" of the composite nanoparticles, making the amount of volume transition lesser. These results for composite nanoparticles are in fact similar to macrogels. As investigated by Burmistrova et al. for crosslinked PNIPAAm-co-AAm, the amount the volume transition decreases with increasing cross-linker content due to decreasing polymer chain length between two cross-linkers and as a consequence increases the gels stiffness (Burmistrova et al., 2011).

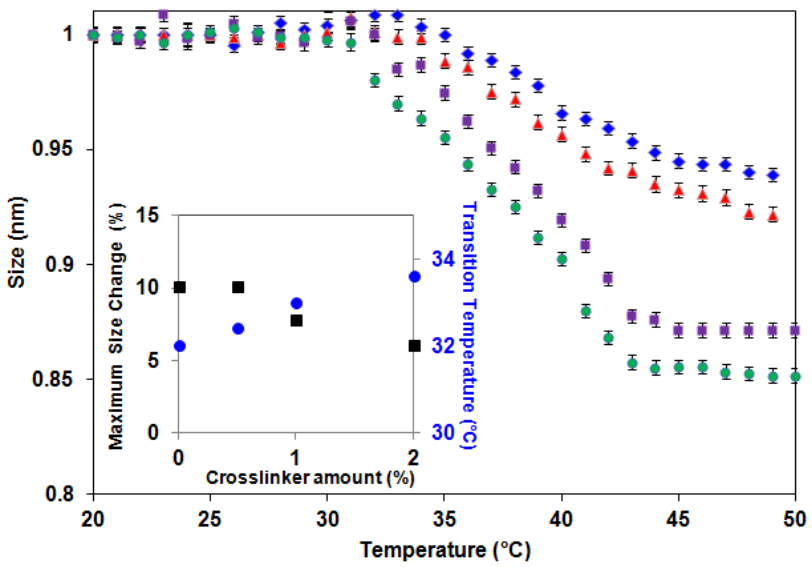

Figure 5.2

Normalized hydrodynamic radius of the composite nanoparticles showing the effect of crosslinker MBA. (Each colored symbol signifies a different amount of MBA percentage used during synthesis; blue diamonds for 2%, red triangles for 1%, purple squares for 0.5% and green circles for 0%). The amount of NIPAAm present in the synthesized composite nanoparticles was 15% as represented in these graphs. Inset shows the relationship between the amount of crosslinker (MBA) with the maximum size change and transition temperature.

Next, we investigate the addition of a co-monomer in the synthesis process to tune the transition temperature of the composite nanoparticles. The temperature effect of the PNIPAAm is due to the disruption of hydrogen bonding with water and increasing hydrophobic interactions among isopropyl groups when temperature increases. In order to raise the transition temperature of the nanoparticles, we hypothesize that an inclusion of an additional hydrophilic

polymer is suitable. It is known that the LCST of bulk PNIPAAm can be tailored by controlling the incorporation of hydrophilic (Zhang et al., 2007) or charged (Tian et al., 2008) co-polymeric components. The additional hydrophilic nature shall increase the tendency of the nanoparticles to hydrogen bond with water thus the contraction in size is hypothesized to occur at a higher temperature.

Bulk composite materials containing copolymers of NIPAAm and DMA have been reported (Aguilar et al., 2007) to have increasing values of transition temperature with increasing DMA content. A similar example shows that when NIPAAm is copolymerized with hydrophilic monomers such as acrylamide (AAm), the transition temperature increases up to about 45ºC when 18% of AAm is incorporated, whereas the transition temperature decreases to about 10ºC when 40% of hydrophobic N-tert-butylacrylamide (N-tBAAm) is added (Aguilar et al., 2007). In this study, we have tried to employ poly (N,N,-dimethylaminoethylmethacrylate (PDMA), which has a LCST of ~50 ^{o}C (Orakdogen, 2011) in order to change the transition temperature of the PNIPAAm based composite nanoparticles. Other polymers with thermoresponsive properties include poly(N,N-diethylacrylamide) (PDEAAm) with an LCST over the range of 25 °C to 32 °C, poly(N-vinlycaprolactam) (PVCL) (Orakdogen, 2011) with an LCST between 25 °C and 35 °C. To increase the transition temperature close to the body temperature (37°C) for future potential use in drug delivery we choose DMA as a comonomer.

Figure 5.3 shows that by incorporating 1.5%, 3% and 6%, DMA monomer, respectively, during the synthesis, the resulting composite

nanoparticles showed an increase in transition temperatures. We anticipate the transition temperature of the composite nanoparticles to change using a simple formula using weighted averages:

$$T = \frac{T_1(X_1) + T_2(X_2)}{X_1 + X_2}$$

Where T is the transition temperature of the composite nanoparticle with varying monomer content. T_1 is the LCST of PDMA, T_2 is the LCST of PNIPAAm, X_1 is the amount of DMA, and X_2 is the amount of NIPAAm used in the synthesis process before. Figure 5.3 suggests that the calculated and experimental values are reasonably consistent over the experimental range.

In their classical study of the LCST of water-soluble polymers, Taylor and Cerankowski proposed as a general rule that the LCST will increase with increasing hydrophilicity of the polymer (Taylor & Cerankowski, 1975). At low temperatures, hydrogen bonding between the hydrophilic segments of the polymer chain and water molecules is dominant, leading to enhanced dissolution in water (Qiu & Park, 2001). The increase in temperature causes partial displacement of water from the polymer coil, weakening the hydrogen bonds, and an increase of the hydrophobic interactions between the hydrophobic segments of the polymer macromolecules (Markicheva et al., 1991). Consequently, the polymers collapse, aggregate, and phase separate because the intra- and intermolecular hydrogen bonds between the hydrophobic parts of the polymer molecules are favored compared to the water molecules, which are re-organized around the non-polar polymer. Similarly we can apply this concept to our system and find that it leads to the shift of transition temperature to higher values. When increasing the

amount of DMA in the reaction, the synthesized material becomes more hydrophilic and forms more hydrogen bonds between the polymer sections and water molecules, requiring more energy to break these hydrogen bonds between the prepared composite nanoparticles and water, therefore exhibiting a higher transition temperature.

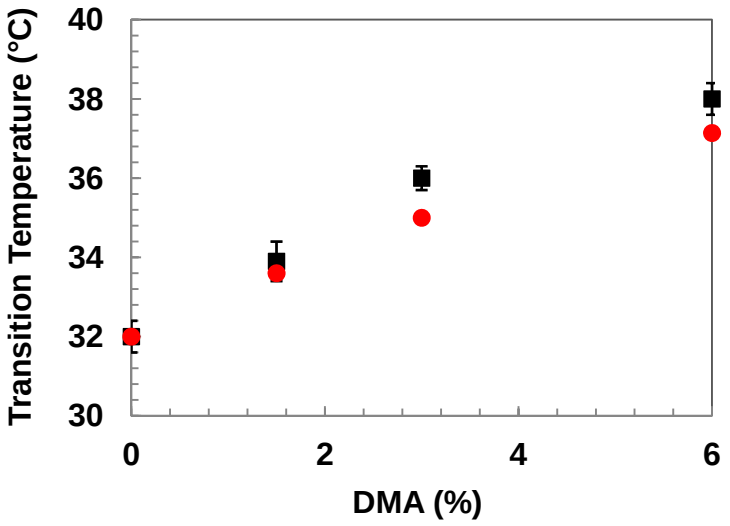

Figure 5.3

The effect of the co-monomer DMA on the transition temperature of the synthesized composite nanoparticles. The red circles are the calculated values and the black squares are the experimental results.

5.3.3 Effect of surfactants on transition temperature

We discussed in the previous section how interactions with hydrophilic or hydrophobic components are known to be essential for inducing a change in the transition temperature of PNIPAAm. In this section we examine the employment of surfactants in post synthesis situations and how they affect the transition temperature of the polystyrene/poly(N-isopropylacrylamide) (PNIPAAm)-silica

core-shell nanoparticles. In general, the entropy of a system should increase with a rise in temperature. In the case of PNIPAAm, as the temperature is raised, the polymer network shrinks to a compact state and its entropy decreases. The entropy decrease of the network should be compensated by an increase of entropy of the water molecules (Kokufuta et al., 1993). It is then expected that a chemical compound in the water with hydrophilic and hydrophobic characters should affect the phase transition properties of PNIPAAm.

Surfactants are well suited for this purpose as they contain both hydrophobic and hydrophilic parts. Surfactants are compounds that lower the surface tension of a liquid, the interfacial tension between two liquids, or that between a liquid and a solid. Surfactants may act as detergents, wetting agents, emulsifiers, foaming agents, and dispersants. Surfactants are usually organic compounds that are amphiphilic, meaning they contain both hydrophobic groups (their tails) and hydrophilic groups (their heads). Therefore, a surfactant contains both a water insoluble (or oil soluble) component and a water soluble component. Surfactants will diffuse in water and adsorb at interfaces between air and water or at the interface between oil and water, in the case where water is mixed with oil. The insoluble hydrophobic group may extend out of the bulk water phase, into the air or into the oil phase, while the water soluble head group remains in the water phase. This alignment of surfactants at the surface modifies the surface properties of water at the water/air or water/oil interface.

In this work, the effects of anionic (SDS), cationic (CTAB) and non-ionic (Triton X-100) surfactants were studied. The composite nanoparticles were

equilibrated in various concentrations of these surfactants and we then examine their transition temperatures as shown in Figure 5.4.

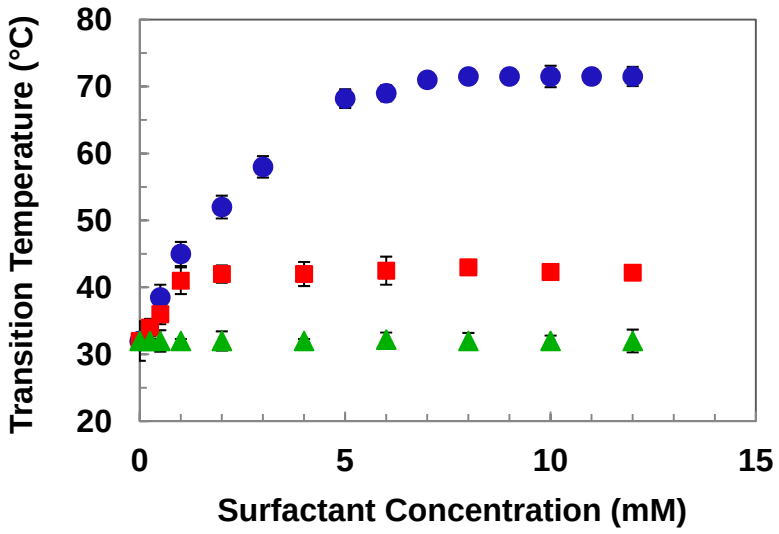

Figure. 5.4

Transition temperatures as a function of the concentration of surfactants, SDS, CTAB and Triton X-100, respectively. The blue circles are for SDS, red squares for CTAB and green triangles for Triton X-100.

The nonionic surfactant does not induce a change in the transition temperature of the composite nanoparticles. It is likely due to the absence of electrostatic interactions between the nonionic surfactant and the composite nanoparticles. Triton X-100 essentially belongs to the class of long chain alcohols and is generally a polyoxyethylene glycol octylphenol ether (C_8H_{17}–(C_6H_4)–(O-C_2H_4)$_{1–25}$–OH). This compound does not have electrostatic interactions as it does not contain any ionic sub group in structure. Another relevant explanation is that Triton X-100 did not complex with the composite nanoparticles to be able to change their nature to hydrophilic or hydrophobic

(Tam et al., 1994). Therefore it does not affect the transition temperature of the composite nanoparticles.

5.3.4 Effect of co-solvent on the transition temperature

The dependence of the transition temperature of dispersions of composite nanoparticles on solvent composition are examined and compared to the reported PNIPAAm bulk behavior in similar solvent mixtures. We chose methanol and THF as solvents for studying the phase transition of the composite temperature sensitive nanoparticles. These solvents were mixed with water and the composite nanoparticles were equilibrated in them. The transition temperatures of these nanoparticles were then measured using the DLS technique detailed previously. With the addition of methanol there is an initial depression of the transition temperature below volume fraction of ~0.5 and then a sudden increase above volume fraction of ~0.5 (Figure 5.5). The experimental measurements are limited due to the temperature limitation of our DLS instrument. The results observed for our composite nanoparticles are well in accordance with previously reported phenomena by analyzing the cloud points for bulk PNIPAAm exhibiting cononsolvency in mixed aqueous solutions using a spectrophotometer (Winnik et al., 1990). Detailed work explaining the driving force for cononsolvency is the preference of water to complex with methanol rather than with bulk PNIPAAm gel has been done by Schild et al. (Schild et al., 1991) Their results have also been digitized and overlayed in Figure 5.5 to draw direct comparisons.

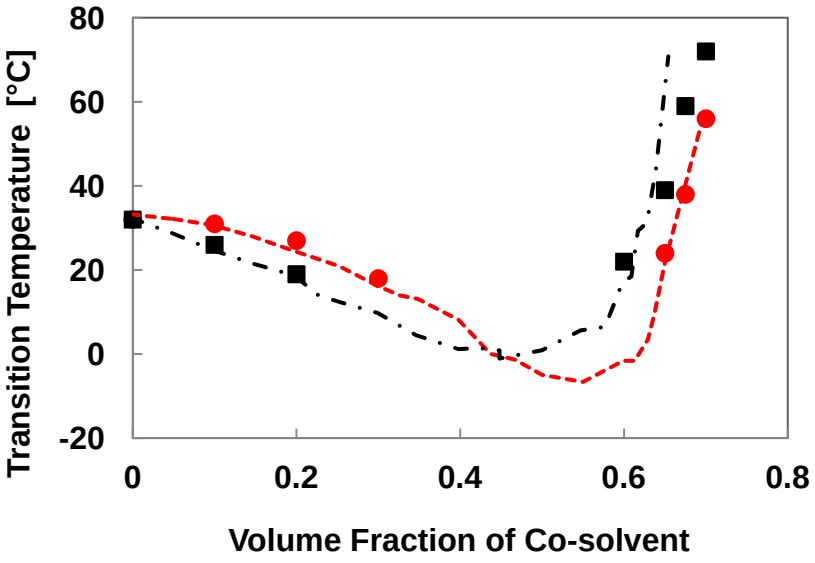

Figure.5.5

*Effect of co-solvents on the transition temperatures of the composite nanoparticles. Black squares are using THF as a solvent and red circles are using methanol as a solvent. Comparison with bulk PNIPAAm gels in mixed aqueous is included by digitizing the experimental data published by Schild et al. (Figure 2 in reference) and overlaying their results (represented by lines) with our work on the composite nanoparticles***.**

The transition temperatures of the composite nanoparticles decrease with increase in concentration of methanol until ~50% methanol, beyond that the transition temperatures increase sharply. It has been discussed previously that the relevant interactions must arise from local contacts between polymer and solvent. The nature of solvent structure of methanol-water mixtures has been studied extensively (Winnik et al., 1990; Schild et al., 1991). At low methanol concentration, water molecules form a disordered tetrahedral structure around an alcohol molecule (Crowther & Vincent, 1998) and water-methanol form a cage-

like hydrated clathrate complex. These clathrate structures compete with PNIPAAm for the water molecules that hydrate the polymer. Due to removal of the water molecules from the interior of the composite nanoparticles to form the clathrate structures, the transition temperature keeps decreasing. However once the methanol amount dominates above 0.5 volume fraction, the transition temperatures increase for higher amounts of methanol in the system. This is in accordance with expected behavior of PNIPAAm in mixed aqueous solutions because methanol is a better solvent than water for PNIPAAm (Hirotsu, 1987). This means as the methanol content increases there is no longer enough water to form clathrate structures for all the methanol molecules, i.e. not enough water to provide spaces for all the methanol molecules. These methanols are now free to interact with polymer segments. This implies that the methanol-polymer interactions become stronger which in turn increases the transition temperature of the composite nanoparticles. Changes in transition temperatures of the composite nanoparticles observed for increasing volume fractions of methanol reveal the importance of the free energy of association in methanol-polymer, water-polymer, and methanol-water. Calculations based on the Flory-Huggins solution theory suggest that the cononsolvency phenomenon occurs from perturbation between water-methanol interactions. Also it seems likely that the water-methanol complexes are preferred to the typical PNIPAAm-water hydrogen bonds resulting in the observed transition phenomena of the system. We have also performed a similar study using THF in water solvent mixtures and observed a similar trend as those of water-methanol mixtures, as included in Figure 5.5.

5.4 Conclusion

The focus of this work is to synthesize thermo-responsive composite core-shell nanoparticles using Pickering emulsion polymerization and more importantly, to tune the transition of these nanoparticles. The synthesized polystyrene/poly(N-isopropylacrylamide) (PNIPAAm)-silica core-shell nanoparticles are temperature sensitive with a transition near 32°C in pure water; an increase of the N-isopropylacrylamide monomer enhances the degree of transition. In addition, the transition temperature can be tuned using facile approaches such as incorporating a crosslinker or co-monomer during the synthesis and by adding a surfactant and co-solvent in the media. The work also suggests that tunability of the transition temperature of these composite nanoparticles follow similar mechanisms like those at the macroscopic level.

Chapter 6

OTHER RESPONSIVE PROPERTIES OF CORE-SHELL COMPOSITE PARTICLES

6.1 pH Responsive Composite Nanoparticles for Oil-Water Interfacial Engineering

Introduction

The recent oil spill (largest spill in history) in the Gulf of Mexico has caused a tremendous and unpredictable environmental disaster. The catastrophic explosion caused discharges of up to 100,000 barrels per day and the oil slick already covers a surface area of 10,000 square miles (Farrell, 2011). Other than the emergency of stopping the oil leak, there is also an urgency to generate effective, efficient and environmentally benign solutions to clean-up the massive spill. Traditional major oil clean-up techniques include controlled burning, utilizing dispersants and bioremediation (http://en.wikipedia.org/wiki/Oil_spill). Although these have been in practice for years, each has significant disadvantages, or may not be applicable for the current massive oil spill. For example, controlled burning is limited to small areas and causes significant air pollution; dispersants break oils into small droplets to be carried away by water current but cause significant water and deep-water contamination; bioremediation often uses microorganisms such as bacteria to decompose oil but doesn't produce short-term results, is pollute-site specific, and only targets certain ingredients of crude oils. It is also worthwhile to note that all of the above only "clean-up" the surface but do not recover oil. There is a critical call for innovative solutions to

meet the challenges to clean-up and recover massive and unpredictable oil spills such as the current disaster in the Gulf of Mexico. This work focuses on performing novel interfacial engineering through functionalized nanoparticles. Surfactants are well-known for equilibrating at oil-water interfaces and serving as emulsion stabilizers (Adamson, 1982; Israelachvili, 1991). In addition to surfactants, as discussed previously in this dissertation, solid particles were identified as a new type of emulsifying agent since the pioneering study by Pickering in 1907 (Pickering, 1907). Recently, there have been growing interests (Lin et al., 2003; Dinsmore et al., 2002; Velev & Nagayama, 1997; Wang & Hobbie, 2003; Melle, et al., 2005; Binks & Lumsdon, 2001; Shah et al., 2003; Binks & Lumsdon, 2000; Tarimala & Dai, 2004; Dai et al., 2005; Ma & Dai, 2009; Dai et al., 2008; Ma & Dai, 2009; Ma & Dai, 2010; Ma et al., 2010) in investigating the particles at oil-water interfaces, for example, Pickering emulsions, due to potential tremendous applications. Here, composite nanoparticles, instead of surfactants, were employed to equilibrate at oil-water interfaces (illustrated in Figure 6.1), with an ultimate objective to subsequently engineer the interface and separate/recover the oil layer.

As previously detailed in this dissertation studies have demonstrated that polystyrene (PS)/poly(N-isopropyacrylamide) (PNIPAAm)-silica core-shell nanoparticles synthesized using Pickering emulsions as templates are temperature responsive (Ma et al., 2010) and the responsiveness of the particle diameter increases with increasing the percentage of NIPAAm, as shown in Figure 4.5. More importantly, these core-shell nanoparticles only release drugs (17-

(Allylamino)-17-demethoxygeldanamycin) at an elevated temperature ("smart" in responsive of a temperature change, Figure 4.6).

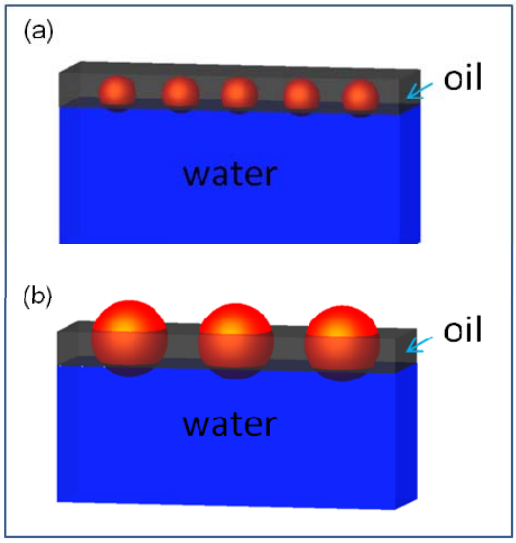

Figure 6.1

Functionalized nanoparticles/ particles equilibrate at oil-water interfaces; they will be designed to either (a) completely immerse in or (b) protrude out of the oil layer.

Similar to the encapsulation of a drug into the PS/PNIPAAm-silica core-shell nanoparticles in Figure 4.7, a rheological thickener, such as hydrophobically modified ethoxylated polyurethane based thickeners (HEUR) (Orgiles-Calpena et al., 2009) can be encapsulated into the pH sensitive composite nanoparticles. It is important to note that rheological modifiers have already been used in certain oilfield treatments such as fracturing and gravel packing. In this research, the rheological thickener is anticipated to be released when the nanoparticles equilibrate at the oil-water interface and environmentally respond to pH.

The aim of this section is to synthesize stable, aqueous dispersions of nanoparticles that respond to pH. For bulk pH sensitive material, the equilibrium degree of swelling can be changed suddenly by several orders of magnitude near the acidity constant of the material (Figure 6.2). Example of monomers used for pH sensitive polymers include acrylic acid, p-styrene sulfonic acid, crotonic acid, vinyl pyridine and aminoethyl methacrylate.

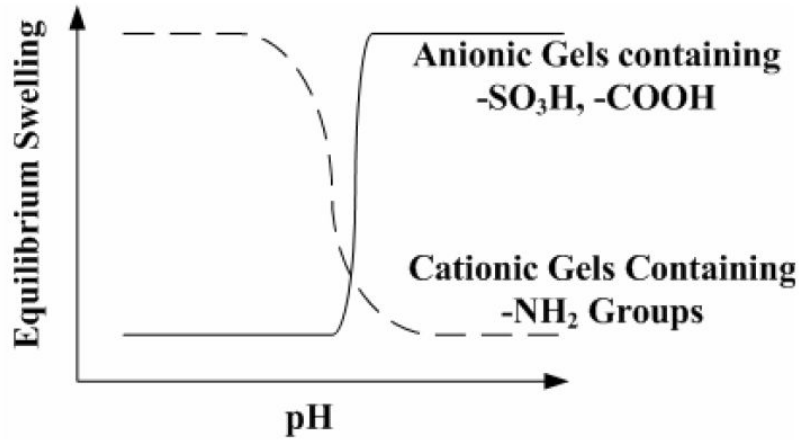

Figure 6.2

Schematic of equilibrium swelling versus pH for pH sensitive polymers. (Adapted from Scranton et al., 1993)

The synthesized pH responsive nanoparticles will encapsulate and release chemicals such as a rheology modifier which temporarily "thicken/solidify" the oil layer that can be removed by "skimming". Skimming is one practical technique to clean-up oil spills but only applies to calm water and the low oil viscosity challenges such a practice; the temporary thickening of the oil layer and the embedding of the nanoparticles will make it feasible. For example,

polystyrene (PS) /poly(N,N,-dimethylaminoethylmethacrylate) (PDMA)-silica nanoparticles will be synthesized to validate the pH responsiveness to sea water: at low pH, the PDMA is hydrophilic whereas at high pH, it is hydrophobic (Dai et al., 2008; Zhang et al., 2008) and the transition pH (approximately 7.6) is in the range of sea water.

pH responsiveness of the composite nanoparticles.

It is known that pH sensitive or pH responsive polymers are materials which will respond to the changes in the pH of the surrounding medium by varying their dimensions. Such materials swell or collapse depending on the pH of their environment. This behavior is exhibited due to the presence of certain functional groups in the polymer chain There are two kinds of pH sensitive materials: one which have acidic group like (-COOH, $-SO_3H$) and swell in basic pH, and others which have basic groups like ($-NH_2$) and swell in acidic environments (Shi et al., 2009). Polyacrylic acid is an example of the former and Chitosan is an example of the latter (Bonina et al., 2004). The mechanism of response is same for both, just the stimuli vary. The response is triggered due to the presence of ionizable functional groups (like -COOH, $-NH_2$) which get ionized and acquire a charge (+/-) in a certain pH. The polymer chains now have many similarly charged groups which cause repulsion and hence the material expands in dimensions. The opposite happens when pH changes and the functional groups lose their charge hence the repulsion is gone and the material collapses back.

In this study, a mixture of styrene (St) monomer, 2-*N,N*dimethylaminoethyl methacrylate (DMA) monomer, L-α-Phosphatidylcholine (lecithin) and VA-086 initiator was used as a dispersed phase and an aqueous phase containing water acted as the continuous phase. A mechanical stirrer was used to form the uniform droplets. Polymerization reaction occurred at 70 ◦C. Representative SEM images of the composite particles are shown in Figure 6.3. These nanoparticles were found to be sensitive to a pH stimulus. As can be seen from Figure 6.4 control polystyrene nanoparticles did not show any change of hydrodynamic diameter with a pH stimulus. However, for a concentration of 50% and 75% DMA the size of the nanoparticles decrease upon increasing the pH of the surrounding environment.

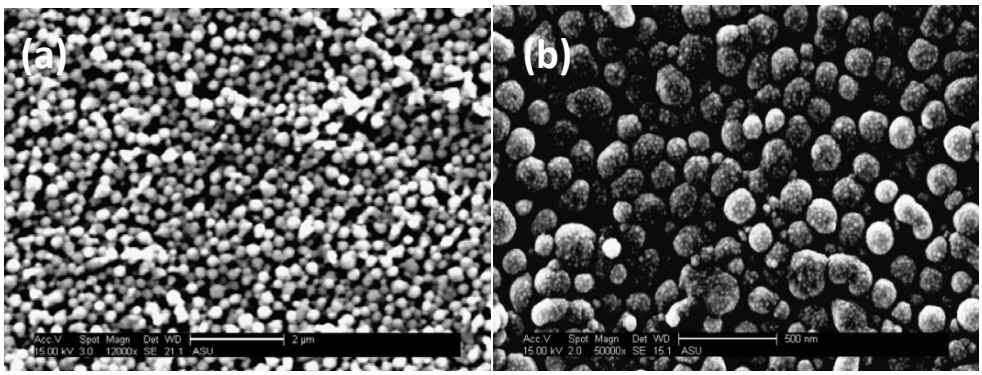

Figure 6.3

SEM images of the composite particles, the rough surface indicating silica outer coverage. Scale bars are (a) 2µm and (b) 500nm

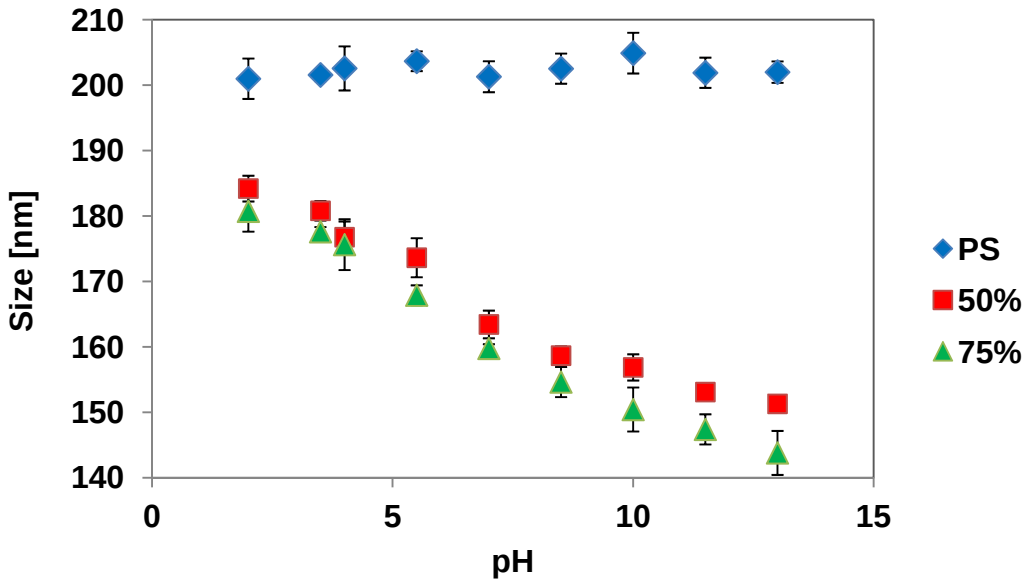

Figure 6.4

The dependence of average diameter of composite nanoparticles with different amounts of DMA on pH. The error bars show standard deviations of particles made in three different batches.

The nanoparticles exhibit pH-sensitive behavior due to protonation/de-protonation of *N*, *N*-dimethylaminoethyl groups in PDMA component of the composite. Owing to bearing weak acidic or basic groups that ionize in a given pH range of the swelling medium, investigations of the swelling behavior of pH-responsive gels has gained noticeable interests (Orakdogen, 2011). Since PDMA is a pH-responsive polybase and it has amine groups in its side chain, in recent years much more attention has been directed to pH-dependent swelling of PDMA (Dai et al., 2008; Zhang et al., 2008; Meng et al., 2009). The tertiary amine groups on PDMA are weakly basic (as they have a lone pair of electrons) and can gain protons under acidic condition and release them under basic condition. In the

structure of PDMA, the presence of hydrophobic basic group together with hydrophilic group makes it a special hydrogel which exhibits a combined pH- and temperature sensitivity.

The variations in the pH of the surrounding medium cause changes in the interactions between polymer chains or between polymer chains and solvent at the molecular level (Carlsson et al., 2010). pH-dependent swelling behavior of the composite PS/PDMA-silica nanoparticles were investigated in buffer solutions of various pH's. Since, in the molecular structure of PDMA, there is an active amino group with strong basicity, the protonation of the tertiary group could induce the size transition to change with changing pH. The tertiary amine groups on PDMA are weakly basic and thus, at room temperature, as the pH is lowered to the acidic region, the tertiary amine side chains of the polymer become protonated, increasing the charge density of the network and causing the PDMA to swell. This leads to the change in size of the composite nanoparticles as characterized by DLS.

Next, during the synthesis process lecithin was included as a starting material and the composite nanoparticles were synthesized with lecithin. The pH responsiveness of these composite nanoparticles was similarly characterized using DLS. The effect of loading lecithin in the nanoparticles was observed (Figure 6.5).

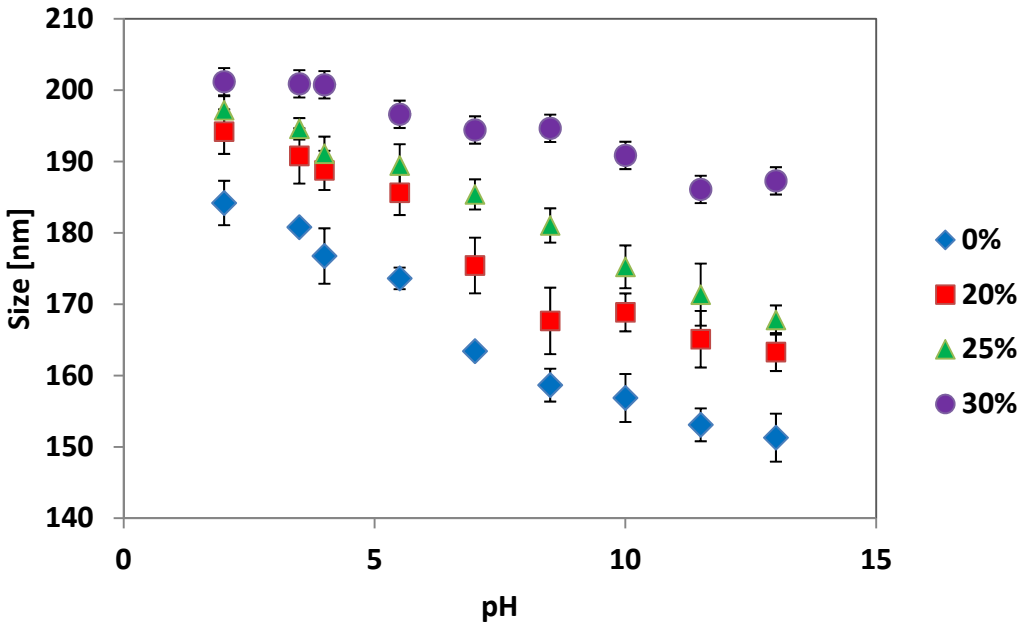

Figure 6.5

The dependence of average diameter of composite nanoparticles with different amounts of lecithin in 50% DMA particles on pH. The error bars show standard deviations of particles made in three different batches.

It was found that increasing the lecithin content leads to decrease in the sensitivity of the nanoparticles to the environmental pH. This is likely because lecithin is not pH sensitive and does not change in size with a pH stimulus. Interestingly, the size of the lecithin incorporated nanoparticles get larger when the amount of lecithin is increased. This is intuitive because just the lecithin content varies in the formulation of these nanoparticles.

Encapsulation and release of a rheology modifier

The science that studies the relation between the flow of materials and applied forces is called rheology. It is important during the processing and

application of innumerable products that occur in everyday life. Rheology properties control the sagging of adhesives, the settling of fillers, the stability of cosmetic emulsions or even the processability of concrete (Galan & Singer, 2011). Careful study of rheological properties using advanced instrumentation and theory is therefore of paramount importance. In case the bulk fluid does not have the desired rheological profile, a rheology modifier is needed to tune the properties of the fluid as needed. For example, lecithin has the property to shear thin water (Schipunov & Hoffman, 2000).

It was found that when the synthesized pH sensitive composite nanoparticles were loaded with lecithin, they show release when subjected to a pH stimulus. These composite nanoparticles were kept in a pH 7 and as well as pH 10 environment. Centrifugation was performed and the supernatants collected. These supernatants were taken as samples and rheology profiles were done on them using a TA Instruments AR-G2 rheometer equipped with a 60 mm cone. A rheometer is a laboratory device used to measure the way in which a liquid, suspension or slurry flows in response to applied forces. It is used for those fluids which cannot be defined by a single value of viscosity and therefore require more parameters to be set and measured than is the case for a viscometer. It measures the rheology of the fluid. Typically for samples with lower viscosity a cone type geometry is used. The sample subjected to a higher pH showed a shear thinning effect as expected from lecithin. However for control polystyrene nanoparticles as well as for lower pH no shear thinning was observed. This implies that lecithin

released from the pH stimuli induced composite nanoparticles has the ability to shear thin water. These results are summarized in Figure 6.6.

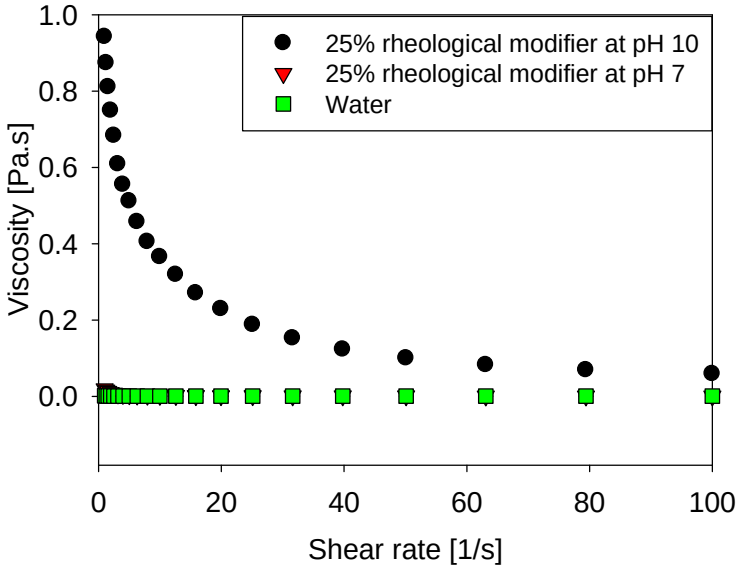

Figure 6.6

Release of lecithin from composite nanoparticles in water indicated by shear thinning flow curves for pH 10. No release observed for pH 7; water is the control.

To confirm lecithin release in water from the pH responsive nanoparticles Fourier transform infrared spectroscopy (FTIR) characterization was done. FTIR is a technique which is used to obtain an infrared spectrum of absorption, emission, or photoconductivity of a solid, liquid or gas. An FTIR spectrometer simultaneously collects spectral data in a wide spectral range. This confers a significant advantage over a dispersive spectrometer which measures intensity over a narrow range of wavelengths at a time. Water was tested as blank control. Next the pH responsive nanoparticles containing lecithin were divided into two

parts. The first part was kept in pH 7 solutions for 48 h and the second was kept in pH 10 solutions for 48 hours. These parts were then centrifuged to spin down the nanoparticles and the supernatants then extracted for making the test samples. It was found that for the higher pH samples characteristic peaks for lecithin were present as shown in Figure 6.7.

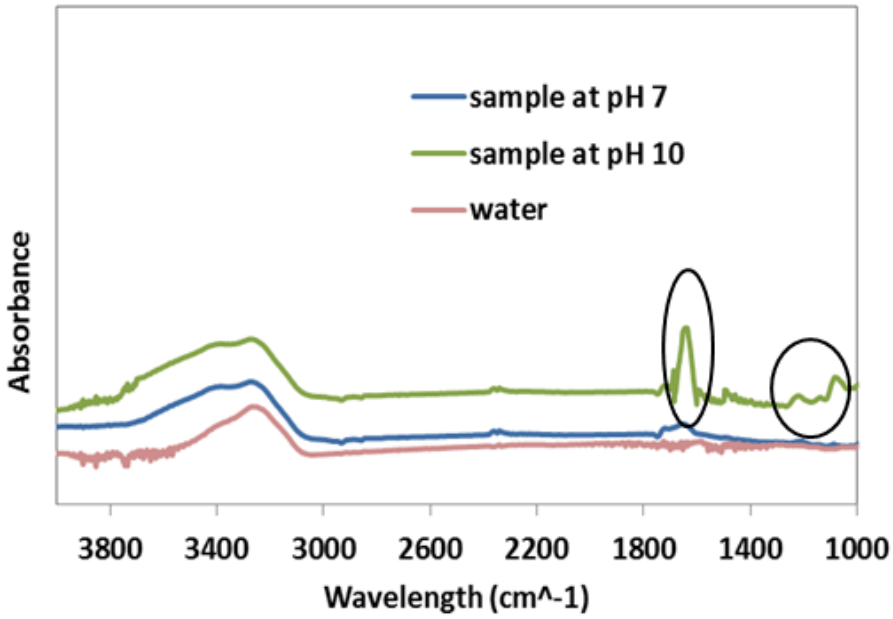

Figure 6.7

FTIR readings of water (control) samples of released lecithin from high pH 10 and no release from low pH 7.

These regions correspond to OH stretching vibrations between 3600–3000 cm^{-1} (high absorbance peak for water; –C=O stretching and OH bending vibrations between 1770–1500 cm^{-1}; and C–O–C, P–O–C and P=O stretching vibration between 1200–1050 cm^{-1}. For water and the sample subjected to lower pH no peaks for lecithin were observed. Once it was established that the released

lecithin can shear thin water we wanted to see if lecithin interacts with dodecane (Figure 6.8).

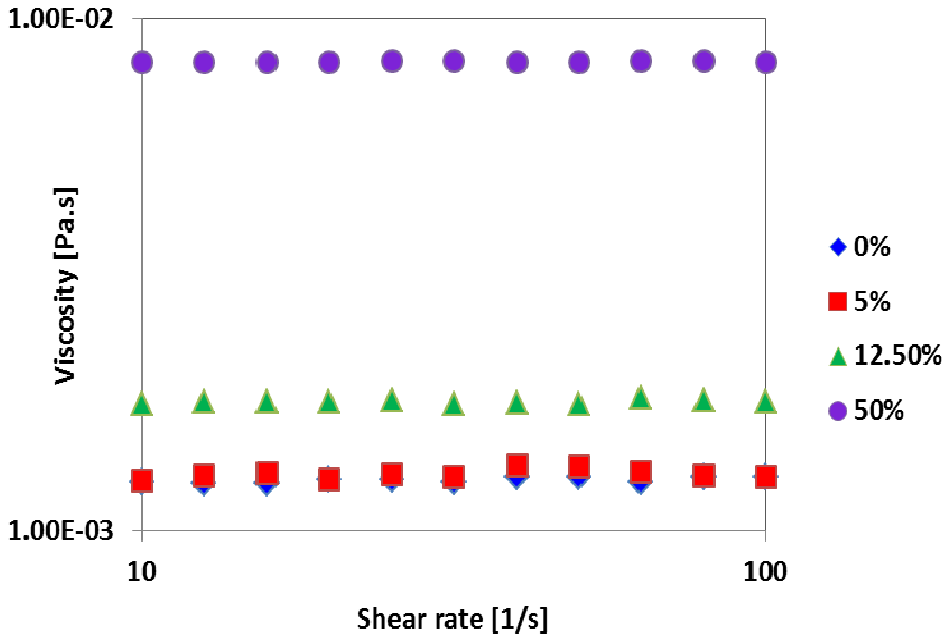

Figure 6.8

For various concentrations of lecithin in dodecane, the viscosity changes as a function of shear rate.

Thus next, different concentrations of lecithin were added to dodecane to see if it changes the bulk viscosity. This means that the bulk fluid was changed to dodecane. Various concentrations of lecithin were added to dodecane and the rheology profile observed. Here no shear thinning behavior is observed for different lecithin concentrations. Now, lecithin has a long non polar tail with a small polar head (Figure 6.9) which is why it is often used as an emulsifier (Weete et al., 1994). When lecithin "dissolves" in dodecane, only van der Waals forces (intermolecular) exist among the nonpolar solvents**.** The same is true for

the nonpolar solutes. Thus, all the lecithin in the solution is subject only to van der Waals forces, and solution can occur. Random motion of solute molecules will cause some of them to leave the surface of the solute. There can be solvation in such cases, but the forces involved are far weaker than those in solutions involving polar compounds. The nonpolar particles are simply dispersed. Thus, lecithin will disperse in dodecane randomly.

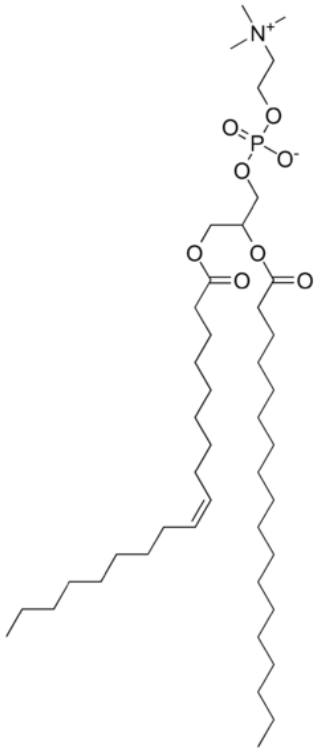

Figure 6.9

Chemical structure of a typical lecithin molecule.(Sigma-Aldrich)

The increase in viscosity for greater amounts of lecithin dispersed in dodecane arises from the multiple Van der Waals attraction forces between these non-polar entities. An analogous increase in viscosity is observed commonly in

the case of syrup compared to water, where sugar syrup has a greater viscosity than water.

Conclusion

It has been demonstrated that pH responsive core-shell composite nanoparticles can be synthesized using the Pickering emulsion polymerization method. The core of these composite nanoparticles has been successfully modified to be pH sensitive by incorporating a polymer that responds to a change of pH in the environment. The amount of responsiveness of the nanoparticles can be tuned by increasing or decreasing the amount of pH responsive monomer added during the synthesis process. A rheology modifier, lecithin was encapsulated within this system and when the system was subjected to basic pH the nanoparticles decreased in size. This direct shrinking of the nanoparticles expelled the encapsulated lecithin into the surrounding fluid, which in turn changed the fluid's rheological properties.

6.2 Development of Metallic Shell Composite Particles

6.2.1 Introduction

. In the last decade, many research interests have focused on polymer-gold nanocomposites for different applications in the fields of electronics, optics, catalysis and biology (Niemeyer, 2001; Daniel & Astruc, 2004). As a well-explored field of research, various polymer-gold nanocomposites have been synthesized using physical or chemical approaches (Sudeep & Emrick, 2007; Wuelfing, Gross, Miles & Murray, 1998; Ohno, Morinaga, Koh, Tsujii & Fukuda, 2005; Ohno, Koh, Tsujii & Fukuda, 2003; Shan & Tenhu, 2007) and have shown

much potential for applications in advanced material science. Particularly, the "smart" nanocomposites consisting of gold nanoparticles and intelligent polymers display fascinating capabilities (Li, Gunari, Fischer, Janshoff & Schmidt, 2004; Liu, Yang, Liu & Tong, 2003; Cui, Tao, Tian, He & Li, 2006; He, Kuller, Grunze & Li, 2007), and therefore there is a need to devise a way to exploit a facile path for fabricating environmentally responsive materials which can be further used in a variety of novel technological applications (Owens et al., 2007; Kim & Lee, 2006; Shan et al., 2004).

A lesser explored field has been the study of a core-shell type of nanoparticle where a polymer serves as the core and inorganic nanoparticles are the shell. This is an interesting class of supramolecular building blocks and can "exhibit unusual, possibly unique, properties which cannot be obtained simply by co-mixing polymer and inorganic particles" (Barthet et al., 1999). We have extended this approach towards making organic cores with gold shells. For these types of composite particles, the polymer cores formed within the surfaces or shells of gold nanoparticles can not only enhance the stability of polymer cores intensively, but also it is possible to functionalize the polymer core due to the special properties which may be imparted by choosing the core polymer after careful consideration. Recently, core-shell composite particles consisting of a polymer core and metal shell have shown much potential in advanced materials (Zhu et al., 2004). Several methods have been developed to fabricate a metal shell around polymer nanoparticles and can be broadly classified into two categories: bottom-up and top-down. Nanotechnology techniques for top down fabrication

vary but can be split into mechanical and chemical fabrication techniques. One of the most well-known top down fabrication technique is nanolithography. In this process, the required material is protected by a mask and the exposed material is etched away. Depending upon the level of resolution required for features in the final product, etching of the base material can be done chemically using acids or mechanically using ultraviolet light, x-rays or electron beams. Areas involving bottom up fabrication are already quite successful. A key method in this approach is "self-assembly" of core-shell composite particles. The bottom-up approaches can be further segmented into three classes: (i) simultaneous fabrication, where both the core and the protective shell formation take place simultaneously; (ii) sequential fabrication, where the core is fabricated followed by the formation of a protective shell, and (iii) displacement reaction (redox) fabrication, wherein the protective shell is fabricated through a typical oxidation-reduction type of displacement chemical reaction mechanism (Wei et al., 2011). Other well-researched preparative methods for mainly (core-shell) nanoparticles have been detailed in literature including the direct-synthesis method, "graft-to" strategy, "graft-from" strategy and physical adsorption method, in which the surface-initiated radical polymerization such as atom-transfer radical polymerization and reversible-addition fragmentation chain-transfer radical polymerization displayed several advantages for well-defined nanostructures (Yong et al., 2006). However, in contrast to these techniques of fabrication, we attempt to synthesize composite nanoparticles with a polymer core and a metal shell using the method of Pickering emulsion polymerization. Previously in this thesis, we have discussed the

synthesis of the composite polymer-silica nanoparticles using Pickering emulsion polymerization. In this section we try to see if the same synthesis strategy can be employed to synthesize core-shell composite particles with a gold shell. To date most of these particles have been synthesized with polymer shells and inorganic cores (as discussed previously in chapter 3) while here, it is proposed to reverse this with polymer cores and metallic shells (example gold) to achieve large radiative property shifts in the visible-infrared wavelengths. One broader impact of the proposed work is listed as follows. The technological opportunities that may be enabled by developing dynamically controllable radiative properties within the proposed composite nanoparticle dispersions are immense. One potential system that may result from such a system is a dual use solar thermal collector/night-sky radiatior, (Figure 6.10). It has been demonstrated that the use of dispersions of nanoparticles acting as direct absorption receivers (Otanicar et al., 2010; Tyagi et al., 2009) offer improved efficiencies over conventional surface based receivers. Furthermore, similar advantages may be available in systems utilizing radiative emission as their main form of heat transfer. By being able to dynamically control where the peak absorption (emission) wavelength occurs, it should be possible to create one system that acts as a direct absorption receiver for capturing solar thermal energy during the day and at night the system would shift operation into a night-sky radiator for cooling purposes.

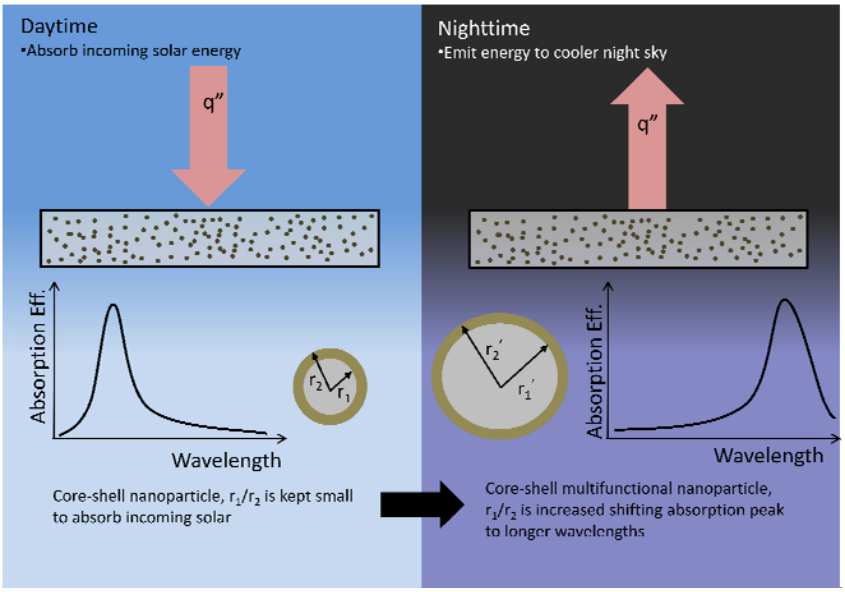

Figure 6.10

Potential dual-use solar thermal collector/night-sky radiator using core-shell multifunctional nanoparticles

6.2.2 Materials

The following materials are used for the core-shell composite nanoparticle synthesis: spherical gold nanoparticles dispersed in iso-propanol, (wt% 3.0%, Nanopartz Inc.), Nonionic azo initiator VA-086 (98%, 2,2-azobis(2-methyl-*N*-(2-hydroxyethyl)propionamide), Wako Chemicals), styrene monomer (99.9%, Fisher), N-isopropylacrylamide monomer (NIPAAm, 97%, Aldrich) and water (HPLC grade, Acros Organics) were used in the polymerization without further purification.

6.2.3 Materials Synthesis

0.1 ml gold nanoparticles dispersion, 5ml water and 0.1 g styrene were sonicated by VCX 500 ultrasound sonicator at 21 amplitude for 15 seconds to

form emulsion. The emulsion was then immediately moved to a 3-neck 15ml flask under magnetic stirring at 300 rpm, and was degassed with nitrogen for 15 minutes. After the solution was heated to 65 °C, 0.007 g VA-086 initiator was injected into the flask; the reaction lasted for 4 hours. The reaction procedure and reaction time was the same with the synthesis of polystyrene-gold composite particles. Before characterization, the synthesized nanoparticles were washed twice by centrifuging-redispersing cycles using a Beckman Microfuge 18 centrifuge for 10 minutes at 4000 rpm. The asymmetric particles were collected by using GD/X™ 0.2 μm PTFE syringe filter.

6.2.4 Characterization Techniques

Particle Size Distribution Measurement

Particle size distributions of the synthesized composite particles were analyzed by NICOMP 380 ZLS with dynamic light scattering (DLS) technique. The washed composite nanoparticles were further diluted with water before measurements to avoid particle aggregation. The NICOMP distribution was adopted to analyze the result.

Transmission Electron Microscopy (TEM) and Energy-dispersive X-ray Spectroscopy (EDX)

The TEM images were obtained by Philips CM-200 FEG. The TEM specimen was prepared by placing one droplet of the sample onto TEM 200 mesh copper grids with Lacey Formvar/Carbon film or Formvar/Carbon film and dried in air.

Scanning Electron Microscope (SEM)

The specimens for scanning electron microscope (SEM) were then sputter coated with gold for 100 seconds and viewed by SEM-XL30 (FEI). Specimens SEM experiments were prepared by placing a droplet of the nanoparticle samples onto mica substrates and dried in air.

6.2.5 Results and Discussion

Asymmetric and non-asymmetric gold-composite articles

Using the Pickering emulsion polymerization synthesis method discussed in the materials synthesis section, there were two kinds of composite particles formed. The first being the usual core-shell type of composite particle of the size order of 400-500 nm with the organic core of the composite particle being covered by gold nanoparticles (these we term as "non-asymmetric"). The formation requirements and process of this type of composite particle has been previously discussed in Chapters 2 and 3. The second, more unusual type of composite particle was of the size order of 160-180 nm and is termed as "asymmetric"; these have an eccentric structure, these nanoparticles were uniform in size and morphology, with each organic bead containing only one gold nanoparticle at its surface. Figure 6.11 depicts the results of the synthesis process:

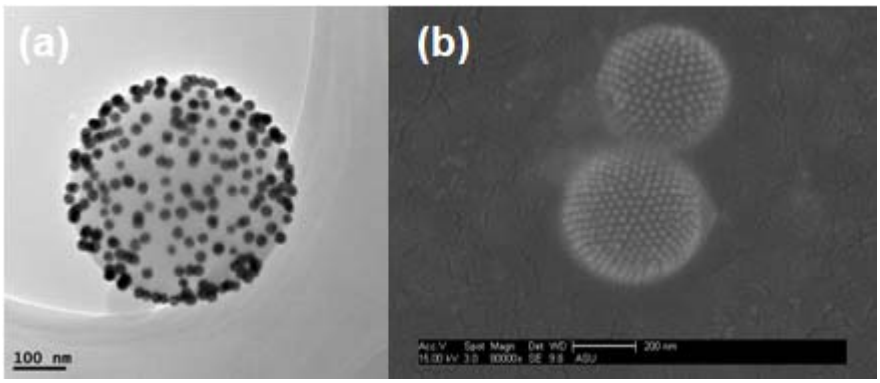

Figure 6.11

(a) TEM micrograph of non-asymmetric composite particles; (b) SEM image of non-asymmetric composite particles.

In this study the preparation procedure of these composite particles was analyzed in detail and applied by varying the type of gold nanoparticles used and by varying the amount of concentration. This type of bimodal distribution is in contrast to a study by Ohnuma et al., where asymmetric gold-polystyrene composites similar to this system were developed (Ohnuma et al., 2009). They had a unimodal size distribution of asymmetric composite particles and their synthesis method was different than the one listed here since they used a precipitation polymerization method. In contrast to emulsion polymerization, precipitation polymerization is a heterogeneous polymerization process that begins initially as a homogeneous system in the continuous phase, where the monomer and initiator are completely soluble, but upon initiation the formed polymer is insoluble and thus precipitates, forming the product. Another major difference from our one-step synthesis process is that they introduced gold nanoparticles into the reaction mixture a few minutes after polymerization had

been induced, whereas in our reaction, the gold nanoparticles act as a stabilizer in the system from the starting of the fabrication process. For the non-asymmetric composite particles (Figure 6.11 a, b) the assumed reaction mechanism is the same type of Pickering emulsion polymerization as discussed in Chapter 3. However, to identify the reaction mechanism of the asymmetric composite particles a study was done on their time dependent growth formation (Figure 6.12). Figure 6.12(a) shows a schematic illustration of the procedure used to form the asymmetric gold composite particles and TEM micrographs of samples obtained at different stages of the synthesis process. As can be seen from Figure 6.12(b) around this point, polystyrene oligomers and/or monomers started to nucleate by attaching onto the surface of the gold nanoparticles, which then grew in size as the polymerization process proceeded and finally grew into spheres the shape of a droplet which has a defined shape dictated by surface tension. Figure 6.12(c) shows the TEM micrograph of an intermediate sample observed at 1 hour into the reaction. An occlusion or bump type of formation of polystyrene can be seen forming on the surface of a gold nanoparticle through a heterogeneous nucleation process. As polymerization continued, this polystyrene nucleus gradually grew larger (around 40 nm) as shown in Figure 6.12(c). This nucleus finally grew into a sphere, as shown in Figure 6.12(d, e) for a sample present 4 hours into the reaction. It is worthwhile to note that all of the polystyrene components showed a spherical shape regardless of their structural morphologies or orientations with the original gold nanoparticles.

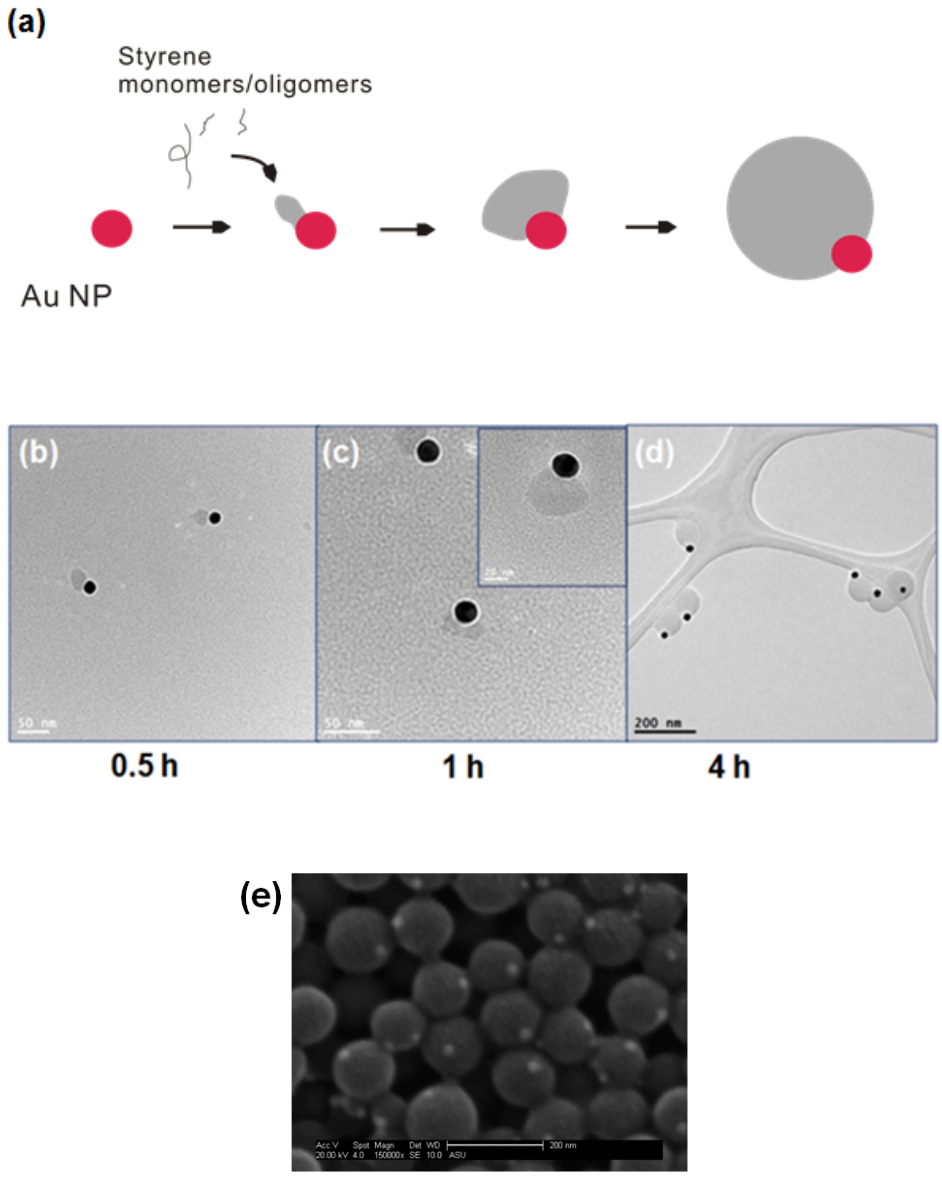

Figure 6.12

Schematic illustration of the procedure for generating asymmetric gold composite particles (a) TEM micrographs indicating reaction intermediates obtained at (b) 0.5 hours (c) 1 hour (d) 4 hours Individual scale bars are as indicated in the figures and inset; (e) SEM image of the asymmetric composite particles

The asymmetric gold composite particles containing gold nanoparticles were uniform in size, with an average diameter 180 nm in size. For every asymmetric composite particle formed, the polystyrene component contained only one gold nanoparticle partially embedded in the surface. As can be clearly seen in Figure 6.12(d, e), the gold nanoparticle slightly protruded from the surface of the polystyrene component, rather than being confined within the center of each composite particle. This appears to be a direct consequence of the growth mechanism detailed before. As clearly indicated by the TEM micrographs in Figure 6.12(b)-(d), the polystyrene component seems to grow in a nonuniform fashion from the surface of the gold nanoparticle while the polymerization took place.

Pickering emulsion polymerization as a formation method of nanoparticles has been established during the course of this dissertation. Also, as has been discussed in a previous study (Binks et al., 2006), many types of nanoparticles, including silica, clay, and polymer species, are very effective as emulsion stabilizers in the absence of any other surface-active species when the particle wettability is suitable. However, in this study involving gold nanoparticles a bimodal kind of structure of composite nanoparticles was found to have been formed. It is therefore relevant to question why the gold particles used here do not stabilize the emulsion drops in the present system in the same way as silica particles do, even when they are clearly observed to adsorb at the oil-water interface (Binks et al., 2006). For most nanoparticle-stabilized emulsion systems reported in literature, the nanoparticle concentration must be on the order of 1 wt

% to provide good long-term emulsion stability. In the system studied here, the concentration of gold particles used initially was only ~0.005 wt %, which may simply be too low to impart long-term emulsion stability against coalescence. To observe how the formation of the composite particles behave as a function of the amount of stabilizing gold nanoparticles, successively higher gold concentrations were used. Another factor that may contribute to the poor emulsion stabilization by gold nanoparticles is that the Hamaker constant for gold surfaces interacting across water or hydrocarbons is 40 X 10^{-20} J. This is indicative of the fact that the van der Waals attractive forces that are involved in destabilizing the gold nanoparticle emulsions are higher than those for silica or polymers for which the corresponding Hamaker constants are in the range of 0.5-0.8 X 10^{-20} J (Binks et al., 2006).

Chapter 7

SUMMARY AND FUTURE WORK

7.1 Summary

This dissertation presents a broad investigation ranging from the synthesis of core-shell composite particles, through Pickering emulsion polymerizations, to their characterizations as well as applications. We started by exploring how to apply the concept of interfacial particle self-assembly in emulsion polymerizations (Pickering emulsion polymerizations) to synthesize organic-inorganic core-shell composite particles and discussed the polymerization mechanisms. Polystyrene-silica core-shell composite particles, with a silica content of 20 wt%, were successfully synthesized by one-step Pickering emulsion polymerization. Possible mechanisms of Pickering emulsion polymerization were also explored. The nanoparticles are thermodynamically favorable to self-assemble and remain at the liquid-liquid interfaces. At the initial stage of polymerization, the nanoparticles provide stability to the monomer droplets. During the nucleation stage, the nanoparticles remain at the interfaces between the monomer and continuous phases. Homogeneous coagulative nucleation was identified as the dominating mechanism in the polymerization when using VA-086 as the initiator. The research has both fundamental and practical applications and has potential impacts in multiple industries, such as the chemical, food, cosmetics, pharmaceutical, electronics and oil industries.

Next, temperature sensitive nanoparticles were synthesized and these were applied in controlled drug delivery. The core-shell nature of these nanoparticles

were determined by etching away the silica shell using HF acid and observing the surface morphology by SEM as well as chemically identifying the absence of the shell using FTIR. We have developed a unique drug delivery model vehicle which can be taken up by cancer cells and release the loaded drug at elevated temperatures. The composite nanoparticles are temperature sensitive and can be taken up by human prostate cancer (PC3 and PC3-PSMA) cells. An anticancer agent 17-(Allylamino)-17-demethoxygeldanamycin (17-AAG) has been loaded into the polymeric cores during formation of the nanoparticles and drug release has been successfully observed at higher than ambient temperatures. The ability of the various nanoparticles for inducing death in human prostate cancer cells has been evaluated.

The transition temperature of the synthesized temperature sensitive core-shell composite nanoparticles was around 32°C. However, if the temperature responsiveness can be tuned to different values, then these composite nanoparticles can have lasting applications in various fields as temperature sensors; also their dimension change property can be exploited as delivery vehicles at specific temperatures. After the efficient implementation of this study in a drug delivery application, we realized the need to tune the transition temperature of these composite nanoparticles to be near the human physiological temperature. A number of methods were investigated for tuning the transition temperature of the nanoparticles which can be broken down into two categories: synthesis modification and post synthesis modification. The polymer core was modified using the addition of either a crosslinker or a co-monomer during the

synthesis and resulted in a maximum transition shift of 2 to 6 degrees respectively over the experimental range. Post synthesis, the nanoparticles were equilibrated in surfactant mixtures as well as co-solvent mixtures. Addition of these increased the transition temperature as has been detailed in chapter 5. Also, it is worthwhile to mention that the tunability of the transition temperature of these nanoparticles show similar trends as those observed for macroscopic bulk gels of similar polymer formulations.

In addition, we have incorporated 2-(*N, N*-dimethylamino) ethyl methacrylate into the Pickering emulsion polymerization and synthesized pH responsive core-shell composite nanoparticles which release rheological modifiers upon pH change. The nanoparticles exhibit pH-sensitive behavior due to protonation/de-protonation of *N*, *N*-dimethylaminoethyl groups in the PDMA component of the composite. During the synthesis process lecithin was included as a starting material and the composite nanoparticles were synthesized with lecithin with a view to release this encapsulated material on a given pH stimulus. Lecithin is a well-studied chemical that is often used as a rheology modifier in applications ranging from the food industry to the pharmaceutical industry. In this case we have demonstrated the release of lecithin from pH sensitive composite nanoparticles by changing the pH levels of the bulk fluid, and that consequently, modifies the rheological properties of water.

Also, the shell material of these core-shell composite nanoparticles has been successfully changed from silica to gold. Following the Pickering emulsion polymerization synthesis method, described in the dissertation, we observed a

bimodal type distribution of particles with polystyrene as a core and gold as a shell having different surface morphologies i.e. asymmetric and non-asymmetric composite particles. The mechanism for the formation of the asymmetric particles was investigated using time as a variable during different stages of the synthesis process and thus we were able to observe the particle growth process with the help of TEM images and a schematic for the formation mechanism was consequently hypothesized.

As seen during the course of this dissertation, Pickering emulsion polymerizations could be used to synthesize a variety of composite particles of different chemistry. This work has consisted of mainly the synthesis, related characterizations and tuning these fabricated composite nanoparticles for a host of interesting applications. Depending on the applications, polystyrene was substituted by other hydrophobic emulsion polymers, or a co-monomer was mixed with styrene to synthesize composite particles with a polystyrene-based polymer core. Also, silica nanoparticles were substituted by other nanoparticles. To be able to change the core as well as the shell of these composite nanoparticles in a facile, one-step manner of synthesis opens up many potentially exciting avenues for future research which shall be discussed further in the next section comprising of future work in succession to this dissertation.

7.2 Future Work

In the case of the pH sensitive composite nanoparticles, future studies include identifying potential rheology modifiers for oils such that they can be encapsulated in the composite pH responsive nanoparticles and then released is currently being studied. In this direction certain hydrostearic acid (HSA) based organogels seems a potentially attractive candidate. These are systems containing a majority oil component as solvent that exhibit elastic, gel-like properties and can be formed by a large variety of different low molecular weight gelators. 12-hydroxy stearic acid (HSA) or other like compounds will be considered and its ability to gel various organic solvents, such as dodecane, silicone oil (PDMS) will be studied. Gelation typically occurs above a concentration of 0.1–0.8 wt% and the gelation concentration is related to the polarity of the oil (Burckhardt et al., 2009) the macroscopic gel properties can be characterized by means of oscillatory rheology experiments, differential scanning calorimetry (DSC) and optical microscopy. A drawback of using macroscopic organogels is releasing them into the bulk surroundings. Hence specific studies need to be done upon the type of modifier that will be used and encapsulation and release studies in the experimental system under consideration should be done.

It is worthwhile to note that the viscoelasticity of the interface can be monitored in-situ by the recently developed interfacial microrheology (Jian & Dai, 2006; Wu & Dai, 2007; Wu et al., 2009). Laser scanning confocal microscopy can be employed, Leica SP5, to perform particle tracking and monitor the rheological change of the oil-water interfaces upon the release of the

rheological thickener. As discussed in experiments in chapter 6, the released rheology modifier will be primarily characterized by rheological experiments (as the feasibility of this technique has been demonstrated.)

For prospective future studies, Pickering emulsion polymerizations could be used to synthesize other composite particles of different chemistry. Synthesis of composite core-shell nanoparticles with a metallic shell and manipulating the core-shell nanoparticle volume ratio and understanding the structure-property of these nanoparticles in dispersions is an objective discussed in this study and its consequent application is outlined next. In the proposed work, the synthesis of the temperature-sensitive core-shell multifunctional nanoparticles will follow the developed experimental protocol: Other than controlling the volume change due to thermal response, it is also proposed to tune the core-shell nanoparticle size in general, as needed. This can be achieved by following an already developed theory (Gilbert, 1995) for use in conventional emulsion polymerizations,

$$M_n \sim R_p \, e^{k_d t} \, M_o / k_d [I]_o \qquad (1)$$

where Rp is the rate of overall emulsion polymerization, k_d is the rate constant of decomposition of the initiator, $[I]_o$ is the initiator concentration, M_o is the initial monomer concentration, and t is the reaction time. M_n is the instantaneous number average molecular weight and directly associated with the particle size.

With respect to applications, the combination of metallic nanoparticles and intelligent polymers provides a facile path for intelligent materials. For example, the metallic shell of the composite core-shell nanoparticles can be chosen to

exhibit spectral radiative properties (for example gold) or magnetic properties (for example iron oxide). Nanoparticles are known to offer a variety of benefits for thermal transport and of particular relevance here are the vast changes to the radiative properties that can be achieved through the dispersion of nanoparticles. In particular, a dispersion of core-shell multifunctional nanoparticles capable of dynamically changing their volume and thus their spectral radiative properties will be created. Preliminary experiments as detailed in Chapter 6 have shown that these multifunctional nanoparticles consisting of a metal shell and polymer core are capable of being synthesized. Further tuning of the size ratio of the core and shell can be done by modifying the synthesis process and by including a temperature responsive polymer in the core of these composite particles. Also, the subsequent experiments will largely focus on measuring the spectral radiative properties of different dispersions at different temperatures and thus different volumes using spectrophotometric and DLS techniques.

REFERENCES

Aguilar, M.R., Elvira, C., Gallardo, A., Vázquez, B., & Román, J.S. (2007). Smart Polymers and their Applications as Biomaterials. *Biomaterials, 3*(6), 1-27.

Akartuna, I., Studart, A. R., Tervoort, E., Gonzenbach, U. T., & Gauckler, L. J. (2008). Stabilization of oil-in-water emulsions by colloidal particles modified with short amphiphiles. *Langmuir, 24*(14), 7161-7168.

Arifin, D.Y., Lee, L.Y., & Wang, C. H. (2006) Mathematical modeling and simulation of drug release from microspheres: implications to drug delivery systems. *Advanced Drug Delivery Reviews, 58*(4), 1274-1325.

Ashby, N. P., & Binks, B. P. (2000). Pickering emulsions stabilised by laponite clay particles. *Physical Chemistry Chemical Physics, 2*(24), 5640-5646.

Barthet, C., Hickey, A. J., Cairns, D. B., & Armes, S. P. (1999). Synthesis of novel polymer-silica colloidal nanocomposites via free-radical polymerization of vinyl monomers. *Advanced Materials, 11*(5), 408-410.

Barua, S., & Rege, K. (2010). The Influence of Mediators of Intracellular Trafficking on Transgene Expression Efficacy of Polymer-Plasmid DNA Complexes. *Biomaterials. 22*(5), 894-902.

Barua, S., & Rege, K. (2009). Cancer-Cell-Phenotype-Dependent Differential Intracellular Trafficking of Unconjugated Quantum Dots. *Small 5*(11), 370-376.

Binks, B. P., & Clint, J. H. (2002). Solid wettability from surface energy components: Relevance to Pickering emulsions. *Langmuir, 18*(4), 1270-1273.

Binks, B. P., Dyab, A. K. F., & Fletcher, P. D. I. (2003). Novel emulsions of ionic liquids stabilised solely by silica nanoparticles. *Chemical Communications,* (20), 2540-2541.

Binks, B. P., & Lumsdon, S. O. (1999). Stability of oil-in-water emulsions stabilised by silica particles. *Physical Chemistry Chemical Physics, 1*(12), 3007-3016.

Binks, B. P., & Horozov, T. S. (2006). *Colloidal particles at liquid interfaces*. Cambridge; New York: Cambridge University Press.

Binks, B. P., & Lumsdon, S. O. (2000). Influence of particle wettability on the type and stability of surfactant-free emulsions. *Langmuir, 16*(23), 8622-8631.

Binks, B. P., & Rodrigues, J. A. (2003). Types of phase inversion of silica particle stabilized emulsions containing triglyceride oil. *Langmuir, 19*(12), 4905-4912.

Binks, B. P., & Rodrigues, J. A. (2005). Inversion of emulsions stabilized solely by ionizable nanoparticles. *Angewandte Chemie-International Edition, 44*(3), 441-444.

Binks, B. P., & Whitby, C. P. (2003). Temperature-dependent stability of water-in-undecanol emulsions. *Colloids and Surfaces A-Physicochemical and Engineering Aspects, 224*(1-3), 241-249.

Binks, B. P., & Whitby, C. P. (2004). Silica particle-stabilized emulsions of silicone oil and water: Aspects of emulsification. *Langmuir, 20*(4), 1130-1137.

Binks, B. P. (2002). Particles as surfactants—similarities and differences. *Current Opinion in Colloid & Interface Science, 7*(1-2), 21-41.

Bon, S. A. F., & Colver, P. J. (2007). Pickering miniemulsion polymerization using laponite clay as a stabilizer. *Langmuir, 23*(16), 8316-8322.

Bonina, P.,. Petrova, T., & Manolova, N. (2004) pH-Sensitive Hydrogels Composed of Chitosan and Polyacrylamide – Preparation and Properties. *Journal of Bioactive and Compatible Polymers, 19*(2), 101-116.

Bouillot, P. & Vincent, B. (2000) A Comparison of the Swelling Behavior of Copolymer and Interpenetrating Network Microgel Particles. *Colloid and Polymer Science, 12*(278) ,74–79.

Bourgeat-Lami, E., & Lang, J. (1998). Encapsulation of inorganic particles by dispersion polymerization in polar media: 1. silica nanoparticles encapsulated by polystyrene. *Journal of Colloid and Interface Science, 197*(2), 293-308.

Burkhardt, M., Kinzel, S., & Gradzielski, M. (2009) Macroscopic properties and microstructure of HSA based organogels: sensitivity to polar additives. *Journal of Colloid and Interface Science, 331*(2), 514-521.

Burmistrova, A., Richter, M., Üzüm, C., & von Klitzing, R. (2011). Effect of cross-linker density of p(NIPAMco-AAc) microgels at solid surfaces on the swelling/shrinking behaviour and the young's modulus. *Colloid and Polymer Science, 289*(67), 613–624.

Carlsson, L., Rose, S., Hourdet, D., & Marcellan, A. (2010) Nano-hybrid self-crosslinked PDMA/silica hydrogels. *Soft Matter, 6*(15), 3619-3631.

Caruso, F. (2000**)** Hollow Capsule Processing through Colloidal Templating and Self-Assembly. *Chemistry-a European Journal, 6*(15), 413-419.

Caruso, F. (2001). Nanoengineering of particle surfaces. *Advanced Materials, 13*(1), 11-22.

Caruso, F., Susha, A. S., Giersig, M., & Möhwald, H. (1999). Magnetic core-shell particles: Preparation of magnetite multilayers on polymer latex microspheres. *Advanced Materials, 11*(11), 950-953.

Caruso, R. A., Susha, A., & Caruso, F. (2001). Multilayered titania, silica, and laponite nanoparticle coatings on polystyrene colloidal templates and resulting inorganic hollow spheres. *Chemistry of Materials, 13*(2), 400-409.

Cauvin, S., Colver, P. J., & Bon, S. A. F. (2005). Pickering stabilized miniemulsion polymerization: Preparation of clay armored latexes. *Macromolecules, 38*(19), 7887-7889.

Cayre, O. J., Noble, P. F., & Paunov, V. N. (2004). Fabrication of novel colloidosome microcapsules with gelled aqueous cores. *Journal of Materials Chemistry, 14*(22), 3351-3355.

Chen, M., Zhou, S., You, B., & Wu, L. (2005). A novel preparation method of raspberry-like PMMA/SiO2 hybrid microspheres. *Macromolecules, 38*(15), 6411-6417.

Chen, T., Colver, P. J., & Bon, S. A. F. (2007). Organic-inorganic hybrid hollow spberes prepared from TiO2-stabilized Pickering emulsion polymerization. *Advanced Materials, 19*(17), 2286-2289.

Cheng, S., Fu, X., Liu, J., Zhang, J., Zhang, Z., Wei, Y., & Han, B. (2007). Study of ethylene glycol/TX-100/ionic liquid microemulsions. *Colloids and Surfaces A-Physicochemical and Engineering Aspects, 302*(1-3), 211-215.

Cheng, X., Chen, M., Zhou, S., & Wu, L. (2006). Preparation of SiO_2/PMMA composite particles via conventional emulsion polymerization. *Journal of Polymer Science Part A-Polymer Chemistry, 44*(12), 3807-3816.

Chern, C. S. (2006). Emulsion polymerization mechanisms and kinetics. *Progress in Polymer Science, 31*(5), 443-486.

Coviello, T., Palleschi, A., Grassi, M., Matricardi, P., Bocchinfuso, G., & Alhaique, F. (2005). Scleroglucan: A versatile polysaccharide for modified drug delivery. *Molecules, 10*(1), 6-33.

Crowther, H. M., & Vincent, B. (1998). Swelling behavior of poly-isopropylacrylamide microgel particles in alcoholic solutions. *Colloid and Polymer Science, 276*(1), 46-51.

Dai, L. L., Tarimala, S., Wu, C., Guttula, S., & Wu, J. (2008). The structure and dynamics of microparticles at Pickering emulsion interfaces. *Scanning, 30*(2), 87-95.

Dai, S., Ravib, P. & Tam K. C. (2008) pH-Responsive Polymers: Synthesis, Properties and Applications. *Soft Matter, 20*(4), 435-449.

Das, M., Mardyani, S., Chan, W.C.W. & Kumacheva, E. (2006) Biofunctionalized pH-responsive microgels for cancer cell targeting: rational design. *Advanced Materials, 18*(1) , 80–83.

Denkov, N. D., Ivanov, I. B., Kralchevsky, P. A., & Wasan, D. T. (1992). A possible mechanism of stabilization of emulsions by solid particles. *Journal of Colloid and Interface Science, 150*(2), 589-593.

Dickinson, E. (2010). Food emulsions and foams: Stabilization by particles. *Current Opinion in Colloid & Interface Science, 15*(1-2), 40-49.

Ding, B.S., Dziubla, T., Shuvaev, V.V., Muro, S., & Muzykantov, V.,R. (2006). Advanced drug delivery systems that target the vascular endothelium. *Molecular Interventions,* 6(1) 98-112.

Ding, X.,F., Jiang, Y.Q., Yu, K.F., Hari-Bala &Tao, N.N. (2004). Silicon dioxide as coating on polystyrene nanoparticles in situ emulsion polymerization. *Material Letters, 58*(2) 1722-1725.

Dinsmore, A. D., Hsu, M. F., Nikolaides, M. G., Marquez, M., Bausch, A. R., & Weitz, D. A. (2002). Colloidosomes: Selectively permeable capsules composed of colloidal particles. *Science, 298*(5595), 1006-1009.

Dokoutchaev, A., James, J. T., Koene, S. C., Pathak, S., Prakash, G. K. S., & Thompson, M. E. (1999). Colloidal metal deposition onto functionalized polystyrene microspheres. *Chemistry of Materials, 11*(9), 2389-2399.

Duan, L.L., Chen, M., Zhou, S., & Wu, L. (2009). Synthesis and Characterization of Poly (N-isopropylacrylamide) / Silica Composite Colloidsomes via Inverse Pickering Emulsion Polymerization. *Langmuir, 25*(8) 3467-3472.

Duracher ,D., Sauzedde, F., Elaissari, A., Perrin, A., & Pichot, C. (1998). Cationic amino-containing *N* -isopropyl- acrylamide–styrene copolymer latex particles: 1-Particle size and morphology vs. polymerization process. *Colloid Polymer Science, 276*(7) 219-231.

El-Sayed, I. H., Huang, X. H., & El-Sayed, M. A. (2005). Surface plasmon resonance scattering and absorption of anti-EGFR antibody conjugated gold nanoparticles in cancer diagnostics: Applications in oral cancer. *Nano Letters, 5*(5), 829-834.

El-Sayed, I. H., Huang, X., & El-Sayed, M. A. (2006). Selective laser photo-thermal therapy of epithelial carcinoma using anti-EGFR antibody conjugated gold nanoparticles. *Cancer Letters, 239*(1), 129-135.

Farrell, C. (2011). *Gulf of Mexico Oil Spill*. ABDO Publishing Company.

Feeney, P. J., Napper, D. H., & Gilbert, R. G. (1984). Coagulative nucleation and particle-size distributions in emulsion polymerization. *Macromolecules, 17*(12), 2520-2529.

Feeney, P. J., Napper, D. H., & Gilbert, R. G. (1987). Surfactant-free emulsion polymerizations - predictions of the coagulative nucleation theory. *Macromolecules, 20*(11), 2922-2930.

Fortuna, S., Colard, C. A. L., Troisi, A., & Bon, S. A. F. (2009). Packing patterns of silica nanoparticles on surfaces of armored polystyrene latex particles. *Langmuir, 25*(21), 12399-12403.

Fournier, C. O., Fradette, L., & Tanguy, P. A. (2009). Effect of dispersed phase viscosity on solid-stabilized emulsions. *Chemical Engineering Research & Design, 87*(4A), 499-506.

Frelichowska, J., Bolzinger, M., Pelletier, J., Valour, J., & Chevalier, Y. (2009). Topical delivery of lipophilic drugs from o/w Pickering emulsions. *International Journal of Pharmaceutics, 371*(1-2), 56-63.

Frelichowska, J., Bolzinger, M., Valour, J., Mouaziz, H., Pelletier, J., & Chevalier, Y. (2009). Pickering w/o emulsions: Drug release and topical delivery. *International Journal of Pharmaceutics, 368*(1-2), 7-15.

Fung, L. K., & Saltzman, W. M. (1997). Polymeric implants for cancer chemotherapy. *Advanced drug delivery reviews, 26*(2), 209-230.

Galan, E., & Singer, A. (2011). Developments in Palygorskite-Sepiolite Research: A New Outlook on These Nanomaterials. *Elsevier,* 1(3), 1572-4352.

Gao, Q., Wang, C., Liu, H., Wang, C., Liu, X., & Tong, Z. (2009). Suspension polymerization based on inverse Pickering emulsion droplets for thermo-sensitive hybrid microcapsules with tunable supracolloidal structures. *Polymer, 50*(12), 2587-2594.

Gao, Y., Li, N., Zheng, L. Q., Zhao, X. Y., Zhang, S. H., Han, B. X., Hou, W. G., & Li, G. Z. (2006). A cyclic voltammetric technique for the detection of micro-regions of bmimPF(6)/Tween 20/H2O microemulsions and their performance characterization by UV-vis spectroscopy. *Green Chemistry, 8*(1), 43-49.

Gao, Y., Zhang, J., Xu, H. Y., Zhao, X. Y., Zheng, L. Q., Li, X. W., & Yu, L. (2006). Structural studies of 1-butyl-3-methylimidazolium tetrafluoroborate/TX-100/p-xylene ionic liquid microemulsions. *Chemphyschem, 7*(7), 1554-1561.

Gao, Y. N., Han, S. B., Han, B. X., Li, G. Z., Shen, D., Li, Z. H., Du, J. M., Hou, W. G., & Zhang, G. Y. (2005). TX-100/water/1-butyl-3-methylimidazolium hexafluorophosphate microemulsions. *Langmuir, 21*(13), 5681-5684.

Gao, Y., Li, N., Zheng, L., Zhao, X., Zhang, J., Cao, Q., Zhao, M., Li, Z., & Zhang, G. (2007). The effect of water on the microstructure of 1-butyl-3-methylimidazolium tetrafluoroborate/TX-100/benzene ionic liquid microemulsions. *Chemistry-a European Journal, 13*(9), 2661-2670.

Garti, N., Binyamin, H., & Aserin, A. (1998). Stabilization of water-in-oil emulsions by submicrocrystalline alpha-form fat particles. *Journal of the American Oil Chemists Society, 75*(12), 1825-1831.

Gong, M.C., Latouche, J., Krause, A., Heston, W.D.W., Bander, N.H., & Sadelain, M. (1999). Cancer patient T cells genetically targeted to prostate-specific membrane antigen specifically lyse prostate cancer cells and release cytokines in response to prostate-specific membrane antigen. *Neoplasia, 1*(3) 123–127.

Gu, S., Kondo, T., & Konno, M. (2004). Preparation of silica–polystyrene core–shell particles up to micron sizes. *Journal of Colloid and Interface Science, 272*(2), 314-320.

Guo, Y. K., Wang, M. Y., Zhang, H. Q., Liu, G. D., Zhang, L. Q., & Qu, X. W. (2008). The surface modification of nanosilica, preparation of nanosilica. *Journal of Applied Polymer Science, 107*(4), 2671-2680.

Grassi, M., & Grassi, G. (2005). Mathematical modeling and controlled drug delivery: matrix systems. *Current Drug Delivery, 2*(1), 97-116.

Han, M. G., & Armes, S. P. (2003). Preparation and characterization of polypyrrole-silica colloidal nanocomposites in water-methanol mixtures. *Journal of Colloid and Interface Science, 262*(2), 418-427.

Han, X., Xu, J., Liu, H. L., & Hu, Y. (2005). A new approach to thick films of a block copolymer with ordered surface structures. *Macromolecular Rapid Communications, 26*(22), 1810-1813.

Harkins, W. D. (1947). A general theory of the mechanism of emulsion polymerization. *Journal of the American Chemical Society, 69*(6), 1428-1444.

Higuchi, T. (1963), Mechanism of sustained-action medication. Theoretical analysis of rate of release of solid drugs dispersed in solid matrices. *Journal of Pharmaceutical Sciences, 52*(1) 1145–1149.

Hirotsu, S., Hirokawa, Y., & Tanaka, T. (1987). Volume-phase transitions of ionized N-isopropylacrylamide gels. *Journal of Chemical Physics, 87*(2), 233-237.

Hong, J., Han, H., Hong, C. K., & Shim, S. E. (2008). A direct preparation of silica shell on polystyrene microspheres prepared by dispersion polymerization with polyvinylpyrrolidone. *Journal of Polymer Science Part A-Polymer Chemistry, 46*(8), 2884-2890.

Horozov, T. S., Aveyard, R., Binks, B. P., & Clint, J. H. (2005). Structure and stability of silica particle monolayers at horizontal and vertical octane-water interfaces. *Langmuir, 21*(16), 7405-7412.

Horozov, T. S., Aveyard, R., Clint, J. H., & Binks, B. P. (2003). Order-disorder transition in monolayers of modified monodisperse silica particles at the octane-water interface. *Langmuir, 19*(7), 2822-2829.

Horozov, T. S., & Binks, B. P. (2005). Particle behaviour at horizontal and vertical fluid interfaces. *Colloids and Surfaces A-Physicochemical and Engineering Aspects, 267*(1-3), 64-73.

Horozov, T. S., & Binks, B. P. (2006). Particle-stabilized emulsions: A bilayer or a bridging monolayer? *Angewandte Chemie-International Edition, 45*(5), 773-776.

Horozov, T. S., Binks, B. P., Aveyard, R., & Clint, J. H. (2006). Effect of particle hydrophobicity on the formation and collapse of fumed silica particle monolayers at the oil–water interface. *Colloids and Surfaces A: Physicochemical and Engineering Aspects, 282-283*, 377-386.

Hou, Y., Matthews, A. R., Smitherman, A. M., Bulick, A. S., Hahn, M. S., Hou, H., Han, A. and Grunlan, M. A. (2008). "Thermoresponsive nanocomposite hydrogels with cell-releasing behavior", Biomaterials, 29(22), 3175-3184.

Hsu, M. F., Nikolaides, M. G., Dinsmore, A. D., Bausch, A. R., Gordon, V. D., Chen, X., Hutchinson, J. W., & Weitz, D. A. (2005). Self-assembled shells composed of colloidal particles: Fabrication and characterization. *Langmuir, 21*(7), 2963-2970.

Huang, H.Y., Remsen, E.E., Kowalewski, T., & Wooley, K.L. (1999). Nanocages Derived from Shell Cross-Linked Micelle Templates. *Journal of American Chemical Society, 121*(2) 3805-3806.

Israelachvili, J. N. (1991). Intermolecular and Surface Forces. *Academic Press*.

Jain, P.K., Lee, K.S., El-Sayed, I.H., & El-Sayed, M.A. (2006). Calculated Absorption and Scattering Properties of Gold Nanoparticles of Different Size, Shape, and Composition: Applications in Biological Imaging and Biomedicine. *Journal of Physical Chemistry, 110*(1) 7238–7248.

Jian, W..& Dai L. L. (2006). One-particle Microrheology at Liquid-Liquid Interfaces. *Applied Physics Letters, 89* (9) 3-7.

Jiao, J., Rhodes, D. G., & Burgess, D. J. (2002). Multiple emulsion stability: Pressure balance and interfacial film strength. *Journal of Colloid and Interface Science, 250*(2), 444-450.

Juang, M. S., & Krieger, I. M. (1976). Emulsifier-free emulsion polymerization with ionic comonomer. *Journal of Polymer Science Part A-Polymer Chemistry, 14*(9), 2089-2107.

Kawaguchi, H. & Fujimoto K. (1999). Smart latexes for bioseparation and bioprocessing. *Bioseparation, 7*(9), 253–258.

Kokal, S. (2005). Crude-oil emulsions: A state-of-the-art review. *SPE Production & Facilities, 20*(1), 5-13.

Komura, S., Hirose, Y., & Nonomura, Y. (2006). Adsorption of colloidal particles to curved interfaces. *Journal of Chemical Physics, 124*(24), 241104.

Kokufuta, E., Wang, B., Yoshida R., Khokhlov, R., & Hirata, M. (1998). Volume Phase Transition of Polyelectrolyte Gels with Different Charge Distributions. *Macromolecules, 31*(20), 6878–6884.

Lee, J., Hong, C. K., Choe, S., & Shim, S. E. (2007). Synthesis of polystyrene/silica composite particles by soap-free emulsion polymerization using positively charged colloidal silica. *Journal of Colloid and Interface Science, 310*(1), 112-120.

Li, C., Liu, Q., Mei, Z., Wang, J., Xu, J., & Sun, D. (2009). Pickering emulsions stabilized by paraffin wax and laponite clay particles. *Journal of Colloid and Interface Science, 336*(1), 314-321.

Li, G., Song, S., Guo, L., & Ma, S. (2008). Self-assembly of thermo- and pH-responsive poly(acrylic acid)-b-poly(N-isopropylacrylamide) micelles for drug delivery. *Journal of Polymer Science Part A-Polymer Chemistry, 46*(15), 5028-5035.

Lin, H., Skaff, T., Emrick, A. D., Dinsmore, & Russell, T. P.(2003). Nanoparticle Assembly and Transport at Liquid-Liquid Interfaces. *Science, 299*(5604), 226-229.

Liu, C., & Zhang, Z.J. (2001). Size-Dependent Superparamagnetic Properties of Mn Spinel Ferrite Nanoparticles Synthesized from Reverse Micelles. *Chemical Materials, 13*(9) 2092-2096.

Lovell, P. A., & El-Aasser, M. S. (1997). *Emulsion polymerization and emulsion polymers*. New York: J. Wiley.

Lu, J., Yan, F., & Texter, J. (2009). Advanced applications of ionic liquids in polymer science. *Progress in Polymer Science, 34*(5), 431-448.

Lu, Y., & Drechsler, M. (2009). Charge-induced self-assembly of 2-dimensional thermosensitive microgel particle patterns. *Langmuir, 25*(22), 13100-13105.

Luo, Y., Dai, C., & Chiu, W. (2008). Polystyrene/Fe_3O_4 composite latex via miniemulsion polymerization-nucleation mechanism and morphology. *Journal of Polymer Science Part A-Polymer Chemistry, 46*(3), 1014-1024.

Lynch, D.E., Nawaz, Y., & Bostrom, T. (2005). Preparation of Sub-micrometer Silica Shells Using Poly(1-methylpyrrol-2-ylsquaraine). *Langmuir, 21*(5) 6572-6575.

Ma, H., & Dai, L. L. (2009). Synthesis of polystyrene-silica composite particles via one-step nanoparticle-stabilized emulsion polymerization. *Journal of Colloid and Interface Science* 333 (2): 807-811.

Ma, H., Luo, M., Sanyal, S., Rege, K., & Dai, L. L. (2010). The one-step Pickering emulsion polymerization route for synthesizing organic-inorganic nanocomposite particles. *Materials* 3: 1186-1202.

Madivala, B., Fransaer, J., & Vermant, J. (2009). Self-assembly and rheology of ellipsoidal particles at interfaces. *Langmuir, 25*(5), 2718-2728.

Madivala, B., Vandebril, S., Fransaer, J., & Vermant, J. (2009). Exploiting particle shape in solid stabilized emulsions. *Soft Matter, 5*(8), 1717-1727.

Markvicheva, E. A., Kuzkina, I. F., Pashkin, I. I., Plechko, T. N., Kirsh, Y. E., & Zubov, V. P. (1991). A novel technique for entrapment of hybridoma cells in synthetic thermally reversible polymers. *Biotechnology Techniques, 5*(3), 223-226.

McClements, D. J. (2004). Protein-stabilized emulsions. *Current Opinion in Colloid & Interface Science, 9*(5), 305-313.

McGorty, R., Fung, J., Kaz, D., & Manoharan, V. N. (2010). Colloidal self-assembly at an interface. *Materials Today, 13*(6), 34-42.

Meakin, P. (1985). Structure of the active zone in diffusion-limited aggregation, cluster-cluster aggregation, and the screened-growth model. *Physical Review A, 32*(1), 453-459.

Melle, S., Lask, M., & Fuller, G. G. (2005). Pickering emulsions with controllable stability. *Langmuir, 21*(6), 2158-2162.

Meng, F., Zhong, Z., & Feijen, J. (2009). Responsive Polymersomes for Programmed Drug Delivery. *Biomacromolecules, 10* (2),197–209

Nagao, D., Yokoyama, M., Saeki, S., Kobayashi, Y., & Konno, M. (2008). Preparation of composite particles with magnetic silica core and fluorescent polymer shell. *Colloid and Polymer Science, 286*(8-9), 959-964.

Nakashima, T., Nonoguchi, Y., & Kawai, T. (2008). Ionic liquid-based luminescent composite materials. *Polymers for Advanced Technologies, 19*(10), 1401-1405.

Neuhausler, U., Abend, S., Jacobsen, C., & Lagaly, G. (1999). Soft X-ray spectromicroscopy on solid-stabilized emulsions. *Colloid and Polymer Science, 277*(8), 719-726.

Nonomura, Y., Komura, S., & Tsujii, K. (2005). Surface-active particles with microstructured surfaces. *Langmuir, 21*(21), 9409-9411.

Nonomura, Y., Komura, S., & Tsujii, K. (2006). Adsorption of microstructured particles at liquid-liquid interfaces. *Journal of Physical Chemistry B, 110*(26), 13124-13129.

Nonomura, Y., & Kobayashi, N. (2009). Phase inversion of the Pickering emulsions stabilized by plate-shaped clay particles. *Journal of Colloid and Interface Science, 330*(2), 463-466.

Nayak, S., Lee, H., Chmielewski, J., & Lyon, L.A. (2004). Folate-Mediated Cell Targeting and Cytotoxicity Using Thermoresponsive Microgels. *Journal of American Chemical Society, 126*(3), 10258-10259.

Nayak, S., & Lyon, L.A. (2004). Photoinduced Phase Transitions in Poly(N-isopropylacrylamide) Microgels. *Chemistry of Materials, 16*(1), 2623-2626.

Nayak, S., & Lyon, L. A. (2004). Ligand-Functionalized Core/Shell Microgels with Permselective Shells. *Angewandte Chemie International Edition, 4*(2), 6706-7708.

Nagao, D., Yokoyama, M., Saeki, S., Kobayashi, Y., & Konno, M. (2008). Preparation of composite particles with magnetic silica core and fluorescent polymer shell. *Colloid and Polymer Science, 286*(8-9), 959-964.

Nakashima, T., Nonoguchi, Y., & Kawai, T. (2008). Ionic liquid-based luminescent composite materials. *Polymers for Advanced Technologies, 19*(10), 1401-1405.

Neuhausler, U., Abend, S., Jacobsen, C., & Lagaly, G. (1999). Soft X-ray spectromicroscopy on solid-stabilized emulsions. *Colloid and Polymer Science, 277*(8), 719-726.

Nonomura, Y., Komura, S., & Tsujii, K. (2005). Surface-active particles with microstructured surfaces. *Langmuir, 21*(21), 9409-9411.

Nonomura, Y., Komura, S., & Tsujii, K. (2006). Adsorption of microstructured particles at liquid-liquid interfaces. *Journal of Physical Chemistry B, 110*(26), 13124-13129.

Nonomura, Y., & Kobayashi, N. (2009). Phase inversion of the Pickering emulsions stabilized by plate-shaped clay particles. *Journal of Colloid and Interface Science, 330*(2), 463-466.

Odian, G. G. (2004). *Principles of polymerization* (4th ed.). Hoboken, N.J.: Wiley.

Ohnuma, A., Cho, E.C., Camargo, P.H.C., Au, L., Ohtani, B., & Xia, Y. (2009). A facile synthesis of asymmetric hybrid colloidal particles. *Journal of American Chemical Society, 131*(4), 1352-1353.

Orakdogen, N. (2011). pH-responsive swelling behavior, elasticity and molecular characteristics of poly(N,N-dimethylaminoethyl methacrylate) gels at various initial monomer concentrations. *Polymer Bulletin, 67*(7) 1347-1366E.

Orgiles-Calpena, E.F., Aran-Ais, A.M., Torro-Palau, C., & Orgiles-Barcelo, J. M. (2009). Influence of the Chemical Structure of Urethane-Based Thickeners on the Properties of Waterborne Polyurethane Adhesives. *Journal of Adhesion, 85* (10), 665-689.

Pickering, S. U. (1907). Emulsions. *Journal of the Chemical Society, 91*, 2001-2021.

Pieranski, P. (1980). Two-dimensional interfacial colloidal crystals. *Physical Review Letters, 45*(7), 569-572.

Pillai, O., & Panchagnula, R. (2001). Polymers in drug delivery. *Current opinion in chemical biology, 5*(4), 447-451.

Pol, V.G., Gedanken, A., Calderon-Moreno, J. (2003). Deposition of gold nanoparticles on silica spheres: a sonochemical approach. *Chemical Materials, 15*(5)1111–1118.

Qiao, X., Chen, M., Zhou, J., & Wu, L. (2007). Synthesis of raspberry-like silica/polystyrene/silica multilayer hybrid particles via miniemulsion polymerization. *Journal of Polymer Science Part A-Polymer Chemistry, 45*(6), 1028-1037.

Qiu, Y., & Park, K. (2001). Environmentally-sensitive polymer hydrogels, in Triggered Release in Drug Delivery Systems. *Advanced Drug Delivery Review, 53*(3), 321-339.

Ramsden, W. (1903). Separation of solids in the surface-layers of solutions and 'suspensions' (observations on surface-membranes, bubbles, emulsions, and mechanical coagulation) - preliminary account. *Proceedings of the Royal Society of London, 72*(479), 156-164.

Rapoport, N. (2007). Physical stimuli-responsive polymeric micelles for anti-cancer drug delivery. *Progress in Polymer Science, 32*(8-9), 962-990.

Rege, K., Patel, S.J., Megeed, Z., & Yarmush, M.L. (2007). Amphipathic peptide-based fusion peptides and immunoconjugates for the targeted ablation of prostate cancer cells. *Cancer Research, 67*(1), 6368-6375.

Rousseau, D. (2000). Fat crystals and emulsion stability — a review. *Food Research International, 33*(1), 3-14

Sahiner, N., Godbey, W.T., McPherson, G.L., & John, V.T. (2006). Microgel, nanogel and hydrogel-hydrogel semi-IPN composites for biomedical applications: Synthesis and characterization. Colloid and Polymer Science, 284 (10), 1121-1129.

Sanchez, C., Julian, B., Belleville, P., & Popall, M. (2005). General Strategies for the Design of Functional Hybrid Materials. *Journal of Materials Chemistry, 15*(2),35-36.

Santipanichwong, R., & Suphantharika, M. (2009). Influence of different β-glucans on the physical and rheological properties of egg yolk stabilized oil-in-water emulsions. *Food Hydrocolloids, 23*(5), 1279-1287.

Schild, H.G., Muthukumar, M. & Tirrell, D.A. (1991). Cononsolvency in mixed aqueous solutions of poly(N-isopropylacrylamide). *Macromolecules, 24*(4), 948-952

Schmid, A., Fujii, S., & Armes, S. P. (2005). Synthesis of micrometer-sized silica-stabilized polystyrene latex particles. *Langmuir, 21*(18), 8103-8105.

Schmid, A., Fujii, S., & Armes, S. P. (2006). Polystyrene-silica nanocomposite particles via alcoholic dispersion polymerization using a cationic azo initiator. *Langmuir, 22*(11), 4923-4927.

Schmid, A., Fujii, S., Armes, S. P., Leite, C. A. P., Galembeck, F., Minami, H., Saito, N., & Okubo, M. (2007). Polystyrene-silica colloidal nanocomposite particles prepared by alcoholic dispersion polymerization. *Chemistry of Materials, 19*(10), 2435-2445.

Schmid, A., Tonnar, J., & Armes, S. P. (2008). A new highly efficient route to polymer-silica colloidal nanocomposite particles. *Advanced Materials, 20*(17), 3331-3336.

Shah, P.S., Sigman, M. B., Stowell, C. A., Lim, K. T., Johnston, K. P., & Korgel B. A. (2003). Single-Step Self-Organization of Ordered Macroporous Nanocrystal Thin Films. *Advanced Materials, 15*(12), 971-974.

Shchipunov, Y.A., & Hoffmann, H. (2000). Thinning and thickening effects induced by shearing in lecithin solutions of polymer-like micelles. *Rheologica Acta , 39*(6), 542-553.

Shi, L., Yang, L., Chen, J., Pei, Y., Chen, M., Hui, B., & Li, J. (2004). Preparation and characterization of pH-sensitive hydrogel of chitosan/poly(acrylic acid) co-polymer. *Journal of Biomaterials Science & Polymer Edition, 15*(4), 65-74.

Shin, H.C., Alani, A.W., Rao, D.A., Rockich, N.C., & Kwon, G.S. (2009), Multi-drug loaded polymeric micelles for simultaneous delivery of poorly soluble anticancer drugs. *Journal of Controlled Release, 140*(2), 294-300.

Siepmann, J., & Siepmann, F. (2008). Mathematical modeling of drug delivery. *International Journal of Pharmaceutics, 364*(2), 328-343.

Simovic, S., & Prestidge, C. A. (2007). Nanoparticle layers controlling drug release from emulsions. *European Journal of Pharmaceutics and Biopharmaceutics, 67*(1), 39-47.

Soppimath, K.S., Tan, D.C.W. & Yang, Y. (2005). pH-Triggered thermally responsive polymer core- shell nanoparticles for drug delivery. *Advanced Materials, 17*(9), 318–323.

Stancik, E. J., Kouhkan, M., & Fuller, G. G. (2004). Coalescence of particle-laden fluid interfaces. *Langmuir, 20*(1), 90-94.

Stankiewicz, J., Vilchez, M. A. C., & Alvarez, R. H. (1993). 2-dimensional aggregation of polystyrene latex-particles. *Physical Review E, 47*(4), 2663-2668.

Steinrueck, H. (2010). Surface science goes liquid ! *Surface Science, 604*(5-6), 481-484.

Stiller, S., Gers-Barlag, H., Lergenmueller, M., Pflucker, F., Schulz, J., Wittern, K. P., & Daniels, R. (2004). Investigation of the stability in emulsions stabilized with different surface modified titanium dioxides. *Colloids and Surfaces A-Physicochemical and Engineering Aspects, 232*(2-3), 261-267.

Sullivan, A. P., & Kilpatrick, P. K. (2002). The effects of inorganic solid particles on water and crude oil emulsion stability. *Industrial & Engineering Chemistry Research, 41*(14), 3389-3404.

Tam, K. C., Ragaram, S., & Pelton R. H. (1994). Interaction of Surfactants with Poly(N-isopropylacrylamide) Microgel Latexes. *Langmuir, 10* (2), 418-422.

Tarimala, S., & Dai, L. L. (2004). Structure of microparticles in solid-stabilized emulsions. *Langmuir, 20*(9), 3492-3494.

Tarimala, S., Wu, C., & Dai, L. L. (2006). Dynamics and collapse of two-dimensional colloidal lattices. *Langmuir, 22*(18), 7458-7461.

Tauer, K., Deckwer, R., Kuhn, I., & Schellenberg, C. (1999). A comprehensive experimental study of surfactant-free emulsion polymerization of styrene. *Colloid and Polymer Science, 277*(7), 607-626.

Tauer, K., Hernandez, H., Kozempel, S., Lazareva, O., & Nazaran, P. (2008). Towards a consistent mechanism of emulsion polymerization - new experimental details. *Colloid and Polymer Science, 286*(5), 499-515.

Taylor, L. D. and Cerankowski, L. D. (1975). Preparation of films exhibiting a balanced temperature dependence to permeation by aqueous solutions—a study of lower consolute behavior. *Journal of Polymer Science: Polymer Chemistry Edition, 13*(11), 2551–2570.

Tcholakova, S., Denkov, N. D., & Lips, A. (2008). Comparison of solid particles, globular proteins and surfactants as emulsifiers. *Physical Chemistry Chemical Physics, 10*(12), 1608-1627.

Teo, B.M., Prescott, S.W., Price, G.J., Grieser, F., & Ashokkumar, M. (2010). Synthesis of temperature responsive poly(N-isopropylacrylamide) using ultrasound irradiation. *Journal of Physical Chemistry. B, 11*(4), 3178-3184.

Tian, P., Wu, Q., & Lian, K. (2008). Preparation of Temperature- and pH-Sensitive, Stimuli-Responsive Poly(N-isopropylacrylamide-co-methacrylic acid) Nanoparticles. *Journal of Applied Polymer Science, 108*(10), 2226–2232.

Tianbin, W., & Yangchuan, K. (2006). Preparation of silica-PS composite particles and their application in PET. *European Polymer Journal, 42*(2), 274-285.

Tiarks, F., Landfester, K., & Antonietti, M. (2001). Silica nanoparticles as surfactants and fillers for latexes made by miniemulsion polymerization. *Langmuir, 17*(19), 5775-5780.

Torii, H., Fujimoto, K., & Kawaguchi, H. (1996). Chemical properties of water-soluble, nonionic azo compounds as initiators for emulsion polymerization. *Journal of Polymer Science Part A-Polymer Chemistry, 34*(7), 1237-1243.

Torimoto, T., Tsuda, T., Okazaki, K., & Kuwabata, S. (2010). New frontiers in materials science opened by ionic liquids. *Advanced Materials, 22*(11), 1196-1221.

Tsuji, S., & Kawaguchi, H. (2008). Thermosensitive Pickering emulsion stabilized by poly(N-isopropylacrylamide)-carrying particles. *Langmuir, 24*(7), 3300-3305.

van Herk, A. (2005). *Chemistry and technology of emulsion polymerization*. Oxford: Blackwell.

Velev, O. D. & Nagayama, K.(1997). Assembly of Latex Particles by Using Emulsion Droplets. Reverse (Water in Oil) System. *Langmuir, 13*(6), 1856-1859.

Voorn, D. J., Ming, W., & van Herk, A. M. (2006). Polymer-clay nanocomposite latex particles by inverse Pickering emulsion polymerization stabilized with hydrophobic montmorillonite platelets. *Macromolecules, 39*(6), 2137-2143.

Wang, H., & Hobbie, E. K. (2003). Amphiphobic Carbon Nanotubes as Macroemulsion Surfactants. *Langmuir, 19*(8), 3091-3093.

Wang, H., An, Y., Huang, N., Ma, R., Li, J., & Shi, L. (2008). Contractive Polymeric Complex Micelles as Thermo-Sensitive Nanopumps. *Macromolecular Rapid Communications, 29*(2), 1410-1414.

Weete, J.D., Betageri, S., & Griffith, G.L. (1994). Improvement of lecithin as an emulsifier for water-in-oil emulsions by thermalization. *Journal of the American Oil Chemists' Society, 71*(7), 731-737.

Wei, H., Zhang, X., Chen, W., Cheng, S., & Zhuo, R. (2007). Self-assembled thermosensitive micelles based on poly(L-lactide-star block-N-isopropylacrylamide) for drug delivery. *Journal of Biomedical Material Research, Part A, 83*(A), 980-989.

Weitz D.A. (2002). Colloidosomes: Selectively Permeable Capsules Composed of Colloidal Particles. *Science, 298*(5595), 1006-1009.

Winnik, F.M., Ringsdorf, H. & Venzmer, J. (1990). Methanol-Water as a Co-Nonsolvent for Poly-(N-isopropylacrylamide). *Macromolecules, 23*(5), 2415-1416

Wu, C., Song, Y., & Dai, L. L. (2009). Two-particle microrheology at oil-water interfaces. *Applied Physics Letters, 95*(14), 144104-144104.

Wu, J., & Dai, L. L. (2006). One-particle microrheology at liquid-liquid interfaces. *Applied Physics Letters, 89*(9), 094107-094107.

Wu, J., & Dai, L. L. (2007). Apparent microrheology of oil-water interfaces by single-particle tracking. *Langmuir, 23*(8), 4324-4331.

Wu, M. H., & Whitesides, G. M. (2001). Fabrication of arrays of two-dimensional micropatterns using microspheres as lenses for projection photolithography. *Applied Physics Letters, 78*(16), 2273-2275.

Wu, W., Shen, S., Cheng, C., Meng, H., Guo, K., & Chen, J. (2009). Investigation on the mechanical strength of magnetic hollow silica prepared from Pickering emulsion route. *Materials Chemistry and Physics, 113*(2-3), 696-701.

Xiong, D., He, Z., An, Y., Li, Z., Wang, H., Chen, X., & Shi, L. (2008). Temperature-responsive multilayered micelles formed from the complexation of PNIPAM-b-P4VP block-copolymer and PS-b-PAA core-shell micelles. *Polymer, 49*(10), 2548-2552.

Yamamoto, T., Kanda, Y., & Higashitani, K. (2004). Molecular-scale observation of formation of nuclei in soap-free polymerization of styrene. *Langmuir, 20*(11), 4400-4405.

Yamamoto, T., Kanda, Y., & Higashitani, K. (2006). Initial growth process of polystyrene particle investigated by AFM. *Journal of Colloid and Interface Science, 299*(1), 493-496.

Yamamoto, T., Nakayama, M., Kanda, Y., & Higashitani, K. (2006). Growth mechanism of soap-free polymerization of styrene investigated by AFM. *Journal of Colloid and Interface Science, 297*(1), 112-121.

Yan, N. X., Gray, M. R., & Masliyah, J. H. (2001). On water-in-oil emulsions stabilized by fine solids. *Colloids and Surfaces A-Physicochemical and Engineering Aspects, 193*(1-3), 97-107.

Yan, N. X., Kurbis, C., & Masliyah, J. H. (1997). Continuous demulsification of solids-stabilized oil-in-water emulsions by the addition of fresh oil. *Industrial & Engineering Chemistry Research, 36*(7), 2634-2640.

Yan, N. X., & Masliyah, J. H. (1995a). Characterization and demulsification of solids-stabilized oil-in-water emulsions .1. partitioning of clay particles and preparation of emulsions. *Colloids and Surfaces A-Physicochemical and Engineering Aspects, 96*(3), 229-242.

Yan, N. X., & Masliyah, J. H. (1995b). Characterization and demulsification of solids-stabilized oil-in-water emulsions .2. demulsification by the addition of fresh oil. *Colloids and Surfaces A-Physicochemical and Engineering Aspects, 96*(3), 243-252.

Yan, N. X., & Masliyah, J. H. (1996). Demulsification of solids-stabilized oil-in-water emulsions. *Colloids and Surfaces A-Physicochemical and Engineering Aspects, 117*(1-2), 15-25.

Yan, N., & Masliyah, J. H. (1996). Effect of pH on adsorption and desorption of clay particles at oil-water interface. *Journal of Colloid and Interface Science, 181*(1), 20-27.

Yang, F., Liu, S., Xu, J., Lan, Q., Wei, F., & Sun, D. (2006). Pickering emulsions stabilized solely by layered double hydroxides particles: The effect of salt on emulsion formation and stability. *Journal of Colloid and Interface Science, 302*(1), 159-169.

Yang, F., Niu, Q., Lan, Q., & Sun, D. (2007). Effect of dispersion pH on the formation and stability of Pickering emulsions stabilized by layered double hydroxides particles. *Journal of Colloid and Interface Science, 306*(2), 285-295.

Yang, J., Hasell, T., Wang, W. X., Li, J., Brown, P. D., Poliakoff, M., Lester, E., & Howdle, S. M. (2008). Preparation of hybrid polymer nanocomposite microparticles by a nanoparticle stabilised dispersion polymerisation. *Journal of Materials Chemistry, 18*(9), 998-1001.

Yasuda, H., Lamaze, C.E., & Ikenberry, L.D. (1968). Permeability of solutes through hydrated polymer membranes. Part I. Diffusion of sodium chloride. *Die Makromolekulare Chemie, 11*(8), 19-35.

Zhang, X., Zhuo R, & Yang, Y. (2002) Using mixed solvent to synthesize temperature sensitive poly(Nisopropylacrylamide) gel with rapid dynamic properties. *Biomaterials, 26*(2), 1313-1318.

Zhang, Y.F., Gu, W. Y., Xu, H. X., & Liu, S. Y. (2008). Facile Fabrication of Hybrid Nanoparticles Surface Grafted with Multi-Responsive Polymer Brushes via Block Copolymer Micellization and Self-Catalyzed Core Gelation. *Journal of. Polymer Science Part A – Polymer Chemistry, 46*(7), 2379-2389.

Zhang, Y., Wu, T. & Liu, S. (2007), Micellization Kinetics of a Novel Multi-Responsive Double Hydrophilic Diblock Copolymer Studied by Stopped-Flow pH and Temperature Jump. *Macromolecular Chemistry and Physics, 208*(23), 2492–2501.

Zhu, M.Q., Wang, L.Q., Exarhos, G.J., & Li, D.Q. (2004). Thermosensitive Gold Nanoparticles. *Journal of American Chemical Society, 126* (9), 2656–2657.

Zrinyi, M. (2000). Intelligent polymer gels controlled by magnetic fields. *Colloid and Polymer Science, 278*(2), 98–103.

APPENDIX A

THE STATUS OF RECYCLING OF PRINTED CIRCUIT BOARD USING A GREEN PROCESS

1. Introduction

Widespread use of electronic equipment and shortening of product life cycles have created the challenging task of dealing with the ever-increasing quantity of obsolete electronic equipments. Among the challenges to successful electronic equipment recycling, printed circuit board (PCB) primary components in every type of electronic products; recycling is recognized as one of the most difficult tasks because of their complex construction and complicated material composition (Pitts &Mizuki, 1996). PCB scraps are generated from almost all kinds of end-of-life electrical and electronic products. It is reported that about 50,000 tons of PCB scraps is produced each year in United Kingdom and only 15% of those is currently subjected to any form of recycling, while remaining 85% is consigned to landfill (Goosey et al., 2003).

PCBs contain three basic components regardless of their construction: 1) a non-conducting substrate or laminate, 2) conductive circuits printed on or inside the substrate and, 3) mounted components. The most widely used substrate is (flame retardant) FR4, which is made up of glass fiber reinforced epoxy resin with a brominated flame retardant in the epoxy matrix. FR2 is another type of commonly seen substrate which is made up of paper reinforced phenolic resin with added flame retardants (Zhang & Gao, 2004). PCBs contain not only a significant amount of precious metals (gold, silver, palladium, etc.) and base metals (copper, iron, aluminum, tin, etc.) but also hazardous elements such as lead, mercury, antimony, cadmium, chromium and beryllium (Zhang & Gao,

2004). This is why it is essential to have proper recycling processes for PCB disposal as these toxic elements could lead to serious environmental contamination.

The traditional PCB recycling technology focuses more on separating objective metals and fiber glasses but pays less attention to efficiency and economic returns. For instance, most recycling processes can only recover 28 wt% metals from PCBs, resulting in more than 70% of PCB scraps not being efficiently recycled and ending up in landfill (Zhang & Gao, 2004). A traditional PCB recycling process usually includes three steps: pretreatment, shredding/separation and mechanical/chemical refining (Zhang & Gao, 2004). The pretreatment stage includes a composition analysis and disassembly of the reusable and hazardous components. Since the main objective of the recycling is to minimize the damage to the environment and maximize material recovery, a composition analysis is necessary not only to obtain the detailed material information of PCBs, but also to give an estimation of the cost incurred and profit realized from the PCB recycling. The purpose of disassembly is to remove reusable and hazardous components in order to isolate them from subsequent treatments. Shredding/separation are the next alternative step after disassembly. The PCB substrates are treated with shredding machines to be fragmented into small particles typically between 100 and 300 μm (Zhang & Gao, 2004). These particles can be further separated by techniques based on component differences in size, density, magnetic, electrostatic, eddy current and gravity (Goosey et al.,

2003). Finally, thermal, mechanical or chemical (or combined) processing are employed to collect the final recycled products. Here we report the development and understanding of an alternative green supercritical fluid (SCF) carbon dioxide (CO_2) based process to delaminate the PCBs such that the metals and glass fibers retain their original form and can be recovered. The process temperature is set higher than the glass transition temperature of the polymer within the PCBs. This can cause polymer decomposition which leads to the delamination of the PCBs.

2. Experimental

2.1 The PCBs and Supercritical CO_2 Process

The PCBs were kindly supplied from S1 Technology Inc. A supercritical carbon dioxide (CO_2) process was designed and developed to delaminate/recycle PCBs with details discussed in Section 3.1. The main components in the process include a HiP GC-21 high pressure vessel, low temperature and high temperature laboratory ovens, pressure transducers, thermometers and a CO_2 supply. The PCB were placed in the high pressure vessel and undergo a supercritical CO_2 process with controllable temperature, pressure and co-solvents (if any) and processing time.

2.2 Material Characterization

In order to understand the mechanisms of PCB delaminating/recycling, we have performed various materials characterization using a differential scanning calorimeter (TA Instruments SDT Q600), a dynamic mechanical analyzer (TA Instruments DMA Q800), and a Fourier Transform Infrared Spectrometer (Bruker

IFS 66V/S). Differential scanning calorimetry (DSC) was used to measure the glass transition temperature of the PCBs before and after supercritical CO_2 treatments. The measurements were performed in a nitrogen atmosphere. After a heating and cooling cycle up to 240 °C at 10 °C/min to eliminate the thermal history, the glass transition temperature was analyzed from data of the second heating scan from 25 to 240 °C at 10 °C/min, with the TA Universal Analysis software. During a dynamic mechanical analyzer (DMA) experiment, the delaminated (supercritical CO_2 treated) and control (untreated) PCBs were dissembled manually and loaded onto the tension clamp. The temperature was varied from 25 to 250°C ramped up at a rate of 3 °C/min. A preload force of 0.01N and force track of 125% was chosen in accordance with the recommended values for the clamp. Fourier transform infrared spectrometer (FTIR) experiments were performed to evaluate the molecular "fingerprints" of PCBs. The polymeric parts were scraped off from the PCBs and then grinded and pressed with potassium bromide (KBr) to form pellets. FTIR spectra were scanned over the range of 400-4,000 cm^{-1}.

3. Results and discussion

3.1 Validation of a Supercritical CO_2 Process for PCB Delaminating/Recycling

An SCF is defined as a substance above its critical temperature (T_c) and critical pressure (P_c), where it remains as a single phase, having gas-like diffusion rate, viscosity, and liquid-like densities (Kazarian, 2000, Smith, Van Ness & Abbott, 2001, Prausnitz, 1999). It can effuse through solids like a gas, and

dissolve materials like a liquid. In addition, close to the critical point, small changes in pressure or temperature result in large changes in density, allowing many properties of a supercritical fluid to be "fine-tuned". Supercritical fluids are suitable as a substitute for organic solvents in a range of industrial and laboratory processes. Carbon dioxide and water are the most commonly used supercritical fluids, being used for decaffeination and power generation, respectively. In addition, there is no surface tension in a supercritical fluid, as there is no liquid/gas phase boundary. By changing the pressure and temperature of the fluid, the properties can be "tuned" to be more liquid- or more gas-like. One of the most important properties is the solubility of material in the fluid. Solubility in a supercritical fluid tends to increase with density of the fluid (at constant temperature). Since density increases with pressure, solubility tends to increase with pressure. The relationship with temperature is a little more complicated. At constant density, solubility will increase with temperature. However, close to the critical point, the density can drop sharply with a slight increase in temperature. Therefore, close to the critical temperature, solubility often drops with increasing temperature, then rises again.

All supercritical fluids are completely miscible with each other so for a mixture a single phase can be guaranteed if the critical point of the mixture is exceeded. The critical point of a binary mixture can be estimated as the arithmetic mean of the critical temperatures and pressures of the two components,

$T_{c(mix)}$ = (mole fraction A) x T_cA + (mole fraction B) x T_cB.

Figure A1 shows a projection of a phase diagram. In the pressure-temperature phase diagram the boiling separates the gas and liquid region and ends in the critical point, where the liquid and gas phases disappear to become a single supercritical phase. At well below the critical temperature, e.g., 280K, as the pressure increases, the gas compresses and eventually (at just over 40 bar) condenses into a much denser liquid, resulting in the discontinuity in the line (vertical dotted line). The system consists of 2 phases in equilibrium, a dense liquid and a low density gas. As the critical temperature is approached (300K), the density of the gas at equilibrium becomes denser, and that of the liquid lower. At the critical point, (304.1 K and 7.38 MPa (73.8 bar)). There is no difference in density, and the 2 phases become one fluid phase. Thus, above the critical temperature a gas cannot be liquefied by pressure. At slightly above the critical temperature (310K), in the vicinity of the critical pressure, the line is almost vertical. A small increase in pressure causes a large increase in the density of the supercritical phase. Many other physical properties also show large gradients with pressure near the critical point, e.g. viscosity, the relative permittivity and the solvent strength, which are all closely related to the density. At higher temperatures, the fluid starts to behave like a gas. For carbon dioxide at 400 K, the density increases almost linearly with pressure.

Many pressurised gases are actually supercritical fluids. For example, nitrogen has a critical point of 126.2K (- 147 °C) and 3.4 MPa (34 bar). Therefore, nitrogen (or compressed air) in a gas cylinder above this pressure is

actually a supercritical fluid. These are more often known as permanent gases. At room temperature, they are well above their critical temperature, and therefore behave as a gas, similar to CO2 at 400K above. However, they cannot be liquefied by pressure unless cooled below their critical temperature. The gas-like and liquid-like properties combined together can give the SCF appropriate thermodynamic properties that make it a highly useful and environmentally benign solvent for various applications.

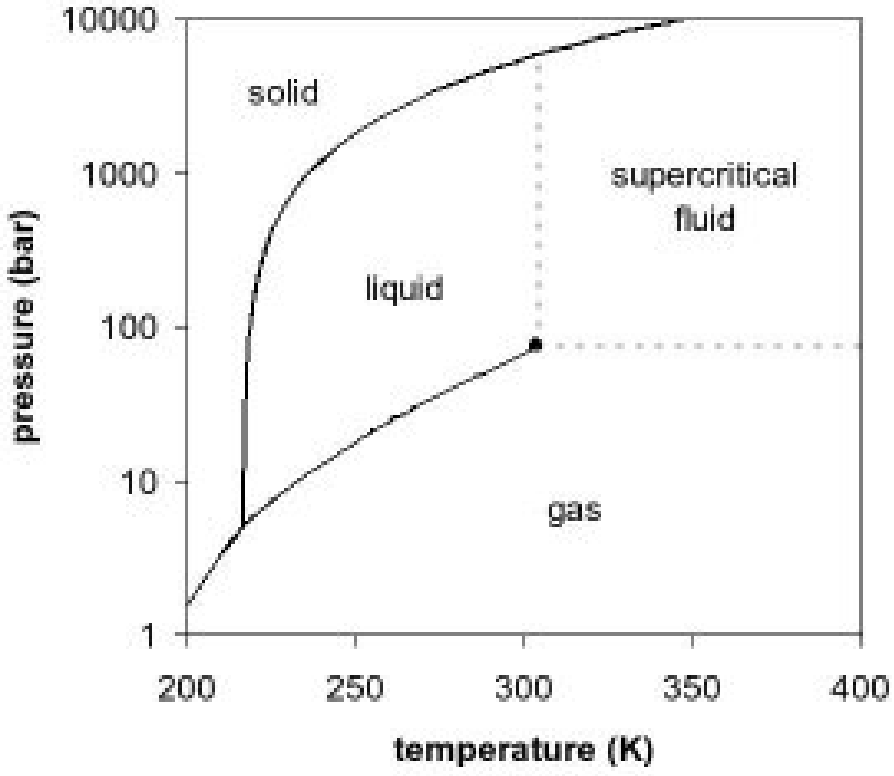

Figure A1

Pressure-temperature phase diagram for carbon dioxide.

Recently, supercritical fluids have been employed for waste material recycling with the potential to satisfy both economic and environmental demands.

It has been found that near critical and supercritical water oxidation techniques can partially or completely break down rubber waste materials (Parl et al., 2001). Electronic wastes can be dissembled with zero emission using supercritical water oxidation. Up to 50% reduction in weight can be achieved and organic epoxy resin material can be converted into carbon dioxide, water, nitrogen and bromide (Eyerer, 1998). The residuals of electronic wastes after the supercritical water oxidation treatment contain merely fiberglass and metals. In this work, we validated a supercritical carbon dioxide (CO_2) process delaminate/recycle PCBs. Supercritical CO_2 has a critical temperature of 31°C and pressure of 73.8 bars (Rothman et al., 2002). Figure A2 is a schematic diagram of the supercritical CO_2 process. During the experiments, we first systematically evaluated the effect of process conditions and time on PCB delaminating. The processing temperature, pressure and time varied from 100-260 ^{o}C, 100-379 bar and 3-6 hours, respectively. We discovered that a combination of medium processing temperature, pressure and time is sufficient to delaminate the PCBs. For example, we found that at a combination of temperature as low as 180 ^{o}C and pressure as low as 138 bar could successfully delaminate PCBs and enable subsequent recycling. In addition, a small amount such as 7% of water as co-solvent improved the effectiveness of delaminating the bonding materials with the process temperature and pressure being below the critical temperature and pressure of water ($T_{c\ water}$ = 374 ^{o}C and P_c = 221 bar (Rothman et al., 2002)).

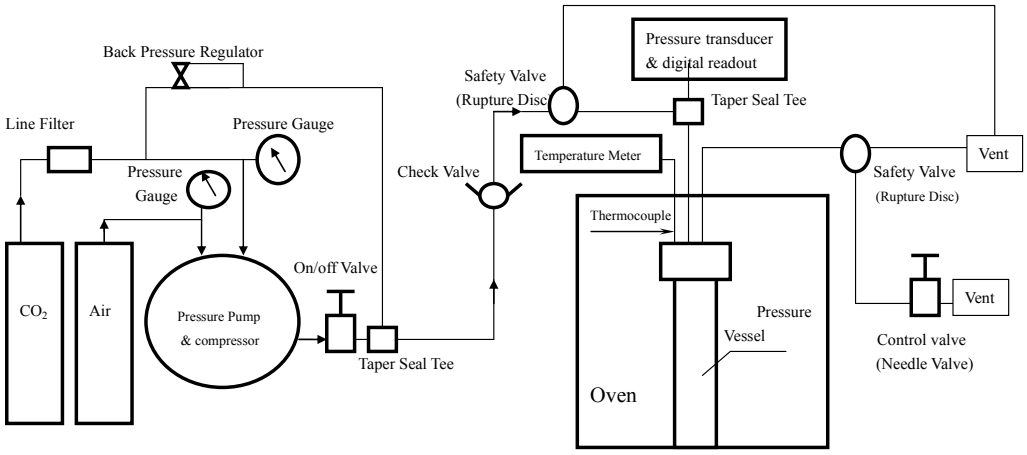

Figure A2

A schematic diagram of the supercritical CO_2 process for delaminating/recycling PCBs.

3.2 Exploring PCB Delaminating Mechanisms

It is intuitive to enquire delaminating mechanisms of the PCB boards under a supercritical CO_2 process such as at 180 ^oC and 138 bar with 7% of water. Thus we have performed a series of materials characterization and compared the PCBs before any supercritical fluid process (control) versus those that went through the process. First, we performed DSC experiments detailed above to quantify the glass transition temperatures. The glass-liquid transition (or glass transition for short) is the reversible transition in amorphous materials (or in amorphous regions within semicrystalline materials) from a hard and relatively brittle state into a molten or rubber-like state. An amorphous solid that exhibits a glass transition is called a glass. Despite the massive change in the physical

properties of a material through its glass transition, the transition is not itself a phase transition of any kind; rather it is a laboratory phenomenon extending over a range of temperature and defined by one of several conventions. Upon cooling or heating through this glass transition range, the material also exhibits a smooth step in the thermal expansion coefficient and in the specific heat, with the location of these effects again being dependent on the history of the material. However, the question of whether some phase transition underlies the glass transition is a matter of continuing research. The glass transition temperature Tg is always lower than the melting temperature, Tm, of the crystalline state of the material, if one exists. The glass transition of a liquid to a solid-like state may occur with either cooling or compression. The transition comprises a smooth increase in the viscosity of a material by as much as 17 orders of magnitude without any pronounced change in material structure. The consequence of this dramatic increase is a glass exhibiting solid-like mechanical properties on the timescale of practical observation. This transition is in contrast to the freezing or crystallization transition, which is a first-order phase transition and involves discontinuities in thermodynamic and dynamic properties such as volume, energy and viscosity. In many materials that normally undergo a freezing transition, rapid cooling will avoid this phase transition and instead result in a glass transition at some lower temperature. Other materials, such as many polymers, lack a well-defined crystalline state and easily form glasses, even upon very slow cooling or compression.

Below the transition temperature range, the glassy structure does not relax in accordance with the cooling rate used. The expansion coefficient for the glassy state is roughly equivalent to that of the crystalline solid. If slower cooling rates are used, the increased time for structural relaxation (or intermolecular rearrangement) to occur may result in a higher density glass product. Similarly, by annealing (and thus allowing for slow structural relaxation) the glass structure in time approaches an equilibrium density corresponding to the supercooled liquid at this same temperature. Tg is located at the intersection between the cooling curve (volume versus temperature) for the glassy state and the supercooled liquid.

The configuration of the glass in this temperature range changes slowly with time towards the equilibrium structure. The principle of the minimization of the Gibbs free energy provides the thermodynamic driving force necessary for the eventual change. It should be noted here that at somewhat higher temperatures than Tg, the structure corresponding to equilibrium at any temperature is achieved quite rapidly. In contrast, at considerably lower temperatures, the configuration of the glass remains sensibly stable over increasingly extended periods of time.

Thus, the liquid-glass transition is not a transition between states of thermodynamic equilibrium. It is widely believed that the true equilibrium state is always crystalline. Time and temperature are interchangeable quantities (to some extent) when dealing with glasses, a fact often expressed in the time-temperature superposition principle. On cooling a liquid, internal degrees of freedom successively get removed out of equilibrium.

Figure A3 shows the overlay of DSC curves of the control (untreated) and the samples that went through the supercritical CO_2 process at the pressure of 172 bar and the temperature of 150 ^oC, 180 ^oC, and 200 ^oC, respectively. The glass transition temperatures (both onset and half-height, as labeled on the curves) did not exhibit significant differences of the samples before (control) and after the supercritical CO_2 processes.

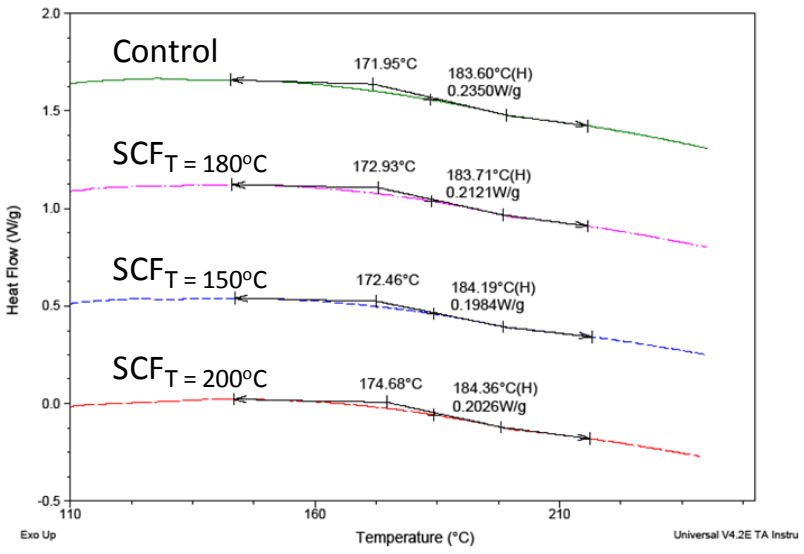

Figure A3

Differential scanning calorimetry (DSC) overlay of the control and the PCBs going through the supercritical CO_2 process at 172 bar, 7% water, but different temperatures.

This is surprising since it is known that a supercritical fluid process can cause a subsequent chain scissoring, often referred to as degradation, which

produces resin fragment with shorter chain length and lower molecular weight (Yu & Zhang, 1998). For example, recycling of high value carbon fiber from polymer composites using supercritical n-propanol (Jiang et al., 2007) and nearcritical and supercritical water (Hernanz et al., 2008) have been reported; both work suggest polymer degradation as the primary mechanism for fiber and resin separation. Since polymer degradation leads to significant changes in physical properties such as glass transition temperature and cross link density, the DSC results do not support such hypothesis when the PCB substrates undergo a supercritical CO_2 process at 172 bar, 150-200 ^oC and 7% water.

Subsequently, we further verified the observation by the DMA experiments and in this study, the peak value of tan δ curve as shown in Figure A4 was used to determine the glass transition temperature. The DMA experiments also suggest that there is no significant difference in glass transition temperature when comparing the samples before (control) and after the supercritical process (same process conditions as those samples in the DSC experiments). It is also worthwhile to note that we characterized the crosslink density through its correlation with rubbery plateau (E′), $3\rho RT/E'$, where ρ is the density, R is the gas constant, and T is the temperature. Taking into account the standard deviation of results, the samples did not reveal meaningful difference in crosslink density, which further eliminates the hypothesis chain scissoring under such process conditions.

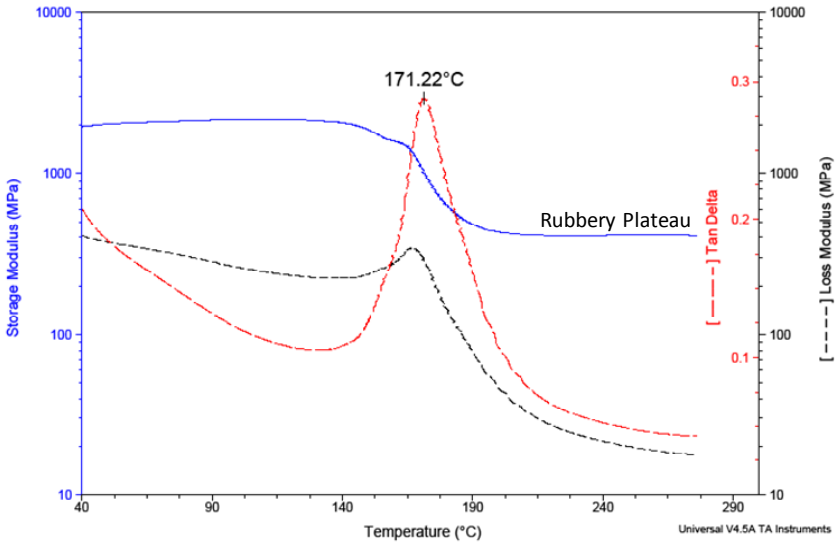

Figure A4

A representative dynamic mechanical analyzer (DMA) run of PCB after going through a supercritical carbon dioxide process at 180°C, 172 bar, and 7% water. The experimental frequency is 1 Hz.

Finally, we try to understand why a small amount (7%) of water improved effectiveness of delamination of the bonding materials when the process temperature was significantly below the critical temperature and pressure of water ($T_{c,\ water}$ = 374 °C and P_c = 221 bar (Prausnitz, 1999)). The commonly used bonding material is brominated bisphenol-A epoxy based material, which includes a basic epoxy resin, crosslinking component, and brominated fire retardants. Water has recently been identified as a unique agent under sub- and supercritical conditions (Shibasaki et al., 2004, Bellissent-Funel, 2001, Goedkoop & Spriensma, 2000, Li et al., 2007, Huisman et al., 2000). For example, sub- and supercritical water has effectively converted an epoxy resin into carbon dioxide

and water through a hydrolysis and oxidation mechanism (Fromonteil et al., 2000). Recovery of waste polystyrene to styrene monomer by supercritical water partial oxidation has also been performed (Lilac & Lee, 2001). Diphenylether can be decomposed into phenol in the reaction in supercritical water with the addition of a base compound Na_2CO_3 (Shibasaki et al., 2004). Surprisingly, our work so far suggests that water caused neither additional chemical reaction nor additional decomposition of the epoxy resins under the tested conditions, likely due to the fact the process was operated at a non-supercritical condition of water. Although 7% water is sufficient to improve the delamination process, we have included high water contents in order to study the mechanism and performed FTIR experiments. The FTIR spectrums suggest that the PCB boards, which went through a high percentage water during the supercritical CO_2 process contained high tracer amount of water molecules. This is evidenced by the more prominent peaks at the wavenumber of 3450 cm^{-1} (where water molecule resonates), as shown in Figure A5. However, the FTIR scans revealed signals of neither formation of any new substances nor changes of other molecular "finger prints" over the experimental wavelength range (Figure A5). The evidence of no formation of new substances such as hydrocarbons and noxious gases commonly found in the pyrolysis of PCBs (Chien et al., 2000) further reinforced the environmentally benign nature of the developed supercritical CO_2 process.

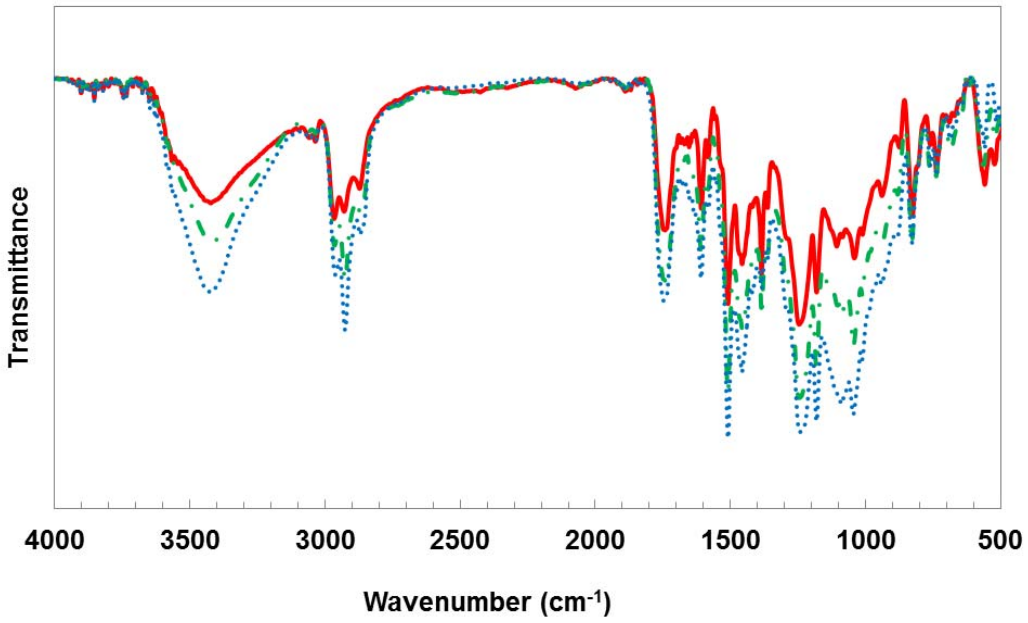

Figure A5

Overlay of Fourier transform infrared spectrum (FTIR) of PCB boards after going through different SCF processes. T = 180°C; P = 172 bar; water percentage: W1(solid red line): 0%, W3(dotted and dashed green line): 20%; W4(dotted blue line): 31%. The water percentage was increased solely for the purpose of studying mechanisms.

4. Conclusion

An environmentally benign supercritical CO_2 process has been designed and validated for PCB recycling. Using supercritical carbon dioxide as a solvent and with an additional small amount of water, the PCB scraps delaminated easily and separated into copper foil, glass fiber and polymer which can then be further recycled. In addition, we have performed a systematic study of the effects of

process conditions such as pressure, temperature, time and co-solvent on PCB delamination/recycling. From the experimental results of DSC, DMA and FTIR, we suggest that neither chain scissoring (polymer degradation) nor any additional reaction occurred during the developed supercritical CO_2 process. Such PCB delaminating/recycling method has the advantages of automatic separation and being environmentally benign compared to the traditional recycling process.

5. Acknowledgments

We are grateful to the financial support from the National Science Foundation CBET-092533 and the Arizona State University Fulton Undergraduate Research Initiative.

References

Bellissent-Funel, M.C. (2001). Structure of supercritical water. *Journal of Molecular Liquids, 12*(90), 313-322.

Chien, Y., Wang, H.P., Lin, K., Huang, Y.J., & Yang, Y.W. (2000). Fate of bromine in pyrolysis of printed circuit board wastes. *Chemosphere, 40*(1), 383-387.

Eyerer, P., & Elsner P. (1998). Using Plastics to Make New Products. *Journal of Polymer Engineering, 18*(2), 301-339.

Fromonteil, C., Bardellec, P., & Cansell, F. (2000). Hydrolysis and oxidation of an epoxy resin in sub- and supercritical water. *Industrial and Engineering Chemistry Research, 39*(3), 922-925.

Goedkoop, M., & Spriensma, R. (2000). *The Eco-Indicator 99, A Damage Oriented Method for Life Cycle Impact Assessment, Methodology Report.* Second Edition, Pre Consultants.

Goosey, M. (2003). Recycling technologies for the treatment of end of life printed circuit boards. *Circuit world, 29*(3), 33-37.

Hernanz, R. (2008). Chemical recycling of carbon fiber reinforced composites in nearcritical and supercritical water. *Composites:Part A, 39*(8) 454-461.

Huisman, J., Boxes, C., & Stevels A. (2000). Environmentally Weighted Recycling Quotes-Better Justifiable and Environmentally More Correct. *International Symposium on Electronics and the Environment.*

Jiang, G., Pickering, S.J., Lester, E., Blood, P., & Warrior, N. (2007). Recycling Carbon Fiber/Epoxy Resin Composites Using Supercritical Propanol. *16th International Conference on Composite Materials*.

Kazarian, S.G. (2000). Polymer Processing with Supercritical Fluids. *Polymer Science Series C+, 42*(7), 78-101.

Li, H., Zhang, H.C., & Tate D. (2007). Energy-saving Based Innovative Product Design Method. *Proceedings of the 2007 IEEE International Symposium on Electronics & the Environment*, 134-136.

Lilac, W.D., & Lee, S. (2001). Kinetics and mechanisms of styrene monomer recovery from waste polystyrene by supercritical water partial oxidation. *Advances in Environmental Research, 6*(8), 9-16.

Park, Y. (2001). Depolymerization of Styrene−Butadiene Copolymer in Near-Critical and Supercritical Water. *Industrial Engineering and Chemistry Research, 40*(3), 756–767.

Prausnitz, J.M., Lichtenthaler, R.N., & Azevedo E.G.D. (1999). *Molecular Thermodynamics of Fluid-Phase Equilibria.* Prentice-Hall, New Jersey.

Pitts, G., & Mizuki, C. (1996). A View of Electronic Products Disposition. *Proceedings of the 1996 IEEE International Symposium on Electronics and the Environment,* 66-72.

Shibasaki, Y., Kamimori, T., Kadokawa, J., Hatano, B., & Tagaya, H. (2004). Decomposition reactions of plastic model compounds in sub- and supercritical water. *Polymer Degradation and Stability, 83*(12), 481-485.

Smith, J.M., Van Ness, H.C., & Abbott M.M. (2001). *Introduction to Chemical Engineering Thermodynamics.* McGraw-Hill, New York.

Tomasko, D.L., Li, H.B., Liu, D.H., Han, X.M., Wingert, M.J., Lee L.J., & Koelling K.W. (2003). A review of CO_2 applications in the processing of polymers. *Industrial and Engineering Chemistry Research, 42*(5), 6431-6456.

Yu, S., & Zhang, H.C. (1998). Environmental Conscious Design Support Model Using Fuzzy Analytic Hierarchy Process. *Transactions of the North American Manufacturing Research Institution of SME, 26*(8), 293-298.

Zhang, H.C., & Gao, Z. (2004). Printed Circuit Boards Recycling: a State-of-the Art Survey. *IEEE Transactions on Electronics Packaging manufacturing, 27*(21), 33-42.